Nano Research Energy

ISSN 2791-0091 (print); 2790-8119 (online)
https://doi.org/10.26599/NRE.2023.9120050

Review Article

Solid polymer electrolytes: Ion conduction mechanisms and enhancement strategies

Dongmei Zhang[§], Xianglong Meng[§], Wenyan Hou[§], Weihao Hu, Jinshan Mo, Tianrong Yang, Wendi Zhang, Qianxiao Fan, Lehao Liu (✉), Bing Jiang, Lihua Chu, and Meicheng Li (✉)

State Key Laboratory of Alternate Electrical Power System with Renewable Energy Sources, School of New Energy, North China Electric Power University, Beijing 102206, China

[§] *Dongmei Zhang, Xianglong Meng, and Wenyan Hou contributed equally to this work.*

Received: 30 September 2022 / **Revised**: 5 December 2022 / **Accepted**: 17 December 2022

ABSTRACT

Solid polymer electrolytes (SPEs) possess comprehensive advantages such as high flexibility, low interfacial resistance with the electrodes, excellent film-forming ability, and low price, however, their applications in solid-state batteries are mainly hindered by the insufficient ionic conductivity especially below the melting temperatures, etc. To improve the ion conduction capability and other properties, a variety of modification strategies have been exploited. In this review article, we scrutinize the structure characteristics and the ion transfer behaviors of the SPEs (and their composites) and then disclose the ion conduction mechanisms. The ion transport involves the ion hopping and the polymer segmental motion, and the improvement in the ionic conductivity is mainly attributed to the increase of the concentration and mobility of the charge carriers and the construction of fast-ion pathways. Furthermore, the recent advances on the modification strategies of the SPEs to enhance the ion conduction from copolymer structure design to lithium salt exploitation, additive engineering, and electrolyte micromorphology adjustion are summarized. This article intends to give a comprehensive, systemic, and profound understanding of the ion conduction and enhancement mechanisms of the SPEs for their viable applications in solid-state batteries with high safety and energy density.

KEYWORDS

solid polymer electrolytes, ionic conductivity, solid-state lithium-ion batteries, electrolyte microstructure, modification strategies

1 Introduction

Since their discovery at the end of the 20th century, lithium (Li)-ion batteries (LIBs) have been widely applied in many fields such as portable electrical devices, electric vehicles (EVs), and grid storage stations, because of their advantages including high energy density, high operating voltage, and excellent cycle stability [1, 2]. Traditional LIBs can offer volumetric and gravimetric energy densities of up to ~ 770 Wh·L^{-1} and ~ 300 Wh·kg^{-1}, respectively [2–8]; however, these levels are still not enough to meet the consumers' requirements [9]. Moreover, due to the volatile, flammable, and explosive properties of the organic liquid electrolytes, the use of large amounts of LIBs especially in energy storage power stations or EVs would easily cause safety hazards [9–12]. Replacing the organic liquid electrolytes by solid state electrolytes (SSEs) cannot only solve the safety problems, but also achieve high-energy-density LIBs by using high-capacity cathodes and Li metal anodes. Besides, the LIB fabrication process can also be simplified by removing the polymer separators.

SSEs can be classified into organic solid electrolytes (OSEs) and inorganic solid electrolytes (ISEs) according to the chemical compositions [9]. Many inorganic oxide electrolytes have been investigated such as NASICON (sodium super ionic conductor)-type phosphates [13], garnet-type $Li_xLa_3M_2O_{12}$ (M = Ta, Nb, and Zr) [14], and perovskite-type oxides [15]. The ionic conductivity of these ISEs can reach ~ 10^{-4} S·cm^{-1} at room temperature. Sulfide electrolytes such as $Li_{10}GeP_2S_{12}$ (LGPS) and $70Li_2S$-$30P_2S_5$ with unprecedented ionic conductivities of 1.2×10^{-2} and 3.2×10^{-3} S·cm^{-1} at room temperature, respectively, have also been reported [16, 17]. Although these ISEs have obvious merits of high ionic conductivity and stiffness, their applications in solid-state batteries are hindered by the poor flexibility, high interfacial resistance, etc. In stark contrast, OSEs have higher flexibility and closer physical contact with the electrodes, and thus have potential applications in solid-state LIBs. OSEs can be divided into plastic crystal electrolytes (PCEs), metal organic framework-based electrolytes (MOFEs), covalent organic framework-based electrolytes (COFEs), and solid polymer electrolyte (SPEs).

Address correspondence to Lehao Liu, lehaoliu@ncepu.edu.cn; Meicheng Li, mcli@ncepu.edu.cn

As early as 2003, a few scholars discovered the ion transport behavior in plastic crystals [18]. Succinonitrile (SN) is a typical organic molecule for preparing PCEs, and it has a strong polarity to dissolve various Li salts [19]. When mixed with 5 mol% lithium bis-trifluoromethanesulphonimide (LiTFSI), the PCEs exhibit a high ionic conductivity of over 10^{-3} S·cm^{-1} at room temperature [20]. Nevertheless, the PCEs have obvious disadvantages of poor film-forming property and high cost.

MOFEs are based on the porous MOF hosts with stable three-dimensional (3D) open solid frameworks to which Li-ion-containing liquids are added as ion conductors. The added Li-ion liquid electrolytes will lose the mobility, however, this would offer high ionic conductivity of 3.0×10^{-4} S·cm^{-1} of the MOFEs [21]. The high ionic conductivity in the MOFEs (e.g., HKUST-1) is also contributed by the good surface contact and ion channels in the MOF [22]. COFs have the similar framework structures as MOFs, but the COFs do not contain metal elements. Jeong et al. [23] developed a single-ion COFE based on a Li-sulfonated covalent organic framework (TpPa-SO_3Li) without lithium salts and organic solvents, and the COFE had high ionic conductivity of 2.7×10^{-5} S·cm^{-1} and Li-ion transference number of 0.9 at room temperature, because of the well-designed directional ion channels, high-concentration lithium ions, and the covalently tethered anion groups. It should be noted that the preparation of the COFEs and MOFEs requires of the mechanical compression of the COF and MOF powders into the electrolyte pellets. Similar to the PCEs, the applications of the COFEs and MOFEs in solid-state batteries are also impeded by the poor flexibility and high cost.

Compared to the ISEs, PCEs, MOFEs, and COFEs, polymer molecule-based SPEs have obvious comprehensive advantages such as high flexibility, low interfacial resistance with the electrodes, excellent film-forming ability, and low price, which are conducive to their large-scale applications in solid-state LIBs. So far, people's research on SPEs has gone through nearly fifty years. In 1973, Wright et al. [24] took the lead in discovering and studying the alkali metal ions transport phenomenon in polyethylene oxide (PEO), which opened the door of the SPE research. Armand et al. [25] proposed the use of PEO-based SPE in LIBs in 1983. Other polymer electrolytes such as polyacrylonitrile (PAN) with wider electrochemical window are also developed [26]. Owing to the main drawback of low room-temperature conductivity of the SPEs, the organic liquid electrolytes are still applied in the commercial LIBs. Besides, the practical applications of the SPEs are also hindered by the insufficient mechanical strength, low thermal stability, and narrow electrochemical window. Thus, a few modification strategies such as copolymer molecule structure design, adding organic plasticizers, polymer blending, and nanoparticle (NP) filling are developed to improve their ionic conductance and other properties.

A few excellent papers have been published on the recent advancement in how to enhance the overall properties of the ISEs and OSEs and how to resolve the interface issues in the solid-state LIBs; however, there are few papers solely regarding the ion transport issue of the SPEs, which is the most important issue hindering their applications. In obvious contrast to the previous review/perspective/progress papers, we scrutinize the ion conduction mechanism of the SPEs, and analyze the main factors determining the ion conduction property. Based on the deep analyses of the SPE microstructure and the ion transport behaviors, we ascribe the increase in the ionic conductivity to the improvement in the carrier concentration and mobility and the fast-ion pathways. Correspondingly, we summarize the up-to-date advance in the modification strategies from the polymer structure design, lithium salt type and content, organic and inorganic additives, and the SPE film morphology (Fig. 1). A scientific step-to-step story why the researchers try to use these modification methods together with proper reasons is also given in the article. Furthermore, a few suggestions related to the development trend to better enhance the ion conduction of the SPEs are proposed. These principles and strategies can be applied to other organic electrolytes such as PCEs, COFEs, and MOFEs for enhancing their ionic conductivity and achieving high-safety LIBs.

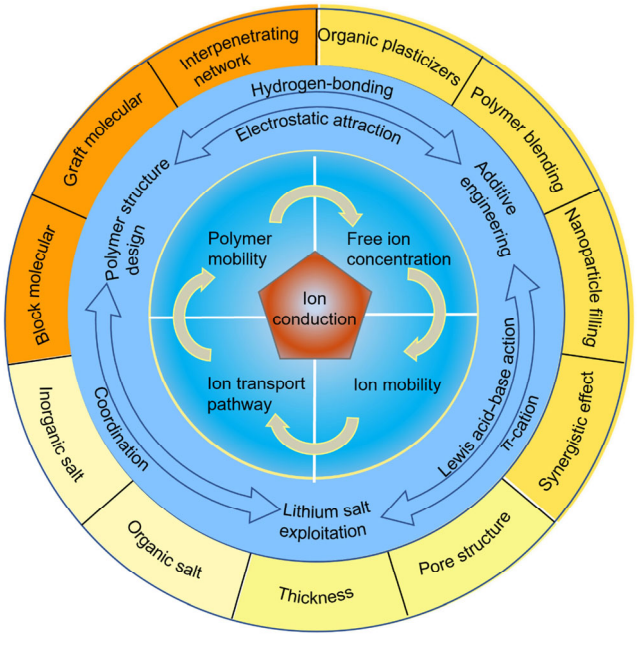

Figure 1 Modification strategies of solid polymer electrolytes for enhanced ion conductance.

2 Ion conduction mechanisms of solid polymer electrolytes

As one of the most important properties of SPEs, the ionic conductivity exerts a direct and critical impact on the impedance, cycle characteristics, and rate performance of the solid-state batteries. Exploring the ion conduction mechanism of polymer electrolytes is the basis for designing high-conductivity electrolytes for high-performance solid-state batteries. As the research moves along, researchers have developed a variety of ion conduction theories and models of the SPEs, and especially the ion conduction mechanisms of the composite polymer electrolytes (CPEs) have aroused more and more attention. In polymer electrolytes, Li^+ mainly transports through the mechanisms such as polymer segment migration and ion hopping. In this section, we summarized the ion conduction models such as Vogel–Tamman–Fulcher (VTF), Arrhenius, and free volume and meanwhile the factors determining the ion transport behaviors, which would guide the design and preparation of high-ion-conductivity polymer electrolytes.

2.1 Polymer segment migration model

In SPEs, there are two different phases, i.e., the crystalline phase and the amorphous phase, in which the lithium salt

dissociates in the polymer matrices and the Li^+ coordinated polymer macromolecules form an ionically conductive phase. The ion transport in the amorphous phase is usually regarded via the polymer segment migration model. For example, in PEO-based electrolytes, the ether oxygen atoms on the polymer backbone coordinate with Li^+ (Fig. 2) [27]. Specifically, in the amorphous region, the polymer molecules perform local segmental motion, and Li^+ migrates from one coordination point to another coordination point along the polymer chain, or from one chain to another chain. Under an electrical field, continuous coordination–decoordination–coordination behaviors result in long-range ion transport [28]. Therefore, both the amount of free Li^+ and the mobility of the polymer segments have important effects on the transport capability of Li^+ in the SPEs. In the past few years, scientists have carried out a lot of researches and established different models based on this ion conduction mechanism. According to the ion conduction models, we can do directional research about the methods to improve the ionic conductivity.

The degree of dissolution and dissociation of the lithium salts will affect the amount of the migrating Li^+. According to the Lewis acid–base properties, the polymers should coordinate with Li^+ to increase the dissociation degree of the lithium salts. Thus, a few polar groups such as –O–, C=O, –N–, –S–, and C=N are usually introduced into the polymer matrices [29]. In order to facilitate the dissociation of the lithium salts in the polymer hosts, the lithium salts should have low lattice energy and the polymers should have high dielectric constant [30]. The ionic conductivity (σ) of the polymer electrolytes can be expressed as follows [31]

$$\sigma = \sum n_i q_i \mu_i \quad (1)$$

in this formula, n_i is the concentration of carriers, q_i is the charge number of the mobile ions, and μ_i is the mobility of the carriers. It can be seen from this formula that, for a certain ion species, the charge q_i is fixed, then the ionic conductivity is proportional to the number of mobile ions and the ion mobility. Therefore, facilitating the dissociation of the lithium salts with large-size anions and decreasing the polymer crystallinity can increase the concentration and mobility of the carriers (include cations and anions) for high ionic conductivity, respectively. It should be mentioned that the strong interaction (or coordination) between the polar groups of the polymers and the cations can promote the dissolution/dissociation of the lithium salts and meanwhile impede the movement of the cations [32], and thus it is necessary to control the interaction between the polymer matrices and the cations. For instance, PEO (–CH_2CH_2O–) is considered as a better solvent for Li salts than either –CH_2O– or –$CH_2CH_2CH_2O$–. In the ion conduction

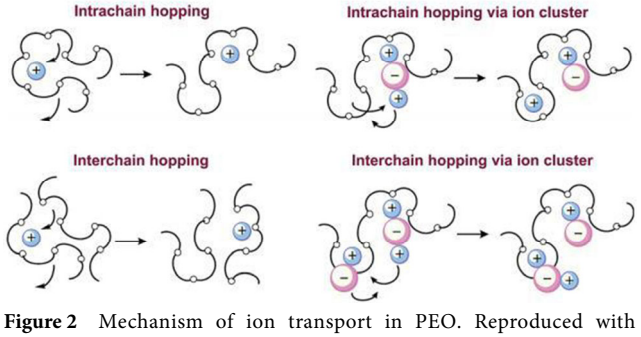

Figure 2 Mechanism of ion transport in PEO. Reproduced with permission from Ref. [27], © The Royal Society of Chemistry 2015.

model, the anion carriers also move fast in the electrical field condition, which usually causes the low Li^+ transference number.

2.2 Vogel–Tamman–Fulcher model

In addition to the above-mentioned ionic conductivity in Eq. (1) regarding the polymer segment migration, the ionic conductivity relationship also satisfies the VTF equation [28]

$$\sigma = AT^{0.5} e^{\frac{-E_a}{K(T-T_0)}} \quad (2)$$

in the formula, A is the pre-exponential factor, E_a is the apparent activation energy, K is a constant, T is the ambient temperature, and T_0 is the ideal glass transition temperature. It is generally considered that T_0 is 50 K lower than the glass transition temperature (T_g). The VTF equation reveals that the transport of Li^+ is related to the segmental motion of the polymer chains. In SPEs, Li^+ migration generally only occurs in the amorphous region above T_g. Polymers with lower T_g have stronger segment mobility, which can promote the ion migration to increase the ionic conductivity [33]. One of the reasons that PEO is the most intensively investigated polymer conductor by far is the relatively low T_g of −60 to −50 °C compared to many other polymers. There are two main ways to reduce the T_g: One is to graft, copolymerize, or crosslink with different polymer molecules, and the other is to add plasticizers or nanofillers into the polymer matrices. The VTF equation also shows that reducing the activation energy can increase the ionic conductivity, and reducing the cross-linking degree of the polymer chains and rejecting high concentrations of the lithium salts are helpful for the fast ion conduction [34]. The high lithium salt concentration may increase the possible charge carrier number, but this would create physical crosslinks between the polymer chains in the system, and thus result in the increase of the activation energy for the main-chain bond rotations, the reduction of the polymer segmental mobility, and the increase of the T_g [35].

2.3 Ionic hopping model

The initial research on the ionic hopping is mainly in inorganic solid-state electrolytes, where Li^+ can diffuse through the vacancy defects and gap sites in the crystals. Therefore, in inorganic electrolytes, the concentration and distribution of the point defects mainly affect the ionic conductivity [36]. Meanwhile, high-temperature sintering is usually adopted to reduce the grain boundary for high ionic conductivity [37]. Actually, most of the SPEs have two different areas, i.e., the amorphous regions and the crystalline regions.

In the abovementioned sections, we have discussed the ion conduction mechanisms in the amorphous regions of the polymer electrolytes. In the crystalline regions, the polymer chains can form pipes by folding and stacking, and Li^+ conducts through the vacancy diffusion in the polymer pipes, similar to the ion hopping in the inorganic electrolytes. Bruce et al. [38, 39] proposed the ion conduction process of $LiAsF_6$ in PEO. When the molar ratio of [EO]:[Li^+] = 6:1 (EO: ethylene oxide), two PEO chains would fold into a double helical tube, forming a cylindrical channel (Fig. 3). Li^+ can migrate along the cylindrical channel, and the anion is outside the cylindrical channel. This double helix structure facilitates the migration of lithium ions and enables the electrolyte to have higher ionic conductivity. They believe that the transport of Li^+ in the crystal part has

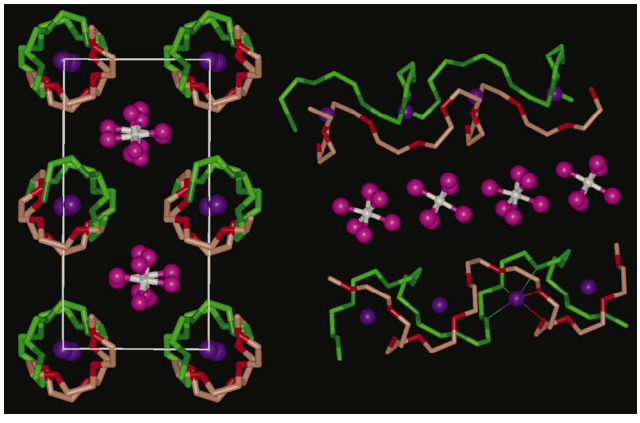

Figure 3 Li^+ hopping over the spiral channels in the static ordered crystalline structure. Reproduced with permission from Ref. [39], © Macmillan Magazines Ltd. 2001.

nothing to do with the chain segment movement, but relies on the hopping of the ions between the helical channels, and the electrolytes with the ordered crystal structure have higher ionic conductivity. Although recent studies have demonstrated the existence of the Li^+ conduction in the polymer crystals with the ordered structures, the ion conduction mechanism needs to be further clarified with more experimental evidences. It is believed that the ion hopping is accompanied by the relaxation, respiration, or segmental motion of the polymer chains, and the ions move along the polymer chains to finally jump from one chain to another chain [40–42]. However, due to the influence of the channel structure, inter-ion Coulomb force, crystalline region, etc., Li^+ moves much slower in the crystalline regions than in the amorphous regions. Therefore, the main strategy to improve the ionic conductivity of polymer electrolytes is still relied on the formation of the amorphous polymer phases.

2.4 Arrhenius model

The Arrhenius equation can be used to describe to the ion hopping as follows [41]

$$\sigma = \frac{A}{T} e^{\frac{-E_a}{RT}} \quad (3)$$

where σ is the ionic conductivity, A is the pre-exponential factor, T is the ambient temperature, E_a is the apparent activation energy, and R is the ideal constant. It can be seen from the equation that the increase of the temperature and the decrease of the activation energy can both greatly increase the ionic conductivity. The motion amplitude and frequency of the polymer backbone and side chains would also increase with the increase of the temperature, and the coordination becomes tighter [40]. The segmental motion of the amorphous polymer would be completely decoupled from the motion of the ions, and the ions need less energy to jump from one site to another.

Baskaran et al. [43] prepared a PVAc-$LiClO_4$ electrolyte and found that the ionic conductivity–temperature change relationship abided by the Arrhenius equation (Fig. 4(a)). It can be seen that there is no sudden change in the ionic conductivity with the increase of temperature from 30 to 100 °C. Li^+ transports within the crystalline regions through the ion jumping in adjacent vacancies. As the temperature increases, the viscosity of the polymer chains decreases, and the increase of the amorphous regions would bring more free volume for the ion transport. Furtherly, Mindemark et al. [35] summarized a diagram to compare the Arrhenius equation and VTF equation (Fig. 4(b)), and proposed that in SPEs, in addition to the common VTF model, some SPEs may have Arrhenius behavior at low and even high temperatures. The line (i) in Fig. 4(b) represents the typical Arrhenius model, which often appears in high-crystallinity rigid solid systems, such as PEO-$LiAsF_6$ [44], PEO-Li_6PS_5Cl [45], ZIF electrolyte [46], and ceramic electrolyte [47, 48]. The line (ii) in Fig. 4(b) represents the typical VTF model, which often appears in low-crystallinity polymer or amorphous conditions, such as crosslinked poly(tetrahydrofuran) (xPTHF) electrolyte [49] and polyhedral oligomeric silsesquioxane ionic liquids (POSS-ILs) [50]. The line (iii) in Fig. 4(b) represents typical semi-crystallinity polymers, such as the most commonly-used PEO, which has high crystallinity at low temperature, and gradually becomes a molten state with the temperature increasing, showing the VFT behavior [51–53]. The line (iv) in Fig. 4(b) represents a solid–solid phase transformation behavior at the turning point during the heating process. The electrolyte keeps crystalline phase whenever before and after the turning point, which is consistent with Arrhenius behavior. Bruce et al. [44] prepared a PEO_8-$NaAsF_6$ electrolyte, and the turning point was ~ 25 °C. The E_a values in the high and low temperature

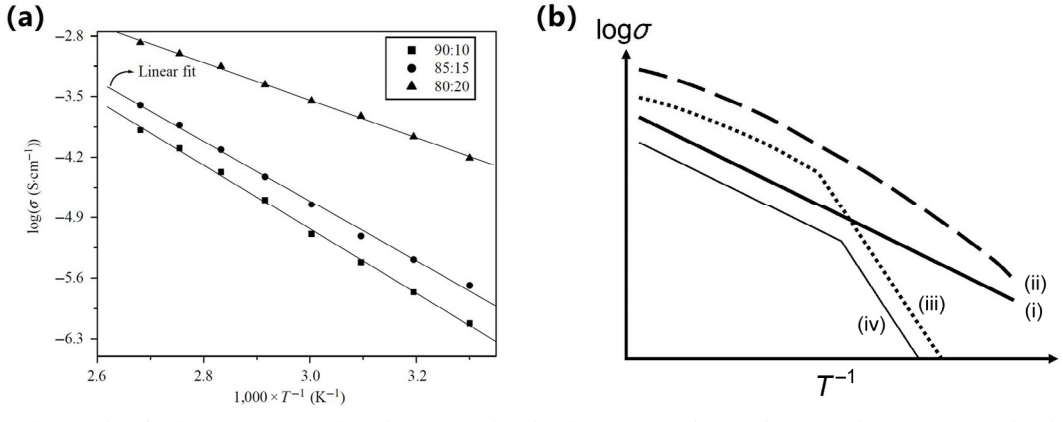

Figure 4 (a) Arrhenius plots for the PVAc:$LiClO_4$ electrolytes. Reproduced with permission from Ref. [43], © Elsevier Ltd 2006. (b) Ideal conductivity and temperature relationships ((i) ionic conductivity satisfying the Arrhenius equation; (ii) ionic conductivity satisfying the VTF equation in amorphous state; (iii) ionic conductivity satisfying the VTF equation in semi-crystalline state; and (iv) solid–solid phase transition occurs in crystal system). Reproduced with permission from Ref. [35], © Elsevier B.V. 2018.

regions were 44 and 291 kJ·mol^{-1}, respectively, so the Arrhenius line showed a smaller slope at the higher temperature region.

2.5 Free volume model

The vibration of the molecular chains in the polymer electrolytes can result in the change of the space near the molecular chains, thus creating voids and forming free volumes. The molecular weight, end groups, temperature, and lithium salts of polymer electrolytes have influence on the free volume [40, 54]. The free volume model emphasizes that the size of the free volume affects the ion migration and the ionic conductivity of the electrolytes. Someone has linked the free volume with the polymer segment motion, and concluded that more free volume can facilitate the mobility of the polymer segments. Bouchet et al. [55] found that the end group and the segment mobility can affect the free volume size, specifically the polymers with –OH end have stronger interaction with the ions than those with the $-CH_3$ end and thus cause the transient crosslinking, less free volume, and lower ionic conductivity.

Yahsi et al. [56] used positron annihilation lifetime spectroscopy and Simha–Somcynsky hole theory to study the effect of the lithium salt content and temperature on the free volume size and fraction. It is disclosed that the free volume (or ortho-positronium lifetime) increases linearly with the temperature, and the free volume fraction also changes with the lithium salt content (Figs. 5(a) and 5(b)). The authors also believe that a small increase in the lithium salt content can make the polymer change from an ordered state to a disordered state, and that an increase of the temperature can promote the structural expansion of the free volume and thus an increase of the ortho-positronium lifetime. The logarithm of the ionic conductivity is approximately linearly related to the inverse of the free volume fraction (Fig. 5(c))

$$\ln\sigma = \ln\sigma^{*} + \frac{\beta}{f_v} \tag{4}$$

where f_v is the free volume fraction, σ^{*} is the ionic conductivity at the highest free volume fraction, and β is the activation coefficient of the thermal free volume fraction.

As we have mentioned above, the temperature has an important impact on the free volume. Specifically, as the temperature increases, the polymer segment vibration ability would strengthen to overcome the potential barriers between the sites, and then the expansion would generate more free volume to facilitate the mobility of the polymer segments, Li^{+}, or solvated molecules. Therefore, the increase of the ionic conductivity actually can be also attributed to the improvement on the polymer segmental mobility and the ion hopping ability.

2.6 Williams–Landel–Ferry (WLF) model

Williams et al. [57] modified the VTF equation considering the influence of the polymer viscosity and the relaxation process of the chain segments, and then deduced the Williams–Landel–Ferry equation

$$\log a_T = \left[\frac{-C_1(T-T_s)}{C_2+(T-T_s)}\right] \tag{5}$$

where a_T is the displacement factor, which represents the ratio of the relaxation time of the chain segments, and T_s is the reference temperature, usually represented by T_g. C_1 and C_2 are constants, which are related to the value of T_s. When T_s is represented by T_g, C_1 and C_2 are 17.44 and 51.60, respectively. The WLF equation further proves that the ion transport in the polymer electrolytes is influenced by the free volume, and the micro-Brownian motion of the chain segments has an important impact on the ion transport in the amorphous regions [58].

Gomes et al. [59] studied the functional crosslinking electrolytes of polyurethane with different molecular weights of PEO, and found that WLF and Arrhenius, two different types of ion conduction mechanisms can appear for the SPEs. When the network size is large, the conductivity of the PEO_{2000} and PEO_{1000} based electrolytes varies with temperature in accordance with the WLF model, showing a curve trend change and following the free volume theory. The differential scanning calorimetry (DSC) curve shows that the conduction of the electrolytes mainly depends on the conduction of amorphous regions [60]. When the molecular weight decreases and the content of LiTFSI increases, the interaction between lithium, PEO, and polyurethane occurs, the cross-linking concentration increases, the crystalline state occupies the main body, and the local mobility decreases. Moreover, the LiTFSI lattice energy is lower and the dissociation degree is larger, but the anion volume is larger, so the energy required for the anion movement cannot be ignored, and there is less free volume space available for the charge movement. Therefore, the conductivity and temperature relationship of the PEO_{600}-LiTFSI electrolyte conforms to the Arrhenius

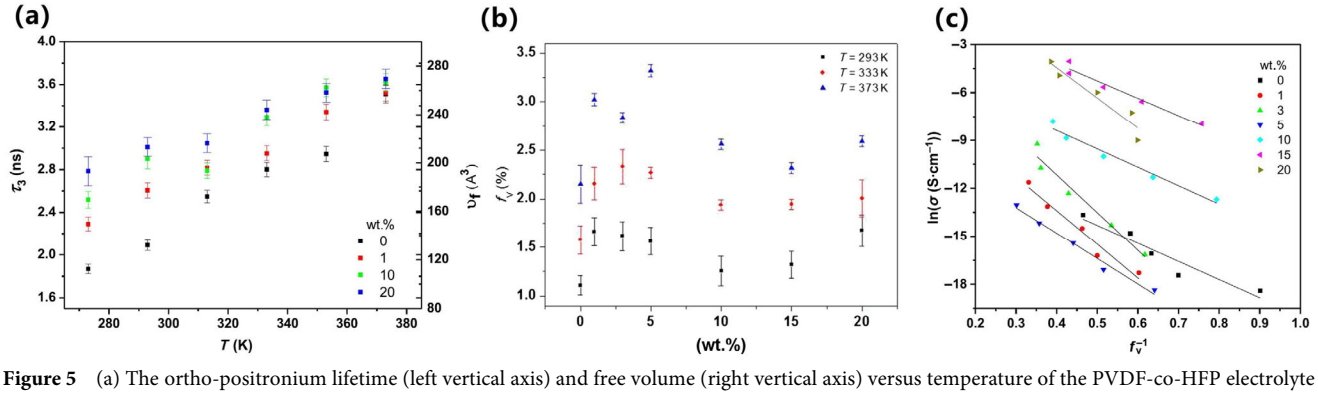

Figure 5 (a) The ortho-positronium lifetime (left vertical axis) and free volume (right vertical axis) versus temperature of the PVDF-co-HFP electrolyte with different weight percentages of $LiClO_4$, (b) the free volume fraction versus weight percentages of $LiClO_4$ added to PVDF-co-HFP, and (c) the logarithmic conductivity versus the inverse of the free volume fraction operated at 1 kHz. Reproduced with permission from Ref. [56], © Informa UK Limited, trading as Taylor & Francis Group 2018.

equation, and the ion movement of the low-molecular-weight system conforms to the ion hopping mechanism.

2.7 Interfacial ion conduction mechanism

In the 1970s, Liang et al. [61] investigated the conduction characteristics of the polycrystalline lithium iodide (LiI) containing aluminum oxide (Al_2O_3), and found that the addition of the Al_2O_3 powders into the LiI phase can effectively increase the ionic conductivity. Surprisingly, the LiI electrolyte containing 33 mol%–45 mol% Al_2O_3 exhibited ionic conductivities in the order of 10^{-5} S·cm^{-1} at 25 °C, which was two orders that of the pristine LiI (10^{-7} S·cm^{-1}). However, they did not realize that the increase of the conductivity was attributed to the LiI/Al_2O_3 interface. In the 1980s, Phipps et al. identified the grain boundaries and LiI–ceramic interfaces as regions of extremely rapid ion transport [62]. They also analyzed the temperature-dependent ionic conductivities of two samples (a LiI sample sandwiched between two fused silica plates and a LiI film deposited on a silica plate), and further confirmed the existence of an LiI/SiO_2 interfacial conduction pathway possessing a high ionic conductivity of ~ 5 S·cm^{-1} at 25 °C, which was much higher than the pristine LiI bulk (~ 10^{-7} S·cm^{-1}). As predicted, the enthalpy of the ion migration along the interface (0.15 eV) was less than the bulk value (0.39 eV). They also proposed that the lattice strain energy associated with a jump from one lattice site to another was identified as the primary contribution to the energy of migration, and the lattice distortion at the microstructural imperfection (i.e., the interfaces) reduced the strain energy associated with ionic transport and led to the greater ion mobility along the interfaces than in the bulk. Someone attributed the enhanced ionic conductivity along the interfaces between the conducting matrices and the dispersant particles to the formation of space-charge layers [63]. Researchers also find that the ionic conductivity of the electrolytes changed with the additive (or dispersant) content. In general, the ionic conductivity shows a marked initial increase with the dispersant concentration, followed by a rapid drop, which seems to extrapolate to zero at some threshold concentration [64]. A percolation theory was then applied to explain this phenomenon.

Recently, different CPEs have been prepared by adding inorganic/organic nanoparticles in the polymer electrolytes to improve the overall properties. It is well accepted that there are three phases in the CPEs, i.e., the nanoparticle, nanoparticle/polymer–Li salt interface (or on the nanofiller surface), and polymer-Li salt regions, and Li^+ transports in these phases at different speeds [65–69]. A few researchers have found that the increase of the ionic conductivity (especially for the inert nanoparticle-containing CPEs) is mainly attributed to the generation of fast-ion pathways at the polymer matrix/nanoparticle interfaces (or on the nanofiller surface) by solid-state nuclear magnetic resonance (ssNMR) measurements. Even in a few active nanoparticle-filled CPEs, the Li^+ ions mostly transport on the surfaces of the inorganic electrolyte particles (e.g., $Li_7La_3Zr_2O_{12}$ (LLZO) [70], $Li_{3/8}Sr_{7/16}Ta_{3/4}Zr_{1/4}O_3$ [71], and $Li_{10}GeP_2S_{12}$ [72]). Numerical analyses (e.g., Comsol Multiphysics) also reveal that the interfacial ionic conductivities of the $Li_{0.33}La_{0.557}TiO_3$ nanowire (1.3×10^{-2} S·cm^{-1} at 30 °C) [65] and $Li_{1.3}Al_{0.3}Ti_{1.7}(PO_4)_3$ (LATP) nanoparticle (2.0×10^{-4} S·cm^{-1} at 20 °C) [69] filled CPEs are much higher than the active nanofillers and comparable to the ionic conductivity of the organic liquid electrolytes. The famous Lewis acid–base theory has also been applied to explain the fast-ion transport pathways at the interfacial regions. Someone has ascribed the high ionic conductivity at the interfaces to the fast polymer segment and ion motion and the high free ion concentration [73]. The molecular dynamics research on a TiO_2 nanoparticle-filled PEO/$LiBF_4$ electrolyte discloses that the TiO_2 nanoparticles are surrounded with three different layers: The first layer of ~ 0.5–0.6 nm in thickness has slower ion mobility of an order of magnitude than the PEO/$LiBF_4$ bulk, the second layer of ~ 0.5–1.5 nm in thickness has the elevated concentrations of the cations and anions, and the third layer beyond 1.5 nm is not affected by the TiO_2 nanoparticles; however, the addition of the nanoparticles with soft-repulsion interactions with PEO leads to the formation of a PEO interfacial layer with reduced PEO density, increased ion concentration, and strengthened PEO and ion mobility [74].

Later, Chen et al. [75] prepared a PAN-$LiClO_4$ electrolyte by an electrospinning method and then discovered the ion conduction mechanism at the polymer/polymer interfaces. The electrospun PAN-$LiClO_4$ electrolyte film had an ionic conductivity of 2.9×10^{-4} S·cm^{-1}, which was much higher than that of the blade-cast PAN-$LiClO_4$ electrolyte film (10^{-7}–10^{-6} S·cm^{-1}) at room temperature (Fig. 6(a)). It was found that the electrospun electrolyte had plenty of polymer/polymer interfaces (specific interface area: ~ 105 cm^{-1}), which was not found in the blade-cast sample, indicating that the high ionic conductivity of the electrospun electrolyte should be attributed to the polymer/polymer interfacial conduction. High-angle annular dark-field scanning transmission electron microscopy (HAADF-STEM) (Figs. 6(b) and 6(d)–6(f)) and electron energy loss spectroscopy (EELS) mapping (Fig. 6(g)) results showed the preferable accumulation of chemically distinctive lithium at the polymer/polymer interfaces. The ^{6}Li NMR measurements (Fig. 6(c)) further disclosed that the blade-cast PAN-$LiClO_4$ electrolyte had a single peak at a chemical shift of −1.45 ppm corresponding to the Li in the bulk of PAN, while the electrospun PAN/$LiClO_4$ sample had a single peak with a distinctive chemical shift of −0.48 ppm. This peak was assigned to the Li at the PAN/PAN interfaces, which was consistent with the predominate location of Li at the PAN/PAN interfaces in the sample as evidenced by STEM-EELS (Figs. 6(d)–6(g)). They also attributed the high ionic conductivity of the electrolyte to the continuous PAN/PAN interfaces generated by the electrospinning method.

2.8 Remarks

As one of the most important properties of SPEs, ionic conductivity has a direct and crucial impact on the battery performance. There are a few famous models to explain the ion conduction mechanism in the polymer electrolytes, such as the polymer segment migration, ionic hopping, free volume, and interfacial ion conduction, which can be utilized to better guide the design and preparation of high-conductivity polymer electrolytes. The polymer electrolytes are usually semi-crystalline below their melting points, and there are two different phases in the electrolytes, i.e., the crystalline phase and amorphous region. Of course, the lithium salts in the polymer electrolytes are also in form of crystal if they are not dissolved/dissociated by the polymers. To increase the free ion concentration for high ionic conductivity, it is better to choose lithium salts with large anion sizes and polymer hosts with

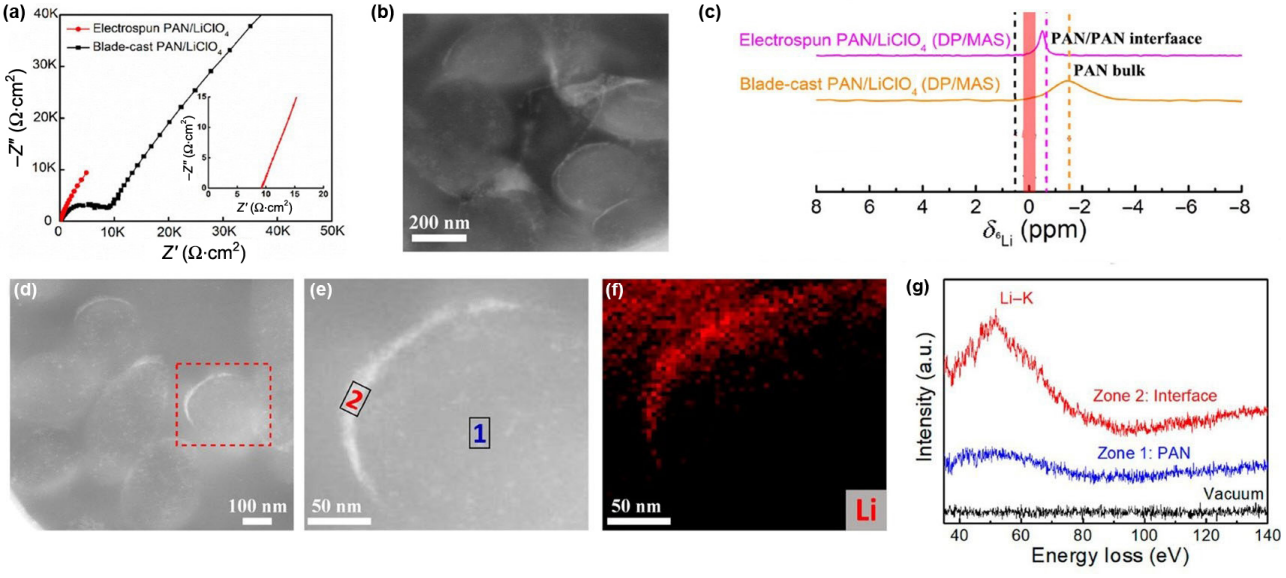

Figure 6 (a) Nyquist plots of the electrospun and blade-cast PAN-$LiClO_4$ samples with a $[Li^+]/[-CN]$ ratio of ~ 1:10 at 25 °C, (b) HAADF-STEM image of the electrospun PAN-$LiClO_4$ microtome slice, (c) ^6Li MAS NMR spectra of the electrospun and blade-cast PAN-$LiClO_4$ electrolytes, (d)–(f) HAADF-TEM images of the electrospun PAN/$LiClO_4$ and the corresponding EELS element concentration map of Li (brightness of the colors represents the relative molar concentration of the mapping element), and (g) EELS spectra integrated from the selected areas of the organic particle phase and the organic/organic interface. Reproduced with permission from Ref. [75], © American Chemical Society 2020.

high dielectric constants. Similar to the ion conduction in the inorganic solid-state electrolytes, the SPEs in highly crystalline condition with the ordered structures also follow the Arrhenius equation, and the ionic conductivity has a linear relationship with the temperature change. The Li^+ movement is not generated by the movement of the polymer chain segments but by the hopping in the nearest vacancies. However, the ion hopping in the crystalline phases is much slower than in the amorphous phases and more experimental evidence is needed to verify the ionic hopping model. Thus, reducing the polymer crystallinity seems to be an important way to increase the ionic conductivity.

Except the ionic hopping model, the polymer segment motion has paid special attention in other ionic conduction models. According to the equation of $\sigma = \Sigma n_i q_i \mu_i$, the increase of the polymer chain mobility can improve the ionic conductivity by strengthening the carrier mobility, and it is necessary to control the interaction between the polymers and the lithium salts to ensure the high concentration and mobility of the free ions. The VTF model reveals that the ion conduction mainly depends on the migration movement of the chain segment in the amorphous region above T_g, and the ionic conductivity has a nonlinear relationship with the temperature. The WLF model further considers the influence of the polymer viscosity and the relaxation process of the chain segments. Decreasing the T_g is another effective way to increase the mobility of the polymer segments for high ionic conductivity. The ions can easily move in the space offered by the free volume of the polymers and migrate between the coordination sites along the polymer chains above the T_g. The free volume, VTF, and WLF models also emphasize the importance of the free volume and the ambient temperature, and the increase of the temperature can greatly change the free volume size/fraction and the crystallinity, but it is not impractical to increase the working temperature of the solid-state LIBs for the fast ion conduction.

The interfacial ion conduction model offers another important route to achieving high ionic conductivity. Although the interfacial ion conduction mechanism was firstly discovered at the LiI/oxide interfaces, it is widely applied in the polymer electrolyte modification field. The fast-ion pathways at the nanoparticle/polymer and polymer/polymer interfaces in the nanoparticle-filled CPEs have been verified by the numerical analyses and the advanced characterization techniques such as ssNMR and EELS, but deep investigation on the ion conduction mechanism at the interfaces is still required. The construction of abundant and continuous fast-ion pathways parallel to the electrical direction would greatly enhance the ionic conductivity of the electrolytes. It should also be mentioned that the anion motion needs more attention, because it has an important influence on the battery performance such as the polarization and metal dendrites. The advantages of the Lewis acid–base interaction or the electrostatic interaction between the additives and the anions provide a feasible way to increase the Li^+ transference number without sacrificing the high ionic conductivity.

3 Modification strategies of solid polymer electrolytes

3.1 Copolymer molecule structure design

SPEs are usually composed of two parts: One is a polymer matrix as a host, and the other is a lithium salt as an ion provider. Generally, the polymer matrix has a low glass transition temperature, which can facilitate the movement of the segment chains in the amorphous phases. Up till now, PEO has long been regarded as one of the most reliable polymer matrices since it was firstly reported by Wright et al. in 1973. The main reason for making PEO irreplaceable is based on its merits, such as the suitable complexation ability with lithium ions, the electrochemical stability against lithium metals, high flexibility, and low cost [76–78].

The lithium ion transportation in the PEO-based SPEs is through the complexation and dissociation with the ethylene oxide units. On one hand, the ether oxygen atoms in the EO chains can interact with different alkali metal cations such as lithium ions, and thus PEO has an extremely strong dissociating property for a wide variety of salts. On the other hand, the excellent chain flexibility and segmental motion ability of the EO segments ensure the fast movement of the metal ions [79]. The ionic conductivity of the pristine PEO-based SPEs usually can be divided into two segments in a wide temperature range. The ionic conductivity in the first segment is extremely low (10^{-8}–10^{-7} S·cm^{-1}), because of the high PEO crystallization degree at the temperatures below the melting point of PEO (~ 65 °C) [77]. When the temperature is close to the melting point, the aggregation of PEO changes from crystalline to almost amorphous, and the ionic conductivity rapidly increases with the temperature and finally keeps constant. Thus, the practical application of the PEO-based electrolytes is severely hindered by the low room-temperature ionic conductivity, and it is necessary to exploit novel polymer matrices with lower crystallinity degree for high-conductivity polymer electrolytes. The degree of crystallinity can be measured by differential scanning calorimetry, X-ray diffraction (XRD), and nuclear magnetic resonance.

3.1.1 *Block molecular design*

To reduce the crystallization degree or the glass-transition temperature (T_g) for higher polymer chain movement ability, the ethylene oxide groups in PEO are usually combined with other polymer segments to construct block, star, and cross-linking polymers as matrices for the polymer electrolytes (Table 1). For the block polymer electrolytes, the diblock- and triblock-based polymers are usually synthesized by copolymerization and widely investigated. David et al. [80] synthesized PEO$_x$- polycarbonate (PC) copolymers using PEO and PC as the precursors by copolymerization. The optimum SPEs (PEO$_{34}$-PC) with the lowest glass-transition temperature of −48 °C had the highest ionic conductivity of 3.7×10^{-5} S·cm^{-1} at room temperature. The T_g of the PEO$_x$-PC copolymer-based SPE also decreased with the increase of the LiTFSI content (up to 30 wt.%). Vidal's group [81] found that the oligomer poly, PPO-PEO-PPO (POP: propylene oxide), based triblock polymer electrolyte showed a highly compliant to Arrhenius model, which is beneficial to the improvement on the ionic conductivity of the PEO-based SPE (Figs. 7(a) and 7(c)–7(f)). PPO can easily lead to an amorphous macromolecular structure, because of the randomly-distributed methyl groups, which greatly boosted the short-range conduction of Li^+. In addition, the synthesized electrolytes were fully amorphous without any endotherm of melting, which is beneficial to the ion conduction (Fig. 7(b)). Xie et al. [82] reported a nanophase-separated elastic epoxy composite electrolyte with the high ionic conductivity of 3.5×10^{-4} S·cm^{-1} at 25 °C. The T_g showed no significant change with the PC increasing, and PC might form percolated Li^+ transport pathways. This elastic epoxy polymer electrolyte was composed of the hard bisphenol A diglycidyl ether segments and the soft poly (propylene glycol) segments, which can both enhance the mechanical properties and the ionic conductivity. Moreover, the molecular weight, molecular structure, and composition can be easily controlled. However, the process of the block copolymer is complicated and difficult to scale up for their practical application.

3.1.2 *Graft molecular design*

In general, polymers with simple, ordered, and symmetrical molecule structure exhibit high crystallinity. The block copolymer-based electrolytes usually show lower ionic conductivity at room temperature, because of the inferior polymer segment migration ability of the hard polymer segments. In contrast, synthesizing graft or star copolymers by grafting short PEO side chains on more flexible backbones is a more effective way to inhibit the PEO crystallization and enhance the segmental mobility of the PEO chains for increasing the ionic conductivity. Zhang et al. [83] designed a super soft polymer matrix with the side chains of ethylene oxide and propylene oxide units. The SPE was fully amorphous at room temperature, and showed a much higher ionic conductivity of 2×10^{-4} S·cm^{-1} at 40 °C. Chen et al. [84] designed novel quasi-solid star brush block copolymer electrolytes (SBBCEs), which had the 2-arm star polymer of [poly [poly (ethylene glycol) methyl ether acrylate]-b-polystyrene]$_2$ ((PPEGMEA-b-PS)$_2$) with a crosslinking structure (Fig. 8(a)). This unique structure was beneficial to reduce the polymer crystallinity and dissolve lithium salts (Fig. 8(b)). Thus, the copolymer-based electrolyte showed a high ionic conductivity of 2.1×10^{-4} S·cm^{-1} at 28 °C (Fig. 8(c)). Simultaneously, the SBBCEs showed a slight decomposition at 5.6 V, and the significantly enhanced electrochemical stability of SBBCEs was attributed to the crosslinked structure and the affinity (Fig. 8(d)). Zhou et al. [85] designed a discotic liquid crystal-based six-arm star copolymer, in which the discotic liquid crystal was arranged along with the flexible arms of the copolymer as the ion

Table 1 Comparison of the copolymer-based electrolytes on the ionic conductivity

Modification strategy	Polymer matrix	Ionic conductivity (S·cm^{-1}, 25 °C)	Glass-transition temperature (T_g, °C)	References
Block	PEO$_x$-PC	3.7×10^{-4}	−48	[80]
Block	PPO-PEO-PPO	4.8×10^{-3} (100 °C)	−32–−21	[81]
Copolymer	eEPE (elastic epoxy polymer electrolyte)	3.5×10^{-4}	−50	[82]
Graft	Jeffamine-PO/EO	2.0×10^{-4} (40 °C)	−55	[83]
Star	[poly [poly (ethylene glycol) methyl ether acrylate]-b-polystyrene]$_2$	2.1×10^{-4} (28 °C)	−64	[84]
Star	DLC-((PS)$_{23}$-b-(PPEGMA)$_x$)$_6$	1.5×10^{-4} (30 °C)	−44	[85]
Crosslink	PE-PEO	2.0×10^{-4}	−65	[86]
Crosslink	3PPEGM-co-GMA	$> 10^{-5}$	−56	[87]

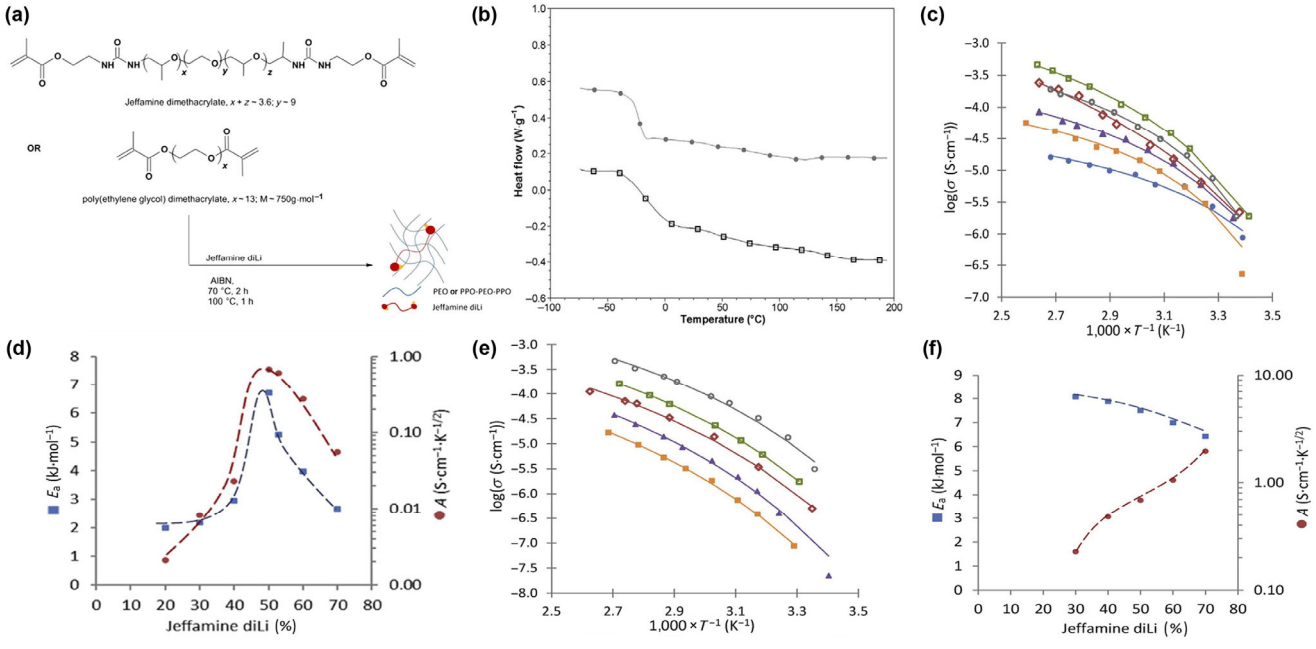

Figure 7 (a) Formation of semi-IPN based on Jeffamine diLi and PEO or PPO-PEO-PPO networks, and (b) typical DSC thermograms of (□) 60/40 PPO-PEO-PPO/Jeffamine diLi and (●) single PPO-PEO-PPO copolymer. Arrhenius plots of the ionic conductivity versus reciprocal temperature of PEO/Jeffamine dLi (c) and PPO-PEO-PPO/Jeffamine dLi (e). Semi-IPNs with network/Jeffamine dLI proportions of ●: 80/20; ■: 70/30; ▲: 60/40; ◇: 50/50; □: 40/60; and ○: 30/70. Solid lines correspond to VTF fit. (d) and (f) The corresponding VTF fit parameters E_a and A factor. Reproduced with permission from Ref. [81], © Elsevier Ltd. 2018.

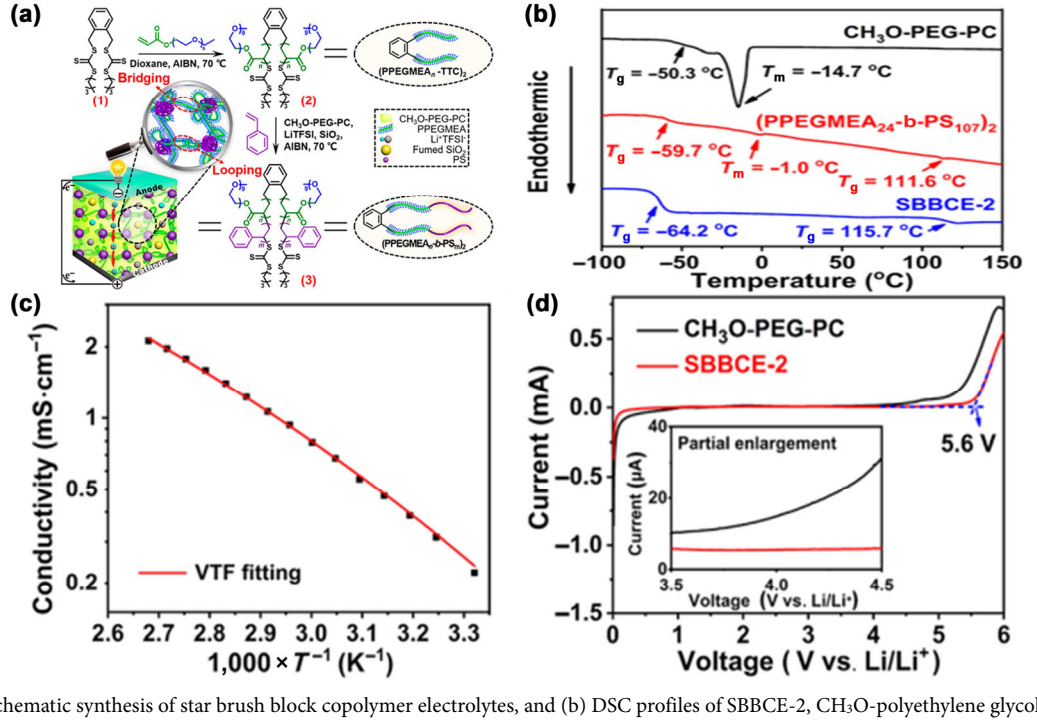

Figure 8 (a) Schematic synthesis of star brush block copolymer electrolytes, and (b) DSC profiles of SBBCE-2, CH_3O-polyethylene glycol (PEG)-PC, and the 2-arm star brush block copolymer of $(PPEGMEA\text{-}b\text{-}PS)_2$. (c) Temperature-dependent ionic conductivity of SBBCE-2, the plot represents the experimental data and the solid line represents VTF fitting results, and (d) Linear sweep voltammetry (LSV) curves of SBBCE-2 and CH_3O-PEG-PC and the enlarged plot of the LSV curves between 3.5 and 4.5 V (inset). Reproduced with permission from Ref. [84], © American Chemical Society 2019.

conduction pathways. The segmental motion ability of the polymer side chains was greater than that of the linear polymers, and thus the copolymer had larger free volume and lower glass transition temperature, and the copolymer-based electrolyte showed a high ionic conductivity of 1.46×10^{-4} S·cm^{-1} at 30 °C. Unfortunately, these copolymer electrolytes usually have a few defects, such as poor mechanical strength and thermal stability, which make them not suitable for the preparation of high-energy-density lithium batteries.

3.1.3 *Interpenetrating network design*

The ion transport across the grafted PEO side chains is not as efficient as that along the PEO backbone. In comparison, designing interpenetrating networks with soft molecules

(especially ethylene oxide units) could greatly reduce the crystalline domain and increase the ionic conductivity. It can also enhance the mechanical properties of the polymer electrolytes by the interconnected networks. Moreover, the interpenetrating networks have high flexibility and can result in the close contact between the polymer electrolytes and the electrode materials. Khurana et al. [86] reported a cross-linked PE/PEO SPE with a high ionic conductivity of 2.0×10^{-4} S·cm^{-1} at 25 °C, and the copolymer structure can also be adjusted by turning the PE and PEO segment lengths to suppress the PEO crystallinity. Dai et al. [87] reported a star-shape polymer of 3-armed poly(ethylene glycol) methyl ether methacrylate-co-glycidyl methacrylate copolymer (3PPEGM-co-GMA), and its ionic conductivity was higher than 10^{-5} S·cm^{-1} at room temperature. This star-shape polymer has an interpenetrating network, and was synthesized via a ring-opening polymerization technique (Figs. 9(a) and 9(b)). This star-shape polymer showed increased thermal stability (a single step decomposition temperature around 350 °C), which can be attributed to the formation of the interpenetrating network and the ester bonds in the polymer backbone. (Fig. 9(c)). The T_g changed with the different molar ratios of the epoxy and amino (Fig. 9(d)), and was also affected by the content of Li salts (Fig. 9(e)). It also had the merits of good processability and cost-effectiveness. However, it should be mentioned that it is difficult to choose ideal crosslinking initiators, and the undesirable by-products are detrimental to the other properties. Especially, the remained free radicals are harmful to the battery cycling performance.

3.1.4 Remarks

PEO is regarded as an important polymer matrix for solid polymer electrolytes; however, PEO-based solid-state electrolytes show relatively low ionic conductivity at room temperature, resulting in the higher battery operation temperatures. Integrating the ethylene oxide groups in other polymer segments (e.g., designing block, star, and cross-linking polymers) for the copolymer electrolytes is an effective strategy to increase the ionic conductivity. The copolymerization method is usually used to prepare the block copolymers as the polymer matrices to decrease the crystallinity for high-ion-conductivity electrolytes, but this method is too complicated to scale up. Constructing graft or star copolymers by grafting short PEO side chains on the more flexible backbones can also enhance the segmental mobility of the PEO chains, but the reduction of the mechanical strength greatly limits their practical applications. Designing cross-linking interpenetrating networks can not only reduce the crystalline domain but also enhance the mechanical properties of the polymer electrolytes. It should also be mentioned that the increase of the ionic conductivity should not sacrifice other properties such as the mechanical strength and the compatibility with the electrode materials, and it is necessary to develop ideal cross-linking initiators and design proper copolymer structures for comprehensively-improved SPEs.

3.2 Lithium salt exploitation

The electrolyte is used as the medium for the ion transmission between the positive and negative electrodes in the lithium batteries, and the lithium salt, as the provider of lithium ions in the polymer electrolyte (not the single-ion polymer electrolyte), is an indispensable part of the electrolyte and has an important impact on the battery performance such as capacity, applicable temperature, cycle capacity, and safety performance [88]. Although there are a lot of lithium salts, only a few types can be used in the polymer electrolyte (Table 2). Ideal lithium salts should meet the following requirements: (1) They should have excellent chemical, electrochemical, and thermal stabilities,

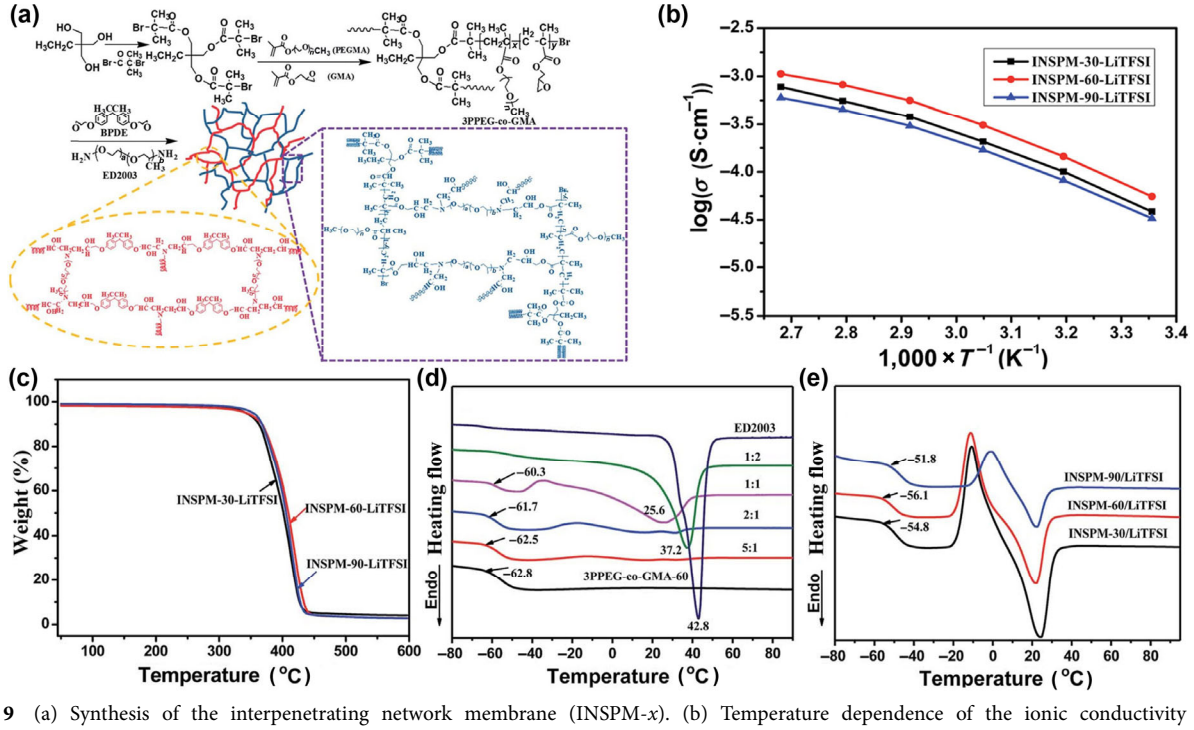

Figure 9 (a) Synthesis of the interpenetrating network membrane (INSPM-*x*). (b) Temperature dependence of the ionic conductivity of the INSPM–*x*/LiTFSI with [O]/[Li$^+$] = 16. (c) Thermogravimetric analysis (TGA) thermograms of INSPM-*x*-LiTFSI, and DSC curves of (d) cross-linking polymers based on 3PPEG-co-GMA-*x* and ED2003 (the molar ratio of the epoxy and amino is 5:1 ,2:1, 1:1, and 1:2), and of (e) INSPM-*x*/LiTFSI electrolytes. Reproduced with permission from Ref. [87], © Royal Society of Chemistry 2018.

Table 2 Properties of lithium salts and their effects on the electrolyte conductivity

Lithium salt	Properties	Polymer matrix	Ionic conductivity ($S \cdot cm^{-1}$, 25 °C)	References
$LiPF_6$	High solubility, form SEI film, low stability	Poly(trimethylene carbonate)	1.78×10^{-8}	[106]
		PEO	4.10×10^{-5}	[93]
$LiClO_4$	High solubility, high ionic conductivity, low cost, high oxidation ability	PEO	1.70×10^{-5} (20 °C)	[89]
		Pectin	5.15×10^{-5}	[107]
$LiAsF_6$	High chemical stability, no current collector corrosivity, As element is poisonous	Polyvinyl alcohol	5.10×10^{-4} (40 °C)	[94]
$LiBF_4$	High thermal stability, suitable for both high and low temperatures, low ionic conductivity	PAN	1.83×10^{-3}	[108]
LiTFSI	High ionic conductivity, high thermal stability, corrosive to current collectors	PVDF-HFP	1.82×10^{-3}	[109]
LiFSI	High ionic conductivity, high thermal stability, corrosive to current collectors	Poly-2,2-dimethoxypropylene carbonate	1.08×10^{-4} (30 °C)	[104]
LiBOB	High ionic conductivity, passivation of electrodes, low solubility	PEO	$> 10^{-5}$ (30 °C)	[105]
LiODFB	Form SEI film, no current collector corrosivity, good low-temperature performance, high cost	PVDF-HFP	2.51×10^{-4} (60 °C)	[110]

and especially do not react with other battery components within a wide potential range; (2) they can be easily solvated to release free lithium ions by the polymer molecules; (3) other characteristics such as low price, non-toxicity, and environmental friendliness [89–91]. The type and content of lithium salts have not only important effects on the film-forming properties of the solid polymer electrolyte, but also on the ionic conductivity and the interface stability between the solid electrolyte and the electrodes. A few low-molecular-weight lithium salts such as LiF and LiCl are not suitable for preparing electrolytes because of their low solubility in organic solvents. Some other lithium salts such as $LiAsF_6$ are also not proper salts because of the toxicity of the elements or compounds.

According to the element component and molecular structure of anions, lithium salts can be divided into inorganic salts and organic salts. At present, inorganic lithium salts are widely utilized in most of the electrolytes in commercial lithium-ion batteries. The inorganic lithium salts generally have the advantages of low cost, environmental friendliness, and are not easy to decompose at high potentials. The commonly-used inorganic lithium salts in solid polymer electrolytes include $LiPF_6$, $LiClO_4$, $LiBF_4$, and $LiAsF_6$, which have large complex anion groups for the solvation.

3.2.1 *Inorganic lithium salts*

$LiPF_6$ [92] is widely used in commercial non-aqueous liquid lithium-ion batteries, because of its comprehensive advantages such as good solubility ability in non-aqueous solvents, high ionic conductivity, excellent thermodynamic and chemical stability, and high electrochemical stability. It can form a dense and stable passivation film on the surface of the aluminum current collector to protect the aluminum current collector from corrosion. $LiPF_6$ also has a good solubilization effect in PC matrix. However, $LiPF_6$ is very sensitive to moisture and has poor thermal stability, which hinders its application [92]. Ibrahim et al. [93] added $LiPF_6$ to a PEO-based polymer to prepare a thin-film electrolyte by solution casting, and explored the impact of $LiPF_6$ on the ionic conductivity of the PEO-based electrolytes. Figures 10(a)–10(c) show the complex impedance plots of the $LiPF_6$-containing electrolytes with different concentrations at room temperature. With the salt concentration increasing, the high-frequency semicircle area gradually decreases, and the low-frequency peak gradually appears, which proves that the ions are charge carriers. As the salt concentration increases, the number and density of the mobile ion increase, and thus the conductivity of the electrolyte increases (Fig. 10(f)). The ionic conductivity of the 20 wt.% $LiPF_6$-containing electrolyte reaches 4.1×10^{-5} $S \cdot cm^{-1}$ (Fig. 10(d)). Not only that, PEO forms a complex with $LiPF_6$ (Fig. 10(g)), and the melting temperature of the electrolyte decreases with the increase of $LiPF_6$ concentration (Fig. 10(e)). XRD analysis also confirmed that with the addition of lithium salt, the intensity of the diffraction peaks greatly decreases, further indicating that the crystallinity of the salt-containing PEO gradually decreases (Fig. 10(h)).

$LiClO_4$ is also an important lithium salt for preparing solid polymer electrolytes, because of the following advantages: Firstly, it has high solubility in polymer matrices for obtaining high ionic conductivity; secondly, it has a wide electrochemical window; thirdly, its price is low. However, the chlorine element in $LiClO_4$ has the highest valence of +7 with a strong oxidizing ability, which is detrimental to the safety of the battery. Therefore, although $LiClO_4$ has many obvious advantages, it is only suitable for scientific research. Wang et al. [69] investigated the effects of $LiClO_4$ content or EO/Li ratio on the polymer matrix crystallinity and the glass-transition temperature (Fig. 11). It can be seen from Fig. 11(a) that the peaks of pure $LiClO_4$ move in the polymer electrolyte, which means that the lithium salt has been completely dissociated and has undergone a complexation reaction with PEO. Figures 11(b), 11(d), and 11(e) show that as the content of the lithium salt increases, the crystallinity, melting endotherm, and the glass-transition temperature of the composite electrolyte also decrease. The inhibitory effect of $LiClO_4$ on the polymer crystallinity was even more pronounced than that of $Li_{1.3}Al_{0.3}Ti_{1.7}(PO_4)_3$ nanoparticles. When the EO/Li ratio is 5, the nanocomposite is almost completely amorphous, suggesting that a large proportion of the polymer chains form complexes with Li^+ and the lithium salt is dissociated. Impedance measurements further show that the samples with low EO/Li ratios exhibit higher ionic conductivity, and the electrolyte with 10 wt.% LATP and EO/Li ratio of 5 has the highest conductivity of 1.71×10^{-4} $S \cdot cm^{-1}$ at 20 °C (Fig. 11(c)).

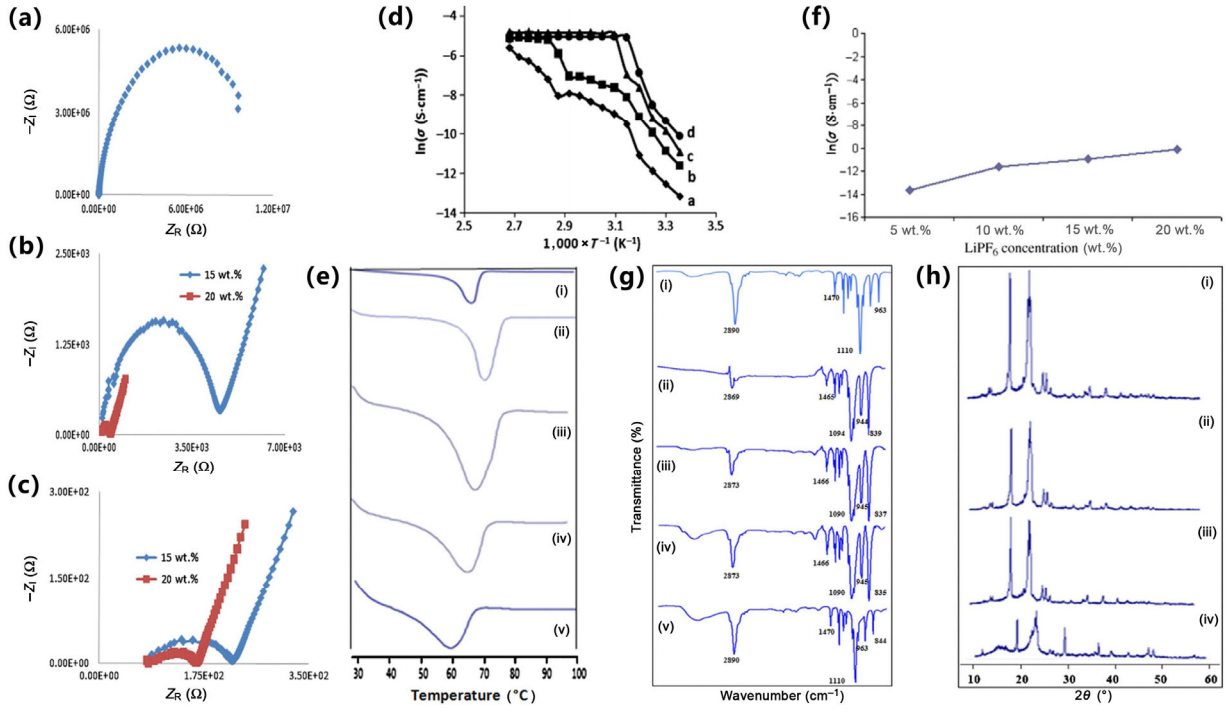

Figure 10 (a)–(c) Impedance plots of samples containing 0 wt.%, 15 wt.%, and 20 wt.% $LiPF_6$, (d) ionic conductivity of the electrolytes with various weight percents of $LiPF_6$ ((i): 5 wt.%, (ii): 10 wt.%, (iii):15 wt.%, and (iv): 20 wt.%), (e) DSC curves of the electrolytes with various weight percents of $LiPF_6$ ((i): 0 wt.%, (ii): 5 wt.%, (iii): 10 wt.%, (iv): 15 wt.%, and (v): 20 wt.%), (f) variation of the conductivity as a function of $LiPF_6$ content at room temperature, (g) FTIR spectra of the pure PEO and electrolytes with various weight percents of $LiPF_6$ ((i): 0 wt.%, (ii): 5 wt.%, (iii): 10 wt.%, (iv): 15 wt.%, and (v): 20 wt.%), and (h) XRD pattern of the electrolytes with various weight percents of $LiPF_6$ ((i): 0 wt.%, (ii): 5 wt.%, (iii): 10 wt.%, and (iv): 15 wt.%). Reproduced with permission from Ref. [93], © Springer-Verlag 2011.

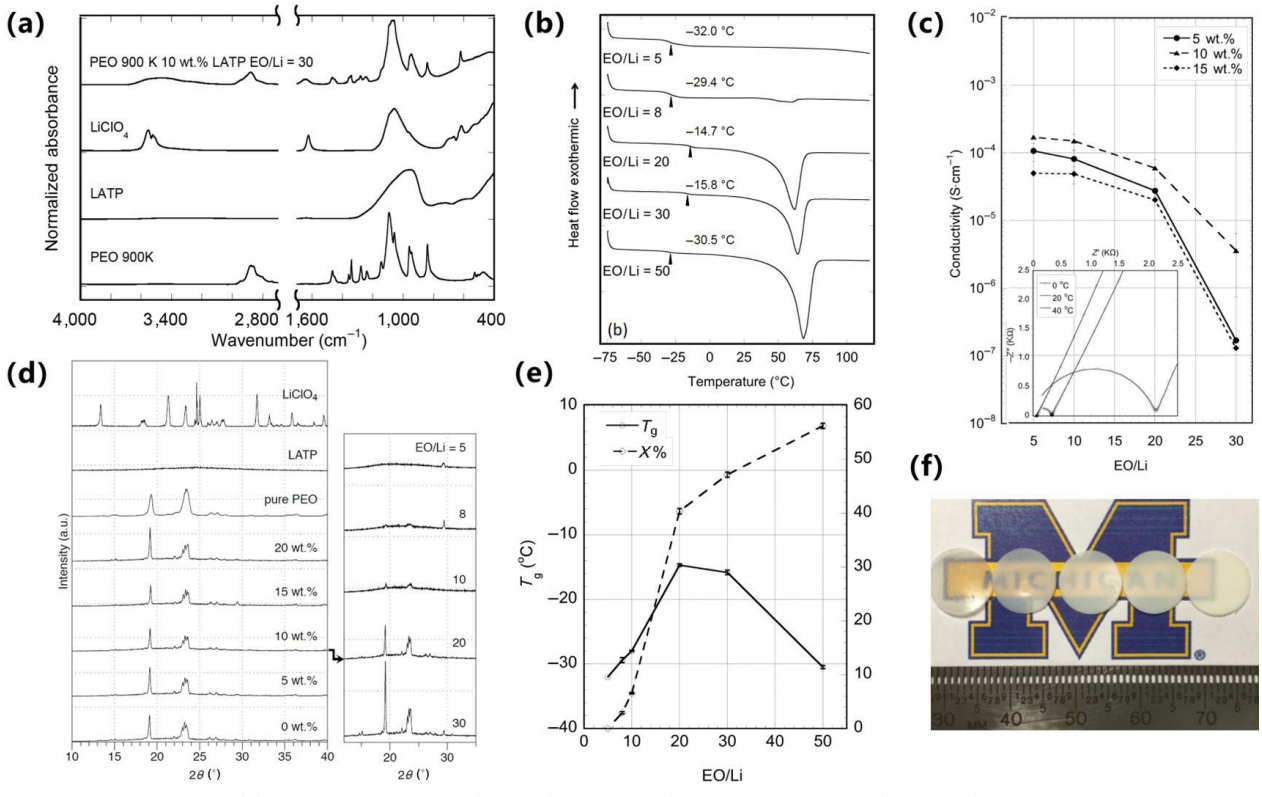

Figure 11 (a) FTIR spectra of the nanocomposite electrolyte, $LiClO_4$, LATP, and PEO, (b) DSC curves of PEO/$LiClO_4$/LATP (10 wt.%) nanocomposites, (c) ionic conductivity as a function of EO/Li with 0 wt.%, 10 wt.%, and 15 wt.% LATP at 20 °C (inset: Nyquist plots for the nanocomposites with 10 wt.% LATP and EO/Li ratio of 10 at 0, 20, and 40 °C), (d) X-ray diffraction patterns of PEO, LATP, $LiClO_4$, and PEO/$LiClO_4$/LATP nanocomposites with EO/Li of 20, (e) the glass-transition temperature and crystallinity of the electrolyte, and (f) photograph of the nanocomposite films. Reproduced with permission from Ref. [69], © American Chemical Society 2017.

$LiAsF_6$ has excellent electrochemical stability. Its anion (AsF_6^-) has high oxidation stability, and the electrochemical window is up to 4.5 V. However, the arsenium element has strong toxicity and thus $LiAsF_6$ is not suitable for commercial batteries. Madhu et al. [94] used a solution casting technique to prepare a composite electrolyte membrane with polyvinyl alcohol (PVA), $LiAsF_6$, and titania filler, and then revealed the principle of $LiAsF_6$ on affecting the ionic conductivity of the electrolyte. After being added to PVA, the vibrational frequency of $LiAsF_6$ changes, indicating that Li^+ interacts with the polar groups of PVA to form a complex (Fig. 12(a)). With the increase of $LiAsF_6$ content, the diffraction peak intensity of the polymer electrolyte gradually decreased, and no salt peak appeared, indicating that after the addition of $LiAsF_6$, the crystallinity decreased and the dissolution was good (Fig. 12(b)). When the $LiAsF_6$ content is 25 wt.%, the amorphous phase dominates the electrolyte. The maximum ionic conductivity of the electrolyte doped with 5 wt.% TiO_2 is 5.10×10^{-4} S·cm^{-1} (Fig. 12(c)), and the Li^+ migration number is 0.52.

$LiBF_4$ has a small anion radius, high solubility, high thermal stability, wide operation temperature range, and low sensitivity to water [95]. Meanwhile, $LiBF_4$ has a good passivation effect on the aluminum collector, and will form the cathode–electrolyte interphase (CEI) containing F^- and B^- during the cycling process [96]. In addition, $LiBF_4$ can decompose and generate a LiF-rich solid electrolyte interphase (SEI) layer [97]. However, $LiBF_4$ is easy to coordinate with organic solvents, which leads to a ring ether polymerization to generate BF_3. Besides, the ionic conductivity of $LiBF_4$ is low when used as a primary lithium salt, and increasing the concentration of $LiBF_4$ will raise the cost. $LiBF_4$ first appeared in liquid batteries in the early 20th century. Later, it is found that $LiBF_4$ had good performance as a co-salt or additive in the electrolytes containing LiTFSI, $LiNO_3$, and LiI [96, 98], but it is still rarely used in SPEs. Rahman et al. [99] studied the influence of $LiBF_4$ on the conductivity of PEO-based SPEs. They found that with the increase of the $LiBF_4$ content in the electrolytes, the crystallinity of the electrolytes gradually decreased, and the electrolyte surface became more smooth. It has been reported that the electrolyte with smooth surface is conducive to the ion mobility [100, 101]. Thus, the ionic conductivity of the PEO-based electrolytes at room temperature increased from 3.91×10^{-9} to 8.75×10^{-4} S·cm^{-1} when adding 30 wt.% $LiBF_4$.

3.2.2 *Organic lithium salts*

In order to improve the thermal and chemical stabilities and the solubility, a series of organic lithium salts with large radius are developed. These lithium salts have high dissociation constants and can be easily dissolved in organic solvents with lower dielectric constants. The commonly-used organic lithium salts are LiTFSI, lithium bisfluorosulfonyl imide (LiFSI), and lithium bis(oxalate)borate (LiBOB). In LiTFSI, S atoms in $N(SO_2CF_3)_2^-$ and ($TFSI^-$) are connected with $-CF_3$ and O atoms, and have strong electronegativity. If there is an electrophilic group connected to the amide group, Li^+ would escape from the molecule, resulting in the dissociation of LiTFSI. The anion radius is large, and the electron delocalization is enhanced. Thus, LiTFSI has high solubility in organic solvents and is regarded as a proper lithium salt for polymer electrolytes. LiTFSI also has high thermal stability. However, $TFSI^-$ will be strongly adsorbed on the surface of Al foil and seriously corrode the aluminum current collector by generating soluble $Al(TFSI)_3$ when the voltage is higher than 3.7 V. Nurul et al. [102] used the solution casting method to prepare solid electrolyte membranes with ultraviolet (UV)-cured glycidyl methacrylate (PGMA) and LiTFSI, and explored the effect of LiTFSI on the ionic conductivity. The Fourier transform infrared (FTIR) spectra showed that with the addition of LiTFSI, there was an interaction between Li^+ ions and the O atoms in the C=O, thus the intensity and sharpness of the C=O peak decreased (Fig. 13(a)). But when the concentration of lithium salt is too high, Li^+ may coordinate with polar atoms in $TFSI^-$ and form ionic aggregates (Fig. 13(b)). Pure PGMA has a prominent semi-crystalline peak at 15°–22°. However, with the addition of salt, the X-ray diffraction peak intensity continued to decrease, the amorphous region increased (Fig. 13(c)), the interchain space increased, and the T_g also decreased from 312 K (0 wt.% LiTFSI) to 291 K (40 wt.% LiTFSI). Correspondingly, the ionic conductivity of the electrolyte increased from 3.09×10^{-10} S·cm^{-1} (0 wt.% LiTFSI) to 4.96×10^{-8} S·cm^{-1} (40 wt.% LiTFSI) at room temperature. However, when the Li salt content increased from 30 wt.% to 40 wt.%, the ionic conductivity of the electrolyte almost did not increase, which may be ascribed to the ion aggregation.

Compared with LiTFSI, the anion of $-CF_3$ is replaced by F atom in LiFSI [103]. The F atom has a strong electron withdrawing property which makes it easier to be dissociated in organic solvents than LiTFSI, and therefore LiFSI has higher ionic conductivity than $LiPF_6$. In addition, LiFSI has a melting point of 145 °C, a decomposition temperature of higher than 200 °C, low sensitivity to water, low toxicity, and good compatibility with electrodes. Takahito et al. [104] used an *in situ* polymerization method to prepare an electrolyte with poly-2,2-dimethoxypropylene carbonate and LiFSI, and

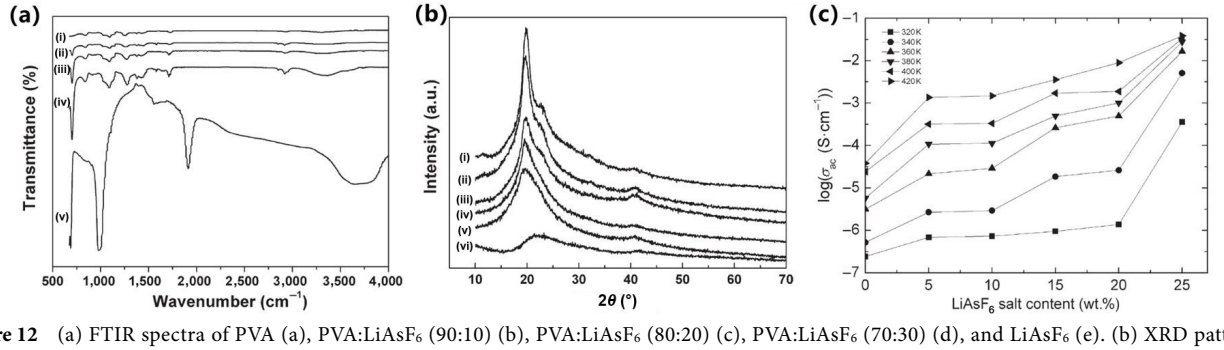

Figure 12 (a) FTIR spectra of PVA (a), PVA:$LiAsF_6$ (90:10) (b), PVA:$LiAsF_6$ (80:20) (c), PVA:$LiAsF_6$ (70:30) (d), and $LiAsF_6$ (e). (b) XRD patterns of PVA (a), PVA:$LiAsF_6$ (95:5) (b), PVA:$LiAsF_6$ (90:10) (c), PVA:$LiAsF_6$ (85:15) (d), PVA:$LiAsF_6$ (80:20) (e), and PVA:$LiAsF_6$ (75:25) (f). (c) Ionic conductivity of PVA:$LiAsF_6$ film. Reproduced with permission from Ref. [94], © Society of Plastics Engineers 2009.

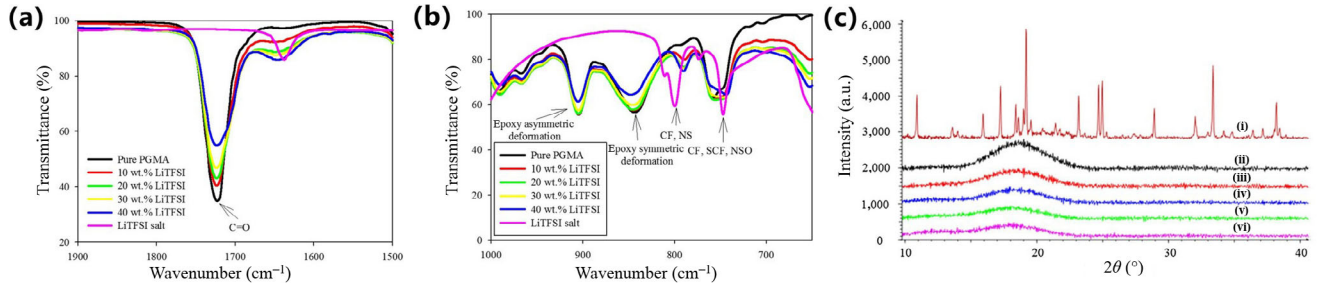

Figure 13 (a) and (b) FTIR spectra and (c) XRD diffractograms of UV-cured PGMA-based SPEs (a: LiTFSI, b: PGMA, and c: 10 wt.%, d: 20 wt.%, e: 30 wt.%, and f: 40 wt.% LiTFSI in PGMA. Reproduced with permission from Ref. [102], © Springer-Verlag Berlin Heidelberg 2015

reached an ionic conductivity 1.08×10^{-4} S·cm^{-1} at 30 °C. The Li^+ transference number was 0.75, and the electrochemical window was above 4 V.

LiBOB also has wide electrochemical window and high ionic conductivity, and can directly react with solvents to form SEI films to protect the electrodes. However, LiBOB is highly sensitive to water and has low solubility in a few low-dielectric-constant solvents. Moreover, LiBOB can generate gas, which seriously threatens the battery safety. Appetecchi et al. [105] prepared a blend electrolyte of PEO and LiBOB by hot pressing, and then verified the plasticizing effect of LiBOB on PEO, which can improve the ionic conductivity by reducing the PEO crystallinity. The ionic conductivity was over 10^{-5} S·cm^{-1} at 30 °C, and the Li^+ transference number was 0.25–0.30.

3.2.3 *Remarks*

Apart from the polymer matrices, lithium salts are also indispensable in polymer electrolytes, and ideal lithium salts should have high dissociation ability, wide electrochemical window, good compatibility with other battery components, high safety, low cost, etc. $LiPF_6$ has balanced performance and is widely used in electrolytes, but it is easy to decompose and sensitive to water; $LiClO_4$ has good solubility and high ionic conductivity, but its strong oxidizing ability causes safety issues; $LiAsF_6$ has high chemical stability, but the As element is poisonous; LiTFSI and LiFSI have high electrical conductivity, but the reaction with current collectors is serious; LiBOB has strong dissociation ability and can passivate electrodes, but its chemical stability and safety are poor. At present, there is no lithium salt with the above-mentioned comprehensive advantages, and it is necessary to exploit new lithium salts including making composite salts or the modification of lithium salts. Novel lithium salts should have large anion radius and weak interaction between the positive and negative ions, which is helpful for facilitating the dissociation of lithium salts to increase the electrolyte conductivity. Applying two or more lithium salts with various molecular structures and properties can take advantages of the synergic effect to improve the electrical, thermal, and electrochemical properties of the electrolytes. With the development of polymer lithium-ion batteries, new lithium salts with better performance will appear in the future to meet the demands.

3.3 Additive engineering

As mentioned in Section 3.1 Copolymer molecule structure design and Section 3.2 Lithium salt exploitation, the optimization of the molecular structures of polymer matrices and lithium salts can increase the ionic conductivity by decreasing the glass-transition temperature and polymer crystallinity and facilitating the lithium salt dissociation. To further improve the ionic conduction capability, a few additives such as organic micro-molecules, polymers, and micro-/nano- particles are then introduced to the polymer electrolytes by enhancing the polymer segment mobility, increasing the carrier concentration, or forming fast-ion pathways.

3.3.1 *Organic plasticizers*

In commercial LIBs, a few high-dielectric-permittivity micro-molecules such as ethylene carbonate (EC), PC, diethyl ethylene (DEC), dimethyl carbonate (DMC), and dimethyl formamide (DMF) are utilized as ion transport mediums [111, 112]. To increase the ionic conductivity of the SPEs, these liquid solvents can be added into the polymer electrolytes as plasticizers (Table 3) because of the following reasons: (1) breaking up the interchain polymer interactions, lowering the glass-transition temperature of the SPEs, and increasing the chain segmental motion; (2) loosening the polymer polar group–Li^+ and anion–Li^+ interactions through the competitive Li^+ coordination with the high-donicity plasticizers, and lowering the activation energy for ion motion [49]. The polymer electrolytes with high-content liquid plasticizer solvents can be defined as gel polymer electrolytes (GPEs). Compared with the SPEs, the ion transport mainly occurs in the liquid phase or swollen gel phase in the GPEs (similar to the liquid electrolytes by the ion-solvent complexation and migration) [113], and thus the GPEs usually show higher ionic conductivities. However, the large amounts of solvents may result in the electrolyte leakage, flammability, electrochemical instability, and mechanical property degradation [114]. Bao et al. [49] prepared a xPTHF electrolyte using LiTFSI as a lithium salt and then scrutinized the effects of PC, DMF, ethyl acetate (EtAc), and chlorobenzene (ClBz) on the ionic conduction of the $xPTHF_5$ electrolyte. The extraction of the VTF parameters showed that the addition of 2:1 DMF:Li equivalencies into $xPTHF_5$ can make the activation energy decrease from 11.1 to 8.7 kJ·mol^{-1} and the VTF prefactor (A) increase from 1.1 to 2.9 S·K$^{0.5}$·cm^{-1}, indicating that DMF (donor number: 26.6, ε = 36.7) can reduce the activation energy for ion motion by the competitive coordination with Li^+ and increase the number of dissociated ions in the electrolyte. Thus, the room temperature ionic conductivity of the $xPTHF_5DMF_{2:1}$ electrolyte (18 wt.% DMF) greatly increased from 1.3×10^{-6} to 1.2×10^{-4} S·cm^{-1} at 30 °C (Fig. 14(a)). The utilization of PC (donor number: 15.1, ε = 64.9) can also increase the A and lower the activation energy for ion motion, thus the $PTHF_5PC_{2:1}$ electrolyte had an appreciable value of 7.8×10^{-5} S·cm^{-1} at 30 °C (Fig. 14(b)). In contrast, the additions of low-dielectric-constant EtAc (donor number: 17.1, ε = 6) and ClBz (donor number: 2, ε = 5.6) can decrease

Table 3 Ionic conductivity of the plasticizer-containing polymer electrolytes

Polymer matrix	Plasticizer	Ionic conductivity (S·cm^{-1}, 25 °C)	References
PEO/PVDF-HFP	POSS-IL	8.0×10^{-4} (22 °C)	[50]
PEO/PVDF	EMIMTFSI	1.6×10^{-4}	[117]
PVDF/PVP	EDTA	7.2×10^{-4}	[124]
PVDF	PC and DGM	1.3×10^{-4}	[114]
PTHF	DMF	1.2×10^{-4}	[49]
PEO	DOP and PEG	10^{-5}–10^{-4}	[115]
ETPTA	Succinonitrile	5.7×10^{-4}	[123]

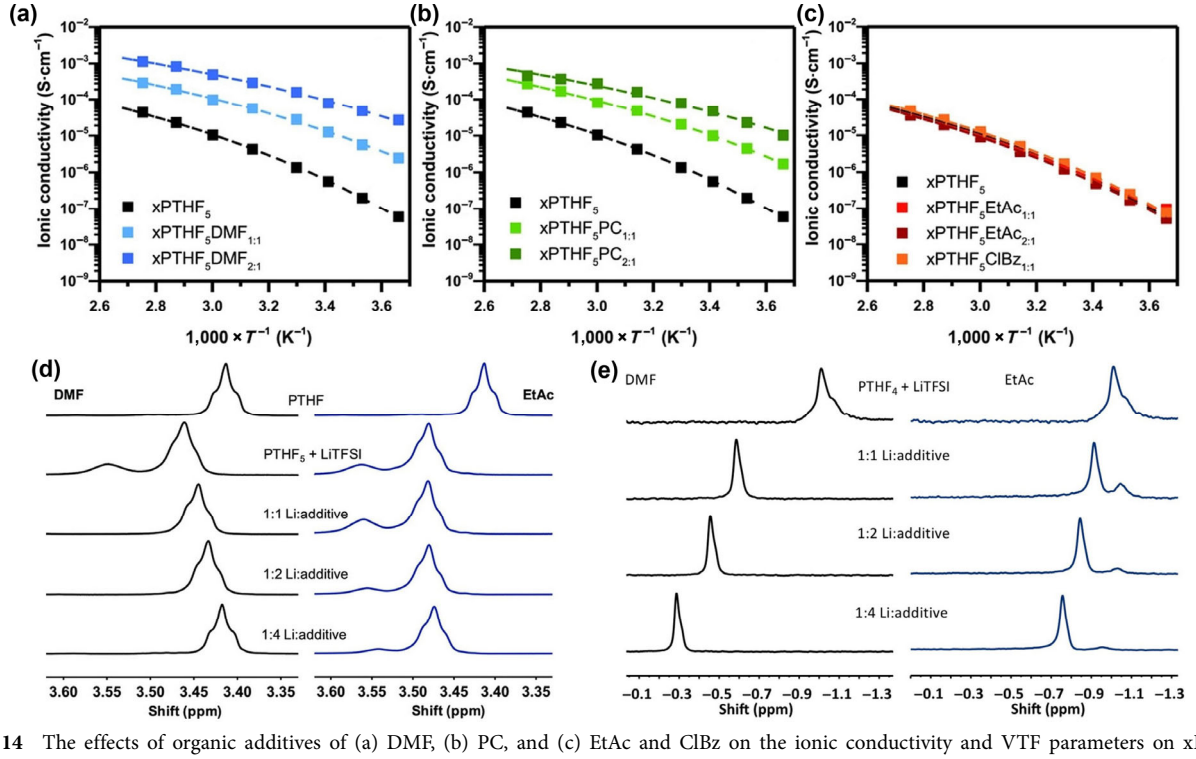

Figure 14 The effects of organic additives of (a) DMF, (b) PC, and (c) EtAc and ClBz on the ionic conductivity and VTF parameters on xPTHF5 electrolyte, and (d) ^{1}H NMR and (e) ^{7}Li NMR spectra of non-crosslinked PTHF$_5$ with increasing amounts of DMF and EtAc. Reproduced with permission from Ref. [49], © WILEY-VCH Verlag GmbH & Co. KGaA, Weinheim 2018.

the T_g, but cannot decrease the A and the activation energy, and therefore they had little effect on the ionic conductivity of the electrolyte (Fig. 14(c)). ^{1}H NMR characterizations showed that the addition of DMF into the PTHF$_5$ electrolyte (dissolved in chloroform) caused the alpha proton peak to shift back upfield, indicating the weakened O–Li$^+$ interaction, while the addition of EtAc had little effect on the alpha proton peak and the O–Li$^+$ interaction (Fig. 14(d)). The additions of DMF and EtAc into the PTHF$_5$ system also caused strong and poor deshieldings of Li$^+$, respectively, indicating a loosening of the strong O–Li$^+$ interaction by DMF (Fig. 14(e)).

Different from the micro-molecule plasticizers, the application of oligomer polymers can increase both the ionic conductivity and mechanical properties of the polymer electrolytes. Pumchusak et al [115] compared the impacts of the dioxyphthalate (DOP) and PEG on the electrical and mechanical properties of the PEO-LiFSI electrolyte. The pristine electrolyte of PEO-15 wt.%LiFSI had a T_g of −64 °C and a PEO crystallinity (X_c) of 37%. With additions of 15 wt.% DOP and PEG, the T_g of the electrolyte increased to −60 and −56 °C and the X_c decreased to 35% and 32%, respectively. Though the slight increase of the T_g was due to the possibility of the crosslinking of the PEO chains with the interaction of the plasticizers, the X_c of the plasticizer-containing electrolyte decreased. Therefore, the ionic conductivity of the plasticizer-containing electrolyte increased from 1.0×10^{-6} to 3.4×10^{-5} S·cm^{-1} (15 wt.% DOP) and 1.7×10^{-5} S·cm^{-1} (15 wt.% PEG) at 25 °C. Moreover, the tensile strength, elongation, and Young's modulus of the polymer electrolyte decreased upon the DOP addition, while the small quantity (5 wt.%–10 wt.%) addition of PEG can effectively reinforce the polymer electrolyte.

Compared with the commercial molecular plasticizers, ILs have obvious thermal advantages such as no measurable vapor pressure and non-flammability, and thus the addition of ILs into the polymer electrolytes can enhance the thermal stability and safety of electrolyte. The IL addition in the polymer electrolyte can also increase the ionic conductivity by effectively swelling the molecular chain of the polymer, weakening the interaction of the polymer segments, and enhancing the movement ability of the polymer molecular chains [116]. Yuan et al. [50] found that the addition of imidazolium-based POSS-ILs consisting of POSS-COO$^-$ anions and a variety of imidazolium cations can greatly increase the ionic conductivity of the PEO/poly(vinylidene fluoride-co-hexafluoropropylene)

(PVDF-HFP)/PC/LiTFSI electrolyte (up to 8.0×10^{-4} S·cm^{-1} at 22 °C). Rathika et al. [117] reported a zinc-ion conducting polymer blend electrolyte system of PEO/PVDF-ZnTFSI with various concentrations of 1-ethyl-3-methylimidazolium bis(trifluoromethylsulfonyl) imide (EMIMTFSI). FTIR spectroscopy measurements showed that there were complexation interactions between $EMIM^+$ and $PEO/TFSI^-$, which can decrease the polymer crystallinity (from 40% to 22%) and facilitate the ZnTFSI dissociation. Thus, the composite electrolyte with 7 wt.% EMIMTFSI had a higher ionic conductivity of 1.63×10^{-4} S·cm^{-1} than the pristine electrolyte at room temperature.

The CPEs with liquid plasticizers can greatly improve the ionic conductivity, but still exhibit all the limits of the liquid plasticizers especially the poor thermal and electrochemical stabilities. In comparison, applying solid-state plasticizers can improve the overall properties of the polymer electrolytes. Succinonitrile is a solid-state organic non-ionic plastic material, where the impurity "trans" isomer imparts a plastic character blow its melting point, and it appears as a stable plastic crystal phase between the phase transition temperature of around −30 °C and melting point of ~ 60 °C [19, 118, 119]. As a solid solvent for various lithium salts, SN has been widely used as a versatile additive to increase the ionic conductivity of the polymer electrolytes. Fan et al. [120] investigated the plasticizing effects of SN on PEO complexed with four kinds of Li salts, and found that the solvating ability of SN on the lithium salts (especially for the lithium salts that are difficult to dissociate) was much higher than that of PEO. Moreover, the introduction of SN can greatly lower the crystallinity of the polymer electrolytes (the crystallinity of the PEO-$LiPF_6$ and PEO-lithium bisperfluoroethylsulfonylimide (LiBETI) electrolytes decreased from 45% and 22% to 40% and 16%, respectively). Thus, the introduction of SN enhanced the ionic conductivity ~ 22,000 and 1,300 times for the LiCl- and $LiPF_6$-containging PEO electrolytes at 20 °C, respectively.

Although the addition of SN can increase the ionic conductivity of the polymer electrolytes, SN is unstable against lithium metal electrodes due to the side reactions or polymerization of nitriles catalyzed by lithium metals [121]. To overcome this drawback, a few SEI forming agents such as fluoroethylene carbonate (FEC) are also introduced into the electrolytes. In addition, to strengthen the mechanical strength of the SN-based electrolytes, the electrolytes are usually deposited on/in the porous substrates as 3D scaffolds. Xie et al. [122] prepared high-strength CPE films by filling PEO-LiTFSI-SN-FEC into the porous PE separators with a thickness of ~ 22 μm. The introduction of SN made the room-temperature ionic conductivity increase from ~ 10^{-5} to ~ 10^{-4} S·cm^{-1}, while the introduction of FEC (10 wt.%) can result in the formation of mechanically stable LiF and ionically conductive Li_3N on the lithium metal surfaces (suppresses the side reactions between SN and lithium metals). Therefore, the electrolyte-based Li/Li symmetrical cells can stably cycle for 700 h with negligible overpotential change at 0.1 mA·cm^{-2}. Lee et al. [123] prepared a deformable CPE film (~ 25 μm) by *in situ* UV-crosslinking of ethoxylated trimethylolpropane triacrylate (ETPTA) monomer with SN in a porous polyethylene terephthalate (PET) nonwoven (NW). Due to the synergistic effect of the SN plasticizer and the PET nonwoven, the CPE film had greatly improved the ionic conductivity (5.7×10^{-4} S·cm^{-1} at 30 °C) and mechanical strength.

3.3.2 *Polymer blending*

The polymer matrices (Fig. 15) commonly used in solid polymer electrolytes include PEO, PAN, polymethyl methacrylate (PMMA), PVDF, and PC. The PEO-based electrolyte has good thermal and mechanical properties along with good interfacial stability when coupled with lithium metal [125, 126]. However, PEO is easy to crystallize at room temperature and its chain segment movement ability is poor, resulting in the low ionic conductivity at room temperature of the PEO-based electrolyte, which cannot meet the needs for solid-state batteries [115]. In contrast, PAN-based electrolyte has high ionic conductivity and good low-temperature working performance, but it has poor thermodynamic stability and mechanical strength.

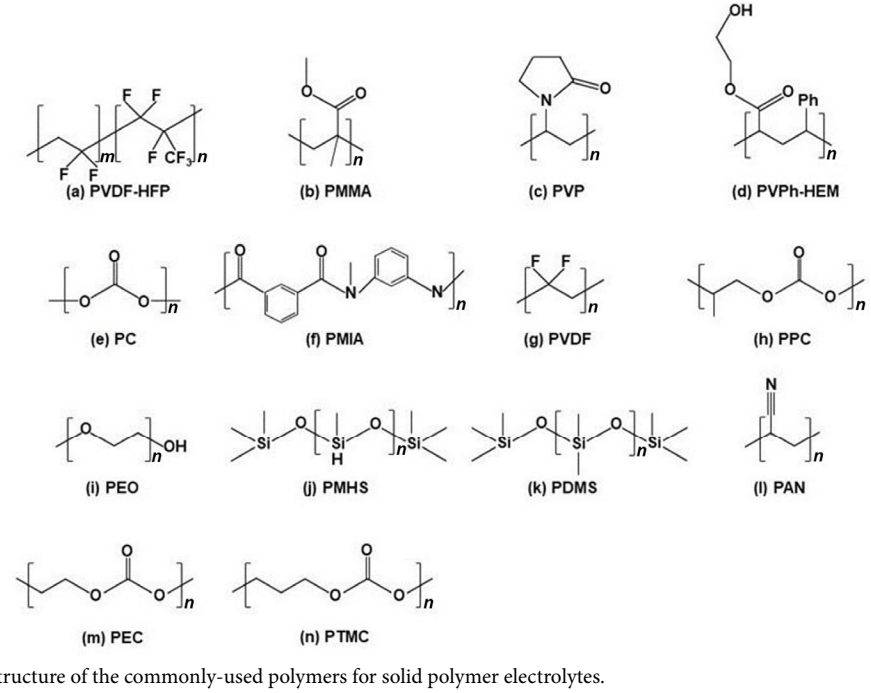

Figure 15 (a)–(n) The structure of the commonly-used polymers for solid polymer electrolytes.

PMMA-based electrolyte has high ionic conductivity at room temperature and low interfacial impedance with lithium metal electrodes, but it has the disadvantages of poor flexibility and low lithium-ion transference number [127]. PVDF-based electrolyte has a high melting point, good thermal stability, and high electrochemical stability, but the homopolymer structure causes high intramolecular crystallinity (65%–78%), which is not conducive to the ion conduction. PC-based electrolyte possesses high lithium-ion transference number and ionic conductivity, but it usually suffers from poor mechanical property. In short, every polymer matrix cannot possesses the comprehensive advantages of high ionic conductivity, mechanical strength, thermostability, and wide electrochemical window.

At present, the blending of two or more polymer matrices is an effective method to improve the performance of the polymer electrolytes by combining the advantages of the polymers (Table 4) [128–131]. Moreover, the electrolyte preparation process is simple and cheap [132, 133]. As for the PEO-based electrolyte, the higher the proportion of the amorphous region in the solid electrolyte, the stronger the lithium-ion transportability. Therefore, a few polymers such as poly(m-phenylene isophthalamide) (PMIA) [130], poly(propylene carbonate) (PPC) [134, 135], poly(vinyl pyrrolidone) (PVP) [126], PVDF [136, 137], and poly(4-vinyl phenol-co-2-hydroxyethyl methacrylate) (PVPh-HEM) [138] can be added into the PEO matrix to obtain high ionic conductivity. Liu et al. [130] prepared novel composite electrolyte films of PMIA/PEO/LiTFSI by the polymer blending technology. The hydrogen bond between PMIA and PEO/$TFSI^-$ can effectively inhibit the crystallization of PEO and promote the dissociation of LiTFSI (Fig. 16(a)), and therefore the PMIA/PEO/LiTFSI electrolytes showed an ionic conductivity of 6×10^{-6} S·cm^{-1}, which was two times that of the pristine electrolyte at room temperature. The integration of the high-strength PMIA additive with robust amide-benzene backbones can also contribute to the mechanical tensile strength (2.96 MPa, Fig. 16(c)), thermostability (419 °C, Fig.16(d)), and interfacial resistance against Li dendrites (468 h at 0.10 mA·cm^{-2} without short circuit, Fig. 16(b)), which are superior to the pristine electrolyte (0.32 MPa, 364 °C, and short circuit after 246 h). Yu et al. [134] reported another blend polymer electrolyte using degradable PPC and PEO. The XRD (Fig. 16(e)) and DSC tests showed that the electrolyte has amorphous properties, which are conducive to the diffusion of ions in the polymer electrolyte. The addition of PPC can reduce the T_g of PEO, and therefore the electrolyte has high ionic conductivity. When the PPC content is 50%, the ionic conductivity reaches 6.83×10^{-5} S·cm^{-1} (Fig. 16(f)). Li et al. [139] reported a polymethylhydrogen-siloxane (PMHS)/PEO blend electrolyte containing SiO_2 nanoparticles by the traditional solution casting method. The crystallinity of the composite electrolyte is greatly reduced (Fig. 16(g)), because Li^+ is connected to the ether oxygen functional groups of PEO and PMHS through the complexation reaction, and therefore the hybrid electrolyte containing 40% PMHS showed high ionic conductivity (2.0×10^{-2} S·cm^{-1} at 80 °C), wide electrochemical window (5.2 V, Fig. 16(h)), and high flexibility and thermostability. When assembled in $LiFePO_4$/Li batteries, the electrolyte provides a reversible capacity of ~ 140 mAh·g^{-1} at 0.1 C and 60 °C. Patla et al. [140] prepared a PEO/PVDF blend electrolyte doped with NH_4I salt. The XRD and DSC tests show that when the salt concentration exceeds 15 wt.%, the PN_x (80 wt.% PEO, 20 wt.% PVDF, and x wt.% NH_4I) system becomes completely amorphous, and thus the ionic conductivity of the PN_{35} system reaches 10^{-3} S·cm^{-1} at room

Table 4 Properties of solid electrolytes with different polymer matrices

Polymer matrices	Li salt	Conductivity (S·cm^{-1}, 25 °C)	t_{Li^+}	References	Pros./cons.
PEO/PMIA = 100:5	LiTFSI	6.00×10^{-6}	0.5	[130]	The hydrogen-bond between PMIA and PEO/TFSI can prevent the PEO crystallization, facilitate the LiTFSI dissociation, and increase the ionic conductivity. The PMIA addition can improve the mechanical strength, thermostability, and interfacial stability against Li dendrites.
PEO/PPC = 1:1	$LiClO_4$	6.85×10^{-5}	—	[134]	PPC can reduce the crystallinity, which is beneficial to the diffusion of ions in the electrolyte and results in high conductivity.
PEO/PVPh	$LiClO_4$	3.69×10^{-5}, ≥ 40 °C	—	[138]	PVPh-HEM isolates the anions from each other, decreasing the number of the ion pairs and enhancing the ion mobility and conductivity.
PEO/PMHS (with silica additive)	LiTFSI	2.00×10^{-2}, 80 °C	0.3	[139]	The Li^+ connected with the ether oxygen groups of PEO and PMHS by the complexation reaction leads to the decrease of the crystallinity. When the PMHS content is more than 50%, the film formability becomes poor.
PEO/PMMA = 47:53	LiTFSI	3.00×10^{-4}	—	[141]	The PMMA-nanoparticle and PEO blend lead to fewer contact between PEO and PMMA and faster PEO segmental dynamics, thus promoting high ionic conductivity.
PEO/PDMS	$LiClO_4$	3.00×10^{-5}	0.7	[142]	The "salting in" phenomenon induced by the ClO_4^-–PEO interactions causes the amorphization of the PEO-PDMS matrix and the high conductivity.
PEO/WPU = 3:1	LiTFSI	8.20×10^{-4}, 60 °C; 3.10×10^{-3}, 80 °C	—	[143]	Hydrogen bonds and Li^+ cross-links between WPU and PEO can improve the mechanical strength, reduce the effective chain length, and restrict the polymer segment motion, thus decreasing the ionic conductivity.
PVDF-HFP/ PEC = 1:1	LiTFSI	1.08×10^{-4}, 30 °C	—	[145]	Dual-path of Li^+ exists in the electrolyte: One path is carried by PECLi phase, and the other is caused by the synergistic effect of PVDF-HFP and PEC, accelerating the Li^+ movement.
PEC/PTMC = 6:4	LiTFSI	1.00×10^{-6}, 50 °C	—	[146]	The interactions between the host matrix and Li^+ lead to the increase in conductivity. PEC and PTMC are immiscible with each other though their chemical structures are similar.

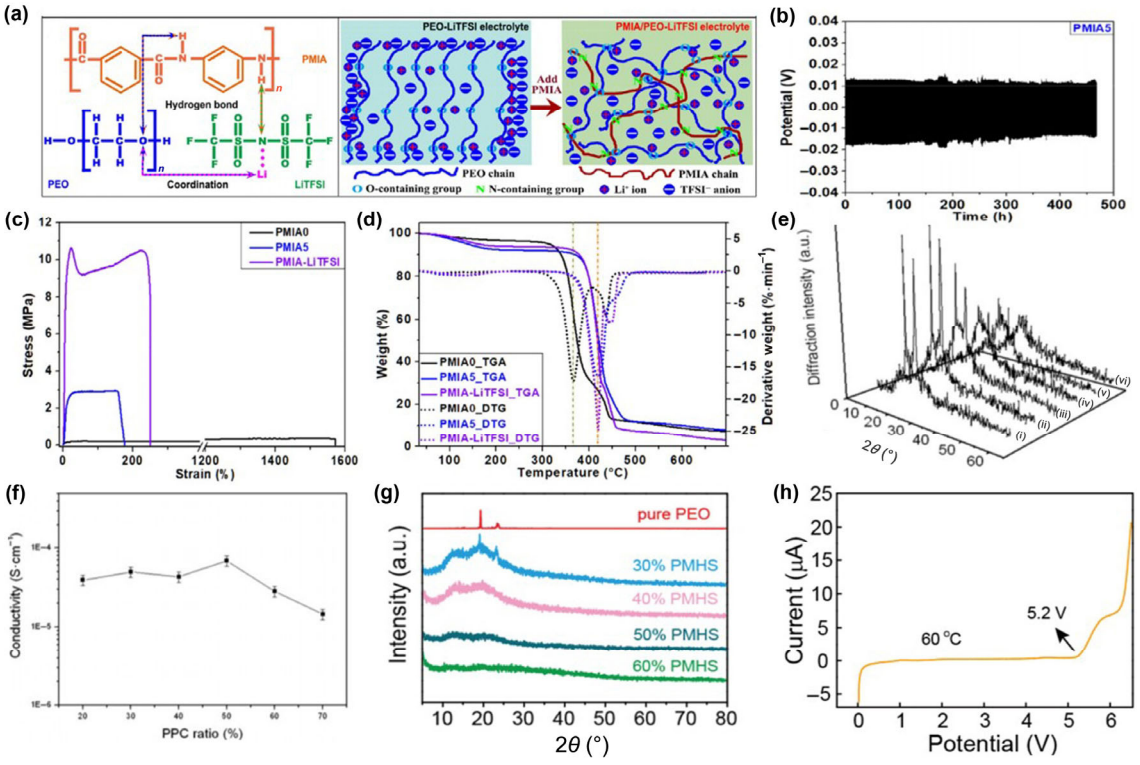

Figure 16 (a) Interactions between PMIA, PEO, and LiTFSI and structures of the PEO-LiTFSI electrolyte before and after the incorporation of PMIA, (b) galvanostatic cycling curves of the PMIA5 electrolyte-based Li/Li symmetric cells under 0.10 mA·cm^{-2} and 60 °C, and (c) mechanical tensile stress-strain curves and (d) TGA curves of the PEO/PMIA electrolytes. Reproduced with permission from Ref. [130], © Science Press and Dalian Institute of Chemical Physics, Chinese Academy of Sciences. Published by Elsevier B.V. and Science Press 2020. (e) XRD traces and (f) ionic conductivity of PEO/x%PPC electrolytes (x = (a) 20, (b) 30, (c) 40, (d) 50, (e) 60, and (f) 70). Reproduced with permission from Ref. [134], © Wiley Periodicals, Inc. 2009. (g) XRD patterns and (h) LSV curves at 60 °C of PPS-CPE with different contents of PMHS. Reproduced with permission from Ref. [139], © The Royal Society of Chemistry 2018.

temperature. When the salt content exceeds 35 wt.%, the carrier ion concentration decreases due to the strong ion interaction, thus reducing the ionic conductivity.

A few researchers have also reported that the addition of PMMA [141], polydimethylsiloxane (PDMS) [142], and waterborne polyurethane (WPU) [143] into PEO can improve the mechanical strength of the polymer electrolyte, but it would reduce the ionic conductivity of the polymer electrolyte. For instance, Bao et al. [143] prepared a polymer electrolyte of PEO/WPU/LiTFSI via a solvent-free process. The mechanical strength of the pure PEO electrolyte (SPE1) is only 0.18 MPa, which is much lower than the composite electrolyte (when WPU:PEOs are 1:1 (SPE2), 1:3 (SPE3), 3:1 (SPE4), and 1:0 (SPE5), the corresponding mechanical strengths are 1.3, 1.6, 2.9, and 4.2 MPa, respectively) (Fig. 17(a)), the main reason of the high mechanical strength of the WPU-containing electrolytes is attributed to the good compatibility and the cross-linking of hydrogen bonds between WPU and PEO. It is worth noting that the ionic conductivity of the PEO/WPU blend electrolyte is a little lower than that of the PEO-only electrolyte (Fig. 17(b)), and it decreases with the increase of the WPU content. This can be attributed to the hydrogen bond interaction between PEO and WPU, restricting the segmental movement of the polymers (Fig. 17(c)).

Apart from PEO, other polymer matrices have also been utilized to prepare high-ion-conductivity blend polymer electrolytes by the polymer blending method [144]. Zhao et al. [145] fabricated a composite electrolyte by controlling the ratio of the PVDF-HFP and polyethylene carbonate and LiTFSI (PECLi). The ion conductivity of the FPEC80/50 electrolyte with 80 wt.% LiTFSI and 50 wt.% PVDF-HFP reached 1.08 × 10^{-4} S·cm^{-1} at 30 °C (Fig. 18(a)), which was attributed to the synergistic effect of the PVDF-HFP and PEC and the establishment of dual lithium-ion transport pathways in the composite electrolyte. Moreover, the FPEC80/50 electrolyte displayed a stable electrochemical window of ~ 4.5 V (Fig. 18(b)). Li et al. [146] prepared another blend electrolyte consisting of amorphous PEC and poly(trimethylene carbonate) (PTMC) with LiTFSI. The PEC/PTMC blends are compatible, and the existence of the interactions between the host matrix and Li$^+$ can facilitate the dissolution of the Li salt, and thus the ionic conductivity of the electrolyte increases with the salt concentration. The PEC_6PTMC_4-LiTFSI blend electrolyte showed an ionic conductivity of 10^{-6} S·cm^{-1} at 50 °C (Fig. 18(c)), which is higher than that of the single PEC- or PTMC-based electrolytes.

3.3.3 *Nanoparticle filling*

Solid-state polymer electrolytes with high ionic conductivity play a critical role in the development of next generation lithium-ion batteries with enhanced safety and energy density. However, the low ionic conductivity of the SPEs at room temperature and their poor mechanical stability need to be improved prior to their practical application. To bypass this problem, a variety of techniques have been attempted such as the introduction of plasticizers, the formation of block copolymers, crosslinking polymers, and the addition of ceramic fillers. Among these strategies, dispersing

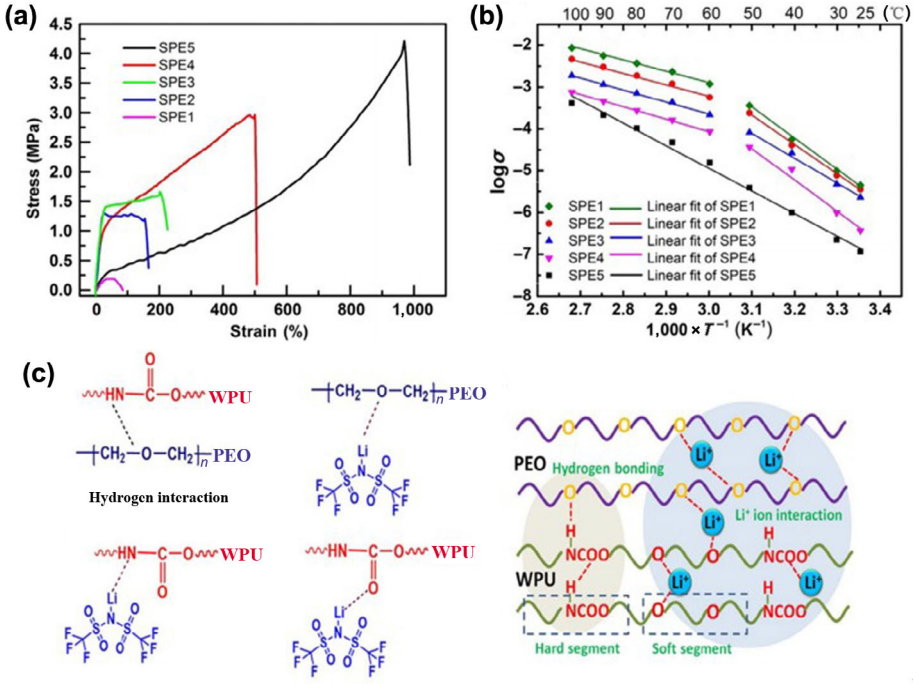

Figure 17 (a) Stress-strain curves, and (b) ionic conductivity of PEO/WPU/LiTFSI electrolytes, and (c) schematics of the hydrogen bonding and Li^+ interactions with WPU and PEO. Reproduced with permission from Ref. [143], © Elsevier B.V. 2018.

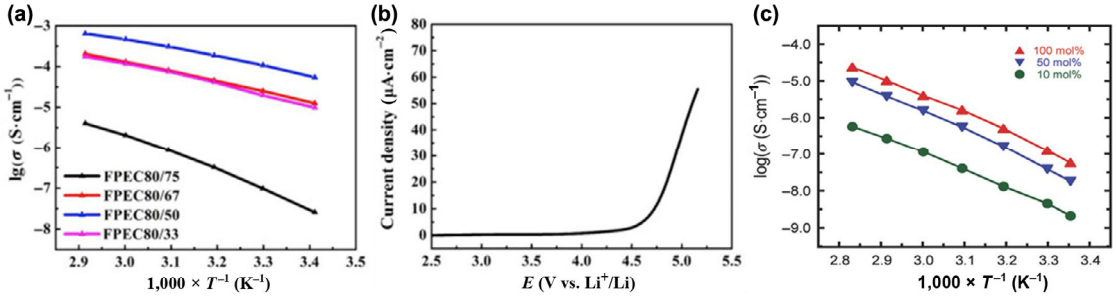

Figure 18 (a) Ionic conductivity of FPEC80 electrolytes with different ratios of PVDF-HFP, and (b) electrochemical window of FPEC80/50. Reproduced with permission from Ref. [145], © Elsevier B.V. 2018. (c) Ionic conductivity of PEC_6PTMC_4-LiTFSI electrolytes with different salt contents. Reproduced with permission from Ref. [146], © WILEY-VCH Verlag GmbH & Co. KGaA, Weinheim 2018.

ceramic nanoparticles in the polymer matrices for fabricating CPEs is attractive, since this can improve both the ionic conductivity and the mechanical and thermal properties (Table 5).

3.3.3.1 *Zero-dimensional (0D) nanofiller*

The commonly-used 0D nanofillers are inert ceramic substances such as Al_2O_3, SiO_2, ZrO_2, and TiO_2. The dispersion of inorganic fillers at the nanoscale can reduce the crystallization of the polymer and improve Li salt dissociation by utilizing their high surface area ratio and strong Lewis acid–base interactions between the nanofillers and the electrolyte ion species. Vignarooban et al. [147] utilized high-dielectric-constant titania nanoparticles (435 vs. 2.8–3.3 of PEO) to facilitate the LiTFSI dissociation and increase the concentration of the mobile carriers for high-conductivity PEO-LiTFSI electrolyte by the Lewis acid–base interaction. The composite electrolyte with 10 wt.% TiO_2 exhibited the maximum conductivity of 4.9×10^{-5} S·cm^{-1} at 30 °C, an order of magnitude higher than that of the nanofiller-free PEO-LiTFSI electrolyte. Masoud et al. [148] used the conventional solution casting technique to prepare PEO-$LiClO_4$ composite membranes filled with Al_2O_3 nanoparticles. The Al_2O_3 nanoparticles with an average size of 42 nm were prepared by pyrolysis method. Using X-ray diffraction, differential scanning calorimetry, and infra-red spectra characterizations, they found that the melting temperature (T_m) of PEO decreased with the addition of Li salts and alumina nanoparticles due to an increase in the amorphous state. The highest ionic conductivity of the nanocomposite films containing 1.25 mol PEO was 8.3×10^{-5} S·cm^{-1}.

In order to increase the interfacial contact area between the polymer matrices and the ceramic nanofillers, porous nanoparticles are also applied. For instance, Wen et al. [149] prepared a nanoporous SSZ-13 particle-filled PEO-LiTFSI electrolyte. SSZ-13 is an aluminosilicate with three-dimensional open structure consisting of Si and Al connected by O atoms. The abundant silicon and aluminum hydroxyl groups on the surface of SSZ-13 introduce Lewis acid–base sites and promote the Lewis acid–base interaction between Li salt and SZZ-13 particles. On the other hand, the nanoporous adsorption effect of the highly ordered nanoporous nanoparticles leads to the coating of high lithium concentration on the surface of the SSZ-13 nanoparticles and nanopores, both of which greatly improve the ionic conductivity. The ionic conductivities of the

Table 5 Polymer electrolyte modification by nanofilling

Dimension	Filler type	Polymer matrix	Ionic conductivity ($S \cdot cm^{-1}$, 25 °C)	Pros./cons.	References
0D	ZrO_2	PAN	1.16×10^{-3}	Large specific surface area, easy to aggregate, incontinuous ion paths	[75]
	TiO_2	PMMA	3×10^{-4} (30 °C)		[199]
	SiO_2 (*in situ*)	PEO	4.4×10^{-5} (30 °C)		[168]
	Al_2O_3 (*in situ*)	TEGDA-BA	3.92×10^{-3}		[200]
	$Li_7La_3Zr_2O_{12}$	PEO	3.9×10^{-4}		[158]
	Ga-LLZO	PEO	7.2×10^{-5} (30 °C)		[201]
	Al-LLZO	PEO	4.4×10^{-4} (30 °C)		[202]
	Ta-LLZO	PPC	5.2×10^{-4} (20 °C)		[165]
	Ta-LLZO	PVDF	5×10^{-4}		[203]
	Ta-LLZO	PEO	4.8×10^{-4} (60 °C)		[204]
	Dopamine-modified LLZTO	PEO	1.1×10^{-4} (30 °C)		[169]
	LATP	PEO	1.7×10^{-4} (20 °C)		[69]
	LAGP	PEO	6.76×10^{-4} (60 °C)		[159]
	$Li_{10}GeP_2S_{12}$	PEO	1.21×10^{-3} (80 °C)		[205]
	$Li_7P_3S_{11}$	PEO	2.1×10^{-3}		[206]
	Hydroxyapatite	PEO	6.4×10^{-5} (30 °C)		[151]
	Carbon quantum dot	PEO	1.39×10^{-4}		[152]
	ZnO quantum dot	PEO	1.5×10^{-5}		[207]
	UIO/Li-IL	PEO	1.3×10^{-4} (30 °C)		[157]
	$BaTiO_3$	PVDF-HFP/PVAc	2.3×10^{-3} (30 °C)		[208]
1D	SiO_2	PVDF-HFP	1.08×10^{-3}	High aspect ratio, 1D continuous ion transport channels, reduction of junction-crossing	[170]
	$Mg_2B_2O_5$	PEO	1.53×10^{-4} (40 °C)		[172]
	Y_2O_3-doped ZrO_2	PAN	1.07×10^{-5} (30 °C)		[173]
	$Al_4B_2O_9$ nanorod	PEO	4.35×10^{-1} (30 °C)		[175]
	LLTO	PAN	2.4×10^{-4}		[171]
	LLTO	PEO	2.4×10^{-4}		[209]
	Aligned LLTO	PAN	6.05×10^{-5} (30 °C)		[65]
	LLZO	PAN	1.31×10^{-4}		[70]
	Ta-LLZO	PEO	2.13×10^{-4}		[210]
	LATP	PEO	5.2×10^{-3}		[166]
2D	Graphene oxide	PEO	$\sim 10^{-5}$	Abundant surface ion transport channels	[177]
	PEG-grafted graphene oxide	PEO	2.1×10^{-4} (30 °C)		[178]
	g-C_3N_4	PEO	1.7×10^{-5} (30 °C)		[180]
	MXene	PEO	2.2×10^{-5} (28 °C)		[182]
	Montmorillonite	PEC	3.5×10^{-4}		[183]
	Carbon nitride	PVDF-HFP	2.3×10^{-4} (30 °C)		[186]
	Hydroxide	PVDF-HFP	2.2×10^{-4}		[185]
3D	Gd-doped CeO_2	PVDF-PEO	2.3×10^{-4} (30 °C)	3D continuous ion transport networks, improved mechanic strength	[211]
	AAO	PEO	5.82×10^{-4}		[66]
	PVDF	PEO	$\sim 10^{-5}$ (30 °C)		[193]
	PI nonwoven	PEO	$\sim 10^{-4}$ (30 °C)		[194]
	Cellulose nanofibril	PEO	3.1×10^{-5}		[195]
	Aramid nanofiber	PEO	8.8×10^{-5}		[73]
	Glass fiber cloth	PEO	2.5×10^{-4} (60 °C)		[212]
	Al-LLZO	PEO	2.5×10^{-4}		[162]
	LLTO	PEO	8.8×10^{-5}		[188]
	Ta-LLZO	PEO	1.17×10^{-4} (30 °C)		[213]
	LATP	PAN	6.5×10^{-4} (60 °C)		[187]
	Li_6PS_5Cl	PEGMEA	4.6×10^{-4}		[214]

composite electrolyte with 10 wt.% SZZ-13 particles at 20 and 70 °C are 4.43×10^{-5} and 2.0×10^{-3} S·cm^{-1}, respectively.

Recent study has shown that the Li^+-insulating nanofillers with lattice defects can improve the ionic conductivity more effectively. For example, Li et al. [150] synthesized insulating fluorite $Gd_{0.1}Ce_{0.9}O_{1.95}$ (GDC) and $La_{0.8}Sr_{0.2}Ga_{0.8}Mg_{0.2}O_{2.55}$ (LSGM) nanoparticles with high concentration of oxygen vacancies to improve the ionic conductivity of the PEO-LiTFSI electrolyte. At 30 °C, the high ionic conductivity of both is above 10^{-4} S·cm^{-1}. To investigate the mechanism of ionic conductance, they applied two methods, namely Li solid-state NMR characterization and density functional theory (DFT) calculations. Li solid-state NMR showed that that Li^+ ions (> 10%) occupy a more fluid A2 environment in the composite electrolytes, indicating a strong interaction between the O^{2-} of LiTFSI and the surface oxygen vacancy of the nanoparticles. The interactions between LiTFSI and GDC, LSGM, and Al_2O_3 nanopowders die surface in polymer electrolyte were further studied by DFT calculations. As shown in Fig. 19(a), the electron accumulation between the O atom of $TFSI^-$ anion and the crystal surface indicates that a bond is formed between the $TFSI^-$ anion and the inorganic ceramic filler surface. Among them, the $TFSI^-$ adsorption capacity on GDC surface is the strongest, while that on Al_2O_3 surface is the weakest (Fig. 19(c)). The strong adsorption of $TFSI^-$ anion on the surface of oxidized particles would reduce the Li^+–$TFSI^-$ interaction and release more Li^+ ions, thus improving the ionic conductivity of GDC and LSGM-containing nanocomposite electrolytes (Fig. 19(b)). In addition, controlling the electronegativity of the filler surface can promote the dissociation of lithium and further improve the ionic conductivity of electrolytes. Liang et al. [151] used hydroxyapatite (HAP) with negative potential as filler for PEO-based SPE to effectively improve the ionic conductivity and mechanical strength of SPE. The surface negative charge on the HAP promotes the lithium dissociation through its attraction to Li^+ in electrochemical reactions (Fig. 19(d)). According to DFT calculations in Fig. 19(e), the unique surface with negative potential vacancies of HAP facilitates the lithium salt dissociation to generate more Li^+ with dissociation energy of 0.76 eV by attracting Li^+, which is superior to that without HAP (0.41 eV). The PEO-LiTFSI-HAP SPE owns a high ionic conductivity of 0.064 mS·cm^{-1} at 30 °C (Fig. 19(f)). Because of the higher conductivity of the HAP-containing electrolyte, the PEO-LiTFSI-HAP SPE-based $LiFePO_4$/Li cell exhibits higher capacities than the PEO-LiTFSI SPE-based cell in the temperature range from 30 to 100 °C at 1 C (Fig. 19(g)). Moreover, the PEO-LiTFSI-HAP SPE-based Li/Li cell can stably cycle for at least 200 cycles without short circuit at 0.05 mA·cm^{-2} and 60 °C due to the enhancement of the mechanical strength by the HAP nanofillers (Fig. 19(h)).

Besides the commonly used oxide nanoparticles, carbon quantum dots (CQDs) have been proved to be important nanofillers owing to the ultra-small size and abundance of oxygen-containing functional groups. Wei et al. [152] used well-dispersed CQDs with a diameter of 2.0–3.0 nm to prepare high-conductivity composite electrolytes. A large number of Lewis acid sites can effectively improve the dissociation degree of lithium and sodium salts by effectively adsorbing anions and the amorphous properties of PEO matrix, and therefore the PEO-$LiClO_4$/CQD and PEO-$NaClO_4$/CQD nanocomposite electrolytes show abnormally high ionic conductivity of 1.39×10^{-4} and 7.17×10^{-5} S·cm^{-1}, and the lithium ion transference numbers are 0.48 and 0.42, respectively.

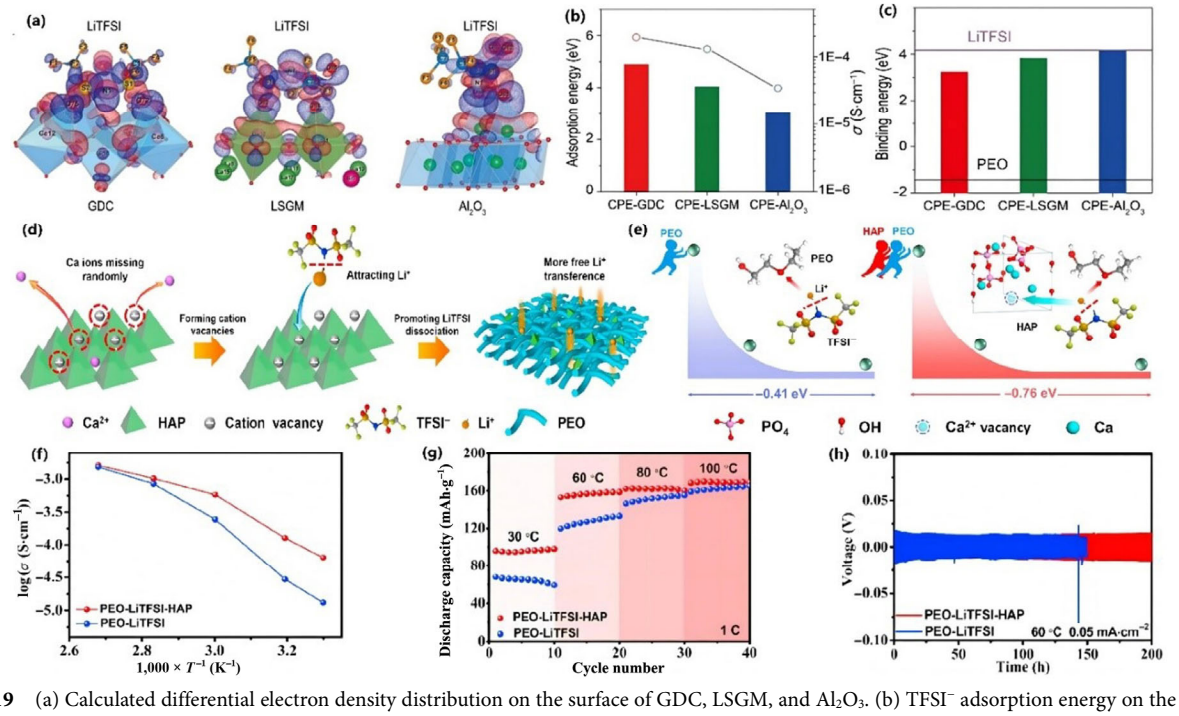

Figure 19 (a) Calculated differential electron density distribution on the surface of GDC, LSGM, and Al_2O_3. (b) $TFSI^-$ adsorption energy on the surface of the crystal and the corresponding experimental measured Li^+ ion conductivity. (c) Calculated Li binding energy of the $TFSI^-$ adsorbed on each ceramic substrate surface, free $TFSI^-$ (purple), and free PEO (black). Reproduced with permission from Ref. [150], © Wiley-VCH Verlag GmbH & Co. KGaA, Weinheim 2019. (d) Design of PEO-LiTFSI-HAP SPEs. (e) Schematic of DFT calculations of the dissociation energy of lithium salt in PEO-LiTFSI SPE and PEO-LiTFSI-HAP SPE. (f) Arrhenius ionic conductivity (σ) plots of PEO-LiTFSI-HAP SPE and PEO-LiTFSI. (g) Cycling performances (1 C) of the $LiFePO_4$-Li cells with PEO-LiTFSI-HAP SPE and PEO-LiTFSI SPE. (h) Galvanostatic cycling performances of the Li/SPE/Li symmetric cell at a current density of 0.05 mA·cm^{-2} at 60 °C. Reproduced with permission from Ref. [151], © Elsevier Ltd. 2021.

Apart from inorganic nanoparticles, organic nanoparticles built with different organic unites have superior chemical tailorability, large surface areas, and high thermal stability, and have also been used as fillers for nanocomposite polymer electrolytes. Liu et al. [153] synthesized mesoporous organic polymer (MOP) spheres by a self-template method, and then used them as nanofillers to prepare PEO-LiTFSI electrolyte membranes. With the addition of the MOP nanofillers, the composite electrolytes showed high ion conductivity of 4.4×10^{-4} S·cm^{-1} at 63 °C and thermal stability of over 270 °C and can effectively block Li dendrite growth. Zhou et al. [154] further fabricated a novel and flexible disk-like liquid crystal-based crosslinked solid polymer electrolyte (DLCCSPE) by controlling the ionic conductive channel through a one-pot photopolymerization of directional reactant, poly (ethylene glycol) diacrylate, and lithium salt. DLC disks also form columns in DLCCSPE and act as ionic conductive channels to facilitate ion transfer in the electrolyte. Therefore, the composite electrolyte has a higher ionic conductivity of 5.48×10^{-5} S·cm^{-1} at 30 °C than the pristine PEO electrolyte (7.93×10^{-6} S·cm^{-1}). Fu et al. [155] developed a new hybrid nanofiller via combining the ion-conductive soy proteins (SPs) and the ceramic nanoparticle, TiO_2. The chain configuration and protein/TiO_2 interactions in the hybrid nanofiller play critical roles in improving not only the mechanical properties but also the ion conductivity, electrochemical stability, and adhesion properties. Particularly, the ion conductivity of the CPE loaded with 5 wt.% TiO_2/(SP-open) hybrid nanofiller is 5×10^{-6} S·cm^{-1}, which is about one magnitude higher than that of the pure PEO-$LiClO_4$ electrolyte.

To further improve the electrolyte properties, MOFs are used as fillers in composite polymer electrolytes. MOFs, consisting of metal ion clusters and organic linkers are typical nanoporous materials, which can provide ideal accommodation for a variety of guest species. By absorbing Li-containing compounds or mixtures in the nanopores, MOFs are converted into lithium ion conductors. Owing to their nanoporous structure and high ionic conductivity, MOF derived ionic conductors are ideal fillers in composite polymer electrolytes. Zhu et al. [156] prepared a PEO-MIL-53(Al)-LiTFSI electrolyte by using MOFs MIL-53(Al) as a filler for all-solid-state LIBs. The MIL-53(Al) nanoparticles have a Lewis acidic surface interaction with $N(SO_2CF_3)_2^-$ anions, and the addition of the particles promotes the dissolution of LiTFSI to increase the ion conductivity. At the same time, the particles, as the crossing-linking center of PEO, can not only increase the thermal stability of the electrolyte, but also enhance the mechanical strength by building a robust network. The synthesized electrolyte has an ionic conductivity of 3.39×10^{-3} S·cm^{-1} at 120 °C, which is higher than that of the MIL-53(Al)-free electrolyte (9.66×10^{-4} S·cm^{-1}). Guo et al. [157] applied a typical MOF material (UIO-66) with the absorption of a nonvolatile and nonflammable Li-containing ionic liquid, i.e., LiTFSI in [EMIM][TFSI], where Li^+, $EMIM^+$, and $TFSI^-$ ions were mobile. The ionic conductivity of the solid electrolytes with 40 wt.% UIO/Li-IL increased by a factor of 37 to 1.3×10^{-4} S·cm^{-1} at 30 °C, and the lithium ion transference number increased to 0.35. The nanoporous UIO/Li-IL fillers can also effectively suppress the growth of Li dendrites in the PEO matrix, and the current density for stable Li plating/stripping in the nanocomposite electrolyte reached to 0.5 mA·cm^{-2}, which was much higher than that of the pristine PEO electrolyte.

Different from the abovementioned inert nanoparticles, a few active Li-containing ceramic electrolytes such as $Li_7La_3Zr_2O_{12}$ [158], $Li_{0.34}La_{0.56}TiO_3$ (LLTO), LATP [69], LAGP [159], and sulfides [160] are also used as fillers to further enhance the lithium ion transfer ability. Finite element simulations reveal that the ion conduction within the composite electrolytes mainly occurs at the ceramic–polymer interface [161, 162]. Recent researches suggest that Li ions can also diffuse through the ceramic electrolyte particles [70, 161]. Thus, the active filler-based composite electrolytes should exhibit higher ionic conductivity than the inert filler-incorporated electrolytes in theory. Hu et al. [163] deeply investigated the ionic transport mechanisms in different nanocomposite electrolytes by the solid-state NMR characterization technology combined with Li isotope labeling. In 2016, they prepared 50 wt.% LLZO microparticle-filled PEO-$LiClO_4$ electrolyte by ball-milling and following slurry coating, and then found that the Li ions favored the pathways through the LLZO ceramic phase instead of the PEO/LLZO interface or PEO matrices. They also investigated the ion transport pathways in other active nanofiller-modified composite electrolytes including LLZO NW/PAN-$LiClO_4$ [70], $Li_{3/8}Sr_{7/16}Ta_{3/4}Zr_{1/4}O_3$ nanoparticle/ PEO-LiTFSI [71], and $Li_{10}GeP_2S_{12}$ nanoparticle/PEO-LiTFSI [72], and proved that most of the Li ions are likely to transport at the active nanofiller/polymer interfaces rather than in the active particles. They also prepared LLZO microparticle/PEO-LiTFSI electrolytes with various LLZO contents (Figs. 20(a) and 20(b)), and then examined the compositional dependence of the three determining factors for ionic conductivity such as ion mobility, ion transport pathway, and active ion concentration [164]. They found that the ion mobility decreased, the ion transport pathway transited from polymer to ceramic routes, and the active ion concentration increased, when increasing the fraction of LLZO phase in the composite electrolytes (Fig. 20(c)). These changes in the ion mobility, transport pathway, and concentration collectively determined the ion conductivity change in the composite electrolytes. In addition, liquid additives altered ion transport pathways and increased the ion mobility, thus resulting in the significant increase of the ionic conductivity. Cui et al. [165] prepared a free-standing PPC/$Li_{6.75}La_3Zr_{1.75}Ta_{0.25}O_{12}$ (LLZTO) electrolyte through a doctor blade coating method for ambient temperature and flexible solid state lithium battery. The composite electrolyte had high ion conductivity (2.2×10^{-4} S·cm^{-1}, 20 °C), high ion transference number (0.75), wide electrochemical window (4.6 V), and satisfactory mechanical strength (6.8 MPa). The addition of LLZTO can reduce the crystallinity of PPC and promote the dissociation of lithium salt, together with the percolation behavior between PPC and LLZTO, improving the ionic conductivity of the composite electrolyte. Moreover, the solid $LiFePO_4$/Li battery showed excellent rate capability (5 C) and cycling stability (95%) at ambient temperature.

It should be noted in the nanoparticle-filled electrolytes, there are two or three ion-conduction pathways: the ion conduction pathways in the ion-conductive nanofillers, the polymer matrices, and the nanofiller/polymer interfaces, and usually the ion conductivity at the interfaces or the nanofillers is the highest. Therefore, arranging the nanofillers in lines is important to increase the ion conductivity by connecting the nanofillers or the interfaces for continuous ion transport pathways. Zhai et al. [166] presented an ice-templating-based method to construct vertically aligned and connected $Li_{1+x}Al_xTi_{2-x}(PO_4)_3$ nanoparticles in the PEO matrix to maximize

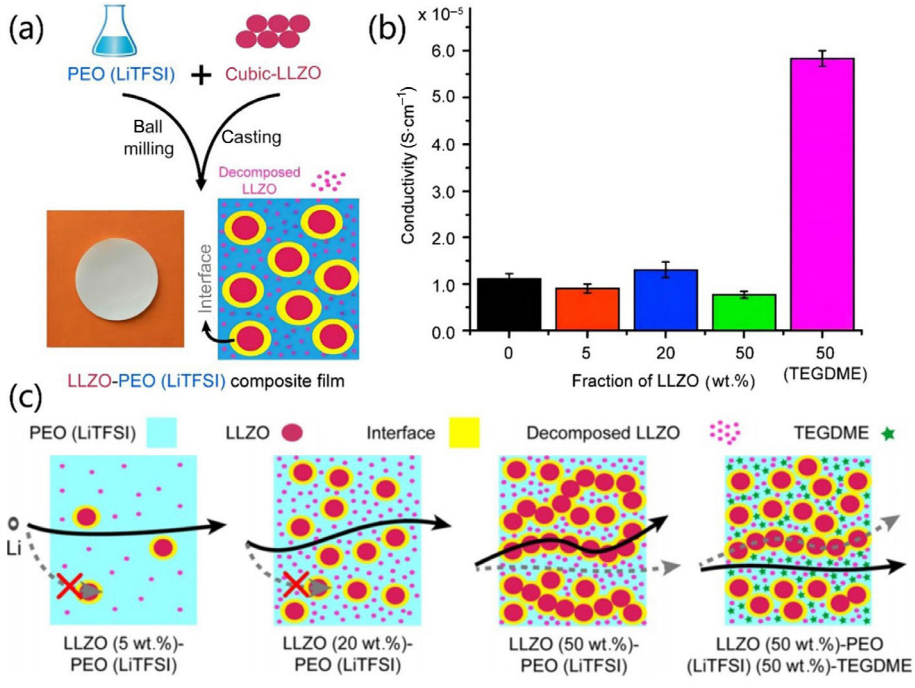

Figure 20 (a) Illustration of the preparation process of LLZO-PEO (LiTFSI) composite electrolytes. (b) Conductivity of PEO (LiTFSI), LLZO (5 wt.%)-PEO (LiTFSI), LLZO (20 wt.%)-PEO (LiTFSI), LLZO (50 wt.%)-PEO (LiTFSI), and LLZO (50 wt.%)-PEO (LiTFSI, 50 wt.%)-TEGDME. (c) Schematic description of the Li-ion pathways in the composite. Reproduced from permission from Ref. [164], © American Chemical Society 2018.

the ionic conduction. The vertically aligned ion-conductive ceramic fillers form fast pathways for Li^+ transport, and its conductivity reaches 0.52×10^{-4} S·cm^{-1}, which is 3.6 times that of the composite electrolyte with the randomly dispersed LATP NPs. In addition to arranging the nanoparticles vertically by the ice-templating-based method, Liu et al. [167] used external AC electric fields to induce the $Li_{1.3}Al_{0.3}Ti_{1.7}(PO_4)_3$ particles and poly(ethylene glycol) diacrylate in poly-(dimethylsiloxane) (LATP@PEGDA@PDMS) assembly into a three-dimensional connected network (Figs. 21(a) and 21(b)). The ionic conductivity of 2.4×10^{-6} S·cm^{-1} at room temperature is higher than that of the random one (8.0×10^{-7} S·cm^{-1}, Fig. 21(e)). This greatly improved ionic conductivity is attributed to the parallel alignment of the LATP particles and the constructed prolonged lithium-ion conductive pathways (Fig. 21(d)). It is clearly observed that the LATP@PEGDA domains were connected to each other and aligned into a stretched necklacelike structure (Fig. 21(c)).

However, the poor interaction between the ceramic nanoparticles and the polymer matrices and the severe agglomeration of the high-surface-area nanoparticles in the polymer matrices have a detrimental effect on the improvement on the electrical and mechanical properties of the electrolytes. Therefore, *in situ* generation of nanoparticles in the polymer matrices or surface functionalization of the nanoparticles are applied to improve the nanofiller dispersity for high-performance polymer electrolytes. Lin et al. [168] established an *in situ* hydrolysis method to obtain a high-monodisperse SiO_2 particle for further synthesis of PEO-based composite electrolyte. This method not only yields stronger PEO–SiO_2 interactions through the chemical bonding and mechanical wrapping, but also enables better SiO_2 dispersion in the PEO matrix, thus greatly increasing the effective surface area of the Lewis acid–base interaction. Both a lower degree of PEO crystallinity and a higher degree of $LiClO_4$ dissociation can be obtained simultaneously in the CPE, and the ionic conductivity is then further improved. Consequently, high ionic conductivities of 4.4×10^{-5} and 1.2×10^{-3} S·cm^{-1} are achieved at 30 and 60 °C, respectively. Li et al. [169] first modified LLZTO nanoparticles with polydopamine (PDA) and then synthesized LLZTO@PDA/PEO electrolyte by solvent casting method (Figs. 22(a) and 22(b)). The uniform polydopamine layer of about 5 nm in thickness on the surface of LLZTO particles was observed by the transmission electron microscopy (Fig. 22(c)). PDA has good compatibility with both inorganic LLZTO and organic PEO materials, which improves the wettability of LLZTO and PEO, resulting in a strong bond between LLZTO and PEO. Meanwhile, due to the excellent wetting ability of dopamine, the composite electrolyte has good compatibility and adhesion with the positive and negative electrodes of the lithium ion battery. This property improves interfacial contact at the electrode/solid electrolyte interface, thereby reducing the overall resistance of the battery. After modification with dopamine, the agglomeration problem of LLZTO particles in the polymer matrix is well improved (Figs. 22(d) and 22(e)). Thus, the ion conductivity of the composite electrolyte increased from 6.3×10^{-5} to 1.1×10^{-4} S·cm^{-1} at 30 °C (Figs. 22(g) and 22(h)), and the interfacial resistance between the composite electrolyte and lithium metal anode decreased from 308 to 65 Ω·cm^2 at 50 °C (Fig. 22(f)). Meanwhile, the discharge capacity curve at 0.2 C and 50 °C between 3.0 and 4.0 V shows that the composite electrolyte-based battery has better cycle stability over 50 cycles (Fig. 22(i)).

3.3.3.2 *One-dimensional (1D) nanofiller*

Compared to the 0D nanofillers, 1D nanowires such as $Mg_2B_2O_5$ nanowire, SiO_2 nanowire [170], and LLTO nanowire [171] with high aspect ratio embedded in polymer electrolytes can create longer continuous fast-ion transport pathways and significantly reduce the junction crossing (Li^+ must crosses a large number

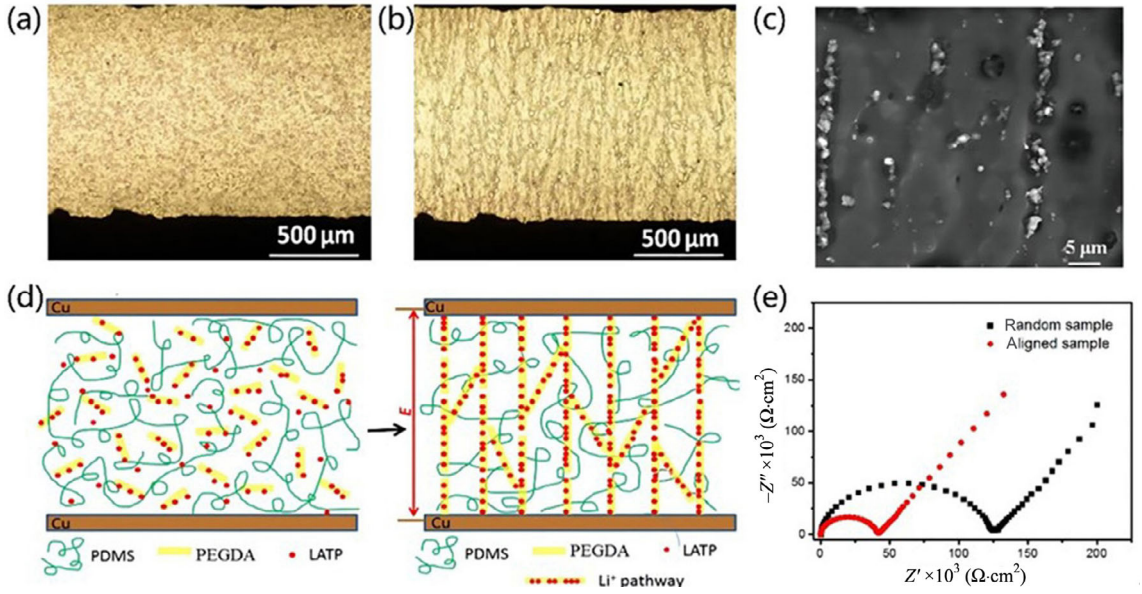

Figure 21 (a) Random morphology of the pristine LATP@PEGDA@PDMS (5:20:100, w/w/w) by *in situ* optical microscopy. (b) Alignment of LATP@PEGDA in PDMS under external AC electric field of 100 Hz and 400 V. (c) SEM morphology of the aligned LATP@PEGDA@PDMS after curing under external an AC electric field of 100 Hz and 400 V. (d) Illustration of electric-field-directed parallel alignment architecting 3D lithium-ion pathways. The electric-field direction is indicated by the vertical arrow. (e) Electrochemical impedance spectroscopy for the LATP@PEGDA@PDMS with or without an external AC electric field at 25 °C. Reproduced from permission from Ref. [167], © American Chemical Society 2018.

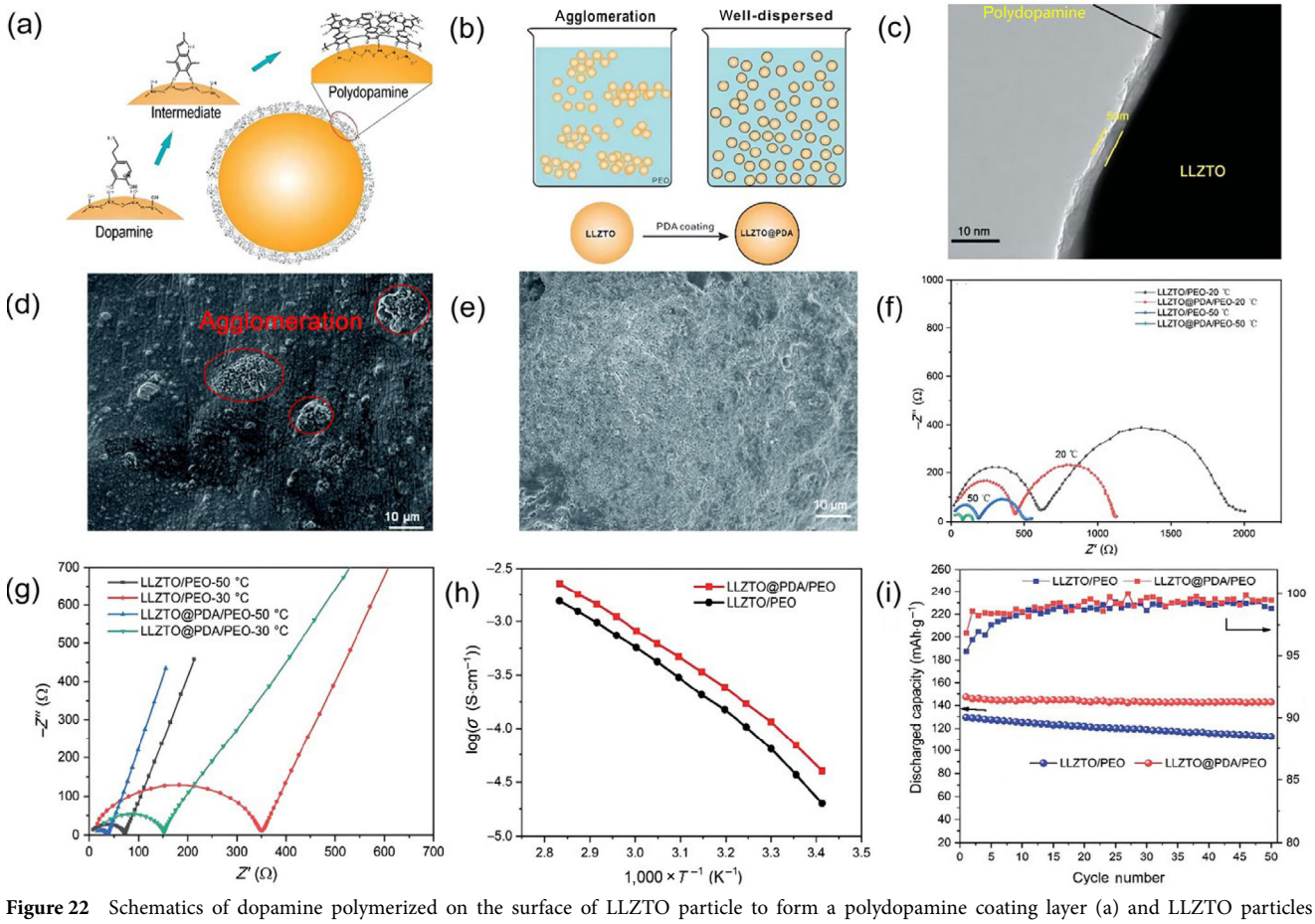

Figure 22 Schematics of dopamine polymerized on the surface of LLZTO particle to form a polydopamine coating layer (a) and LLZTO particles (coated and uncoated with PDA) dispersion in PEO solution (b). (c) TEM micrograph of the PDA coating layer on the LLZTO particle. SEM micrographs of (d) LLZTO/PEO and (e) LLZTO@PDA/PEO. (f) Nyquist plots of lithium symmetric cells at 20 and 50 °C. (g) Nyquist plots of LLZTO@PDA/PEO and LLZTO/PEO at 30 and 50 °C. (h) Arrhenius plots of LLZTO@PDA/PEO and LLZTO/PEO electrolytes in the temperature range from 80 to 20 °C. (i) Discharge capacity retention and Coulombic efficiency evolution with cycle number of Li|SSE|$LiFePO_4$ all-solid-state batteries with a rate of 0.2 C at 50 °C. Reproduced from permission from Ref. [169], © The Royal Society of Chemistry 2019.

of particle-particle junctions in the 0D nanoparticle-based electrolytes because of the incontinuity of the nanoparticles or the nanoparticle/polymer interfaces). Tao et al. [172] reported PEO-LiTFSI electrolytes filled with $Mg_2B_2O_5$ nanowires. The average diameter of these nanowires was about 270 nm. The electrolyte sample with 10 wt.% $Mg_2B_2O_5$ nanowires had a high ionic conductivity of up to 1.53×10^{-4} and 3.7×10^{-4} S·cm^{-1} at 40 and 50 °C, respectively, attributing to the improved motion of the PEO chains and the increased Li migrating paths at the interfaces between the $Mg_2B_2O_5$ nanowires and the PEO-LiTFSI matrices. The interaction between the $Mg_2B_2O_5$ nanowires and the $-SO_2-$ groups in the $TFSI^-$ anions also contributes to the improvement of the ion conductivity. The maximum stress of the nanofilm containing 5 wt.% $Mg_2B_2O_5$ nanowires is 2.29 MPa, which is much higher than that of the electrolyte without nanowires (1.31 MPa). Liu et al. [173] synthesized a solid composite polymer electrolyte with Y_2O_3-doped ZrO_2 (YSZ) nanowires that are rich in positive-charged oxygen vacancies. The oxygen vacancy in YSZ has a positive charge and can act as a Lewis acid site in a composite polymer electrolyte, binding to anions and then releasing more lithium ions. Compared with the nanofiller-free electrolyte (3.62×10^{-7} S·cm^{-1}), the electrolyte filled with 7 mol% YSZ nanowires has the highest ionic conductivity of 1.07×10^{-5} S·cm^{-1} at 30 °C, while the composite polymer electrolyte with 0D YSZ nanoparticles only shows 2.98×10^{-6} S·cm^{-1}. It indicates that the nanowires form a more continuous fast-ion conduction pathway than the 0D nanoparticles.

Cui et al. [65] further studied the effect of the orientation of the LLZO nanowires on the ionic conductivity of the PAN-$LiClO_4$ electrolyte. The ionic conductivity of the electrolyte without nanofillers is very low, i.e., 3.62×10^{-7} S·cm^{-1}, while the LLZO nanoparticle and random LLZO nanowire-containing electrolytes show higher conductivities of 1.02×10^{-6} and 5.4×10^{-6} S·cm^{-1} at room temperature. When the nanowires are arranged, the ion conductivity reaches the highest (6.05×10^{-5} S·cm^{-1}), which is one order of magnitude higher than the polymer electrolytes with the randomly aligned nanowires. The large enhancement in conductivity is attributed to a fast ion-conducting pathway with no cross-junctions on the surfaces of the aligned nanowires (Fig. 23). Comsol multiphysics numerical analysis of the ion distribution in composite polymer electrolytes with the nanowires at different orientation angles (0°, 30°, 45°, 60°, and 90°) is also utilized to prove the faster ion transport pathways at the LLZO/PAN interfaces (1.26×10^{-2} S·cm^{-1} at 30 °C, comparable to that of liquid electrolyte).

In addition to the nanowires, nanorods and nanotubes, as new designed structures of 1D ceramic nanofillers, also greatly contribute to the improvement of the composite electrolyte ion conductivity. Romero et al. [174] prepared hydrogen titanate nanotube filler-based PAN-$LiClO_4$ composite electrolytes, and then combined with two characterization methods, Raman microscopy analysis and *ab initio* molecular dynamics simulations to reveal the ion conduction mechanism. The acidic hydrogen titanate nanotubes can promote the dissociation of lithium perchlorate at the interface between the polymer and the nanotube fillers, and thus the PAN-$LiClO_4$ composite electrolyte with 10 wt.% nanofillers showed a high ionic conductivity of ~ 4×10^{-4} S·cm^{-1} at room temperature, which was almost two orders of magnitude higher than the original electrolyte. Guo et al. [175] synthesized $Al_4B_2O_9$ (ABO) nanorods by an economical sol-gel method and then added ABO into PEO matrix to prepare PEO based SPEs (ASPEs). Due to the longer-range ordered Li^+ transfer channels generated by the interaction between the ABO nanorods and PEO, the optimal ASPE exhibited high ionic conductivities of 4.35×10^{-1} and 3.1×10^{-1} S·cm^{-1} at 30 and 60 °C, respectively.

3.3.3.3 *Two-dimensional (2D) nanofiller*

In addition to the 0D and 1D inorganic nanofillers, 2D graphene oxide (GO) also acts as an effective additive to enhance the performance of polymer electrolytes, due to its unique laminated structure, high specific surface area, abundant oxygen-containing functional groups, strong mechanical strength, and high thermal stability [176]. Yuan et al. [177] synthesized solid PEO-$LiClO_4$-GO nanocomposite electrolyte by solution blending and evaporation casting method (Fig. 24(a)). The PEO electrolyte containing 0.5% GO shows a wave-like morphology and the GO sheets appear to be well integrated into the polymer matrix (Figs. 24(b) and 24(c)). With the addition of GO nanosheets,

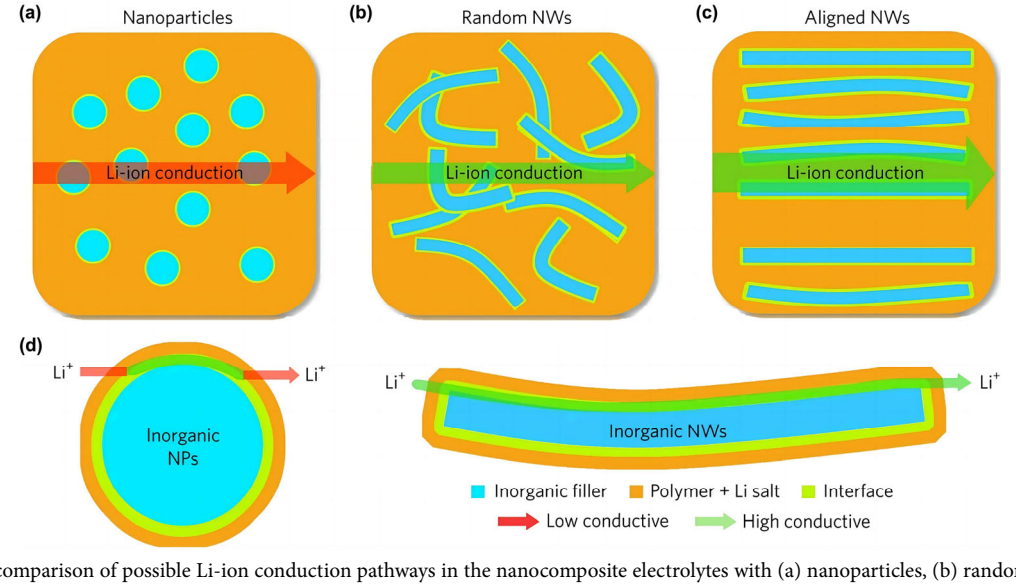

Figure 23 The comparison of possible Li-ion conduction pathways in the nanocomposite electrolytes with (a) nanoparticles, (b) random nanowires, and (c) aligned nanowires. (d) Compared with the isolated nanoparticles, the random nanowires could supply a more continuous fast conduction pathway for Li ions and the aligned nanowires are free of crossing junctions. Reproduced with permission from Ref. [65], © Nature Publishing Group 2017.

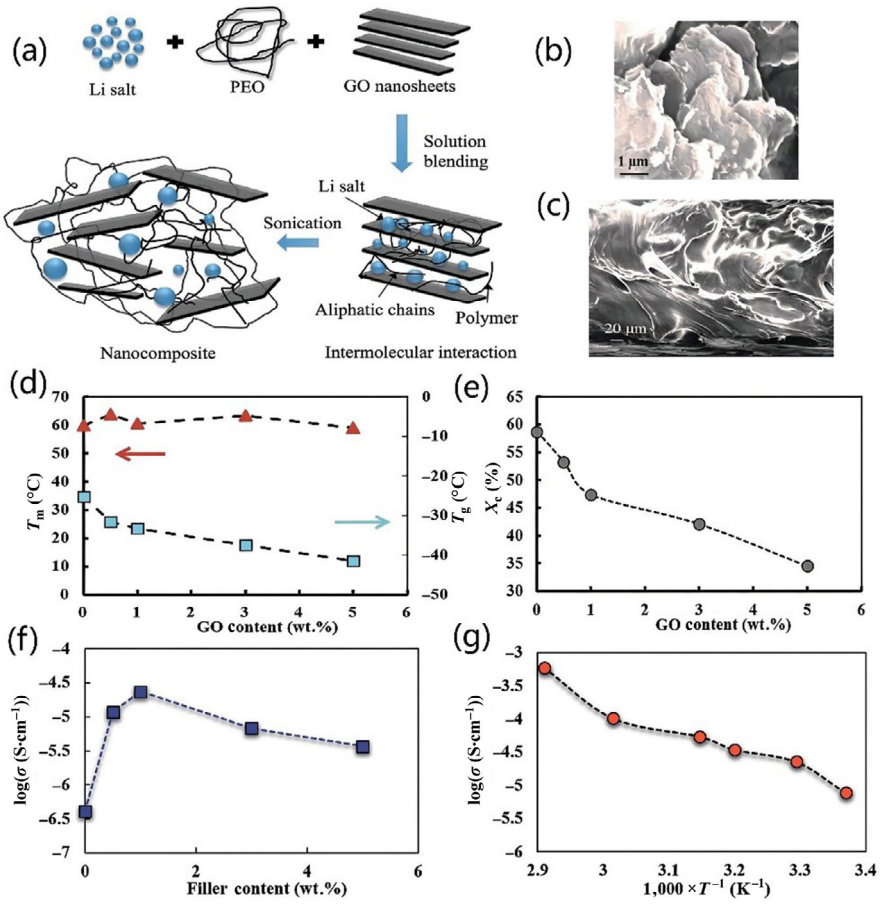

Figure 24 (a) The preparation schematic of PEO/GO/Li salt membrane. (b) SEM image of GO. (c) SEM image of cross-section of 0.5 wt.% GO/PEO-Li polymer electrolyte. (d) Melting point (T_m) and glass transition temperature (T_g) of polymer electrolyte films. (e) Crystalline fraction (Xc) of polymer electrolyte films. (f) Ionic conductivity (σ) at room temperature of polymer electrolyte films. (g) Temperature dependence of ion conductivity (1 wt.% GO content). Reproduced with permission from Ref. [177], © The Royal Society of Chemistry 2014.

the T_g of the polymer electrolyte decreases (Fig. 24(d)) and the proportion of amorphous regions increases (Fig. 24(e)), which could improve the mobility of the polymer chains. By comparing the fraction of free ClO_4^- calculated by the FTIR spectra of the pure PEO and nanocomposites with different GO contents, they found that the number of dissociated lithium ions in pure PEO was about 70%. With the addition of the GO sheets to the polymer electrolyte, the free ions increase to a maximum of 80% in the 1 wt.% GO-based electrolyte. This suggests that the GO sheets can also promote the dissociation of lithium salts by weakening the bonds between the ion pairs, and leading to an increase in carrier concentration. The combination of these factors leads to an increase in the ionic conductivity of the composite electrolyte (Figs. 24(f) and 24(g)), and the room-temperature ionic conductivity of the 1 wt.% GO-containing composite electrolyte (~ 10^{-5} S·cm^{-1}) is about two orders of magnitude greater than that of the pristine electrolyte (~ 10^{-7} S·cm^{-1}).

A few polymers such as PEG [178] and polymeric ionic liquids (PILs) [179] are further used to functionalize GO to enhance the compatibility with the polymer matrices and the dispersion of graphene in the polymer matrices, thus resulting in the increased Lewis acid–base interactions with lithium salts. The highly dispersed 2D graphene in the polymer matrix can also form 3D continuously interconnected ion conduction channels, and greatly enhance the segment motion ability of the polymer chain, thus further increasing the Li^+ ionic conductivity of the composite polymer electrolyte (~ 10^{-4} S·cm^{-1} at room temperature) [176, 178]. In addition, the incorporation of the graphene materials can improve the mechanical strength and thermal stability of the composite polymer electrolytes. Although a few studies have shown that the graphene oxides and the polymer-functionalized graphene oxides are insulators, safety issues such as internal short circuits, heat, and ignition should be carefully considered because the graphene-based composite polymer electrolytes also act as separators in the batteries.

Other 2D nanomaterials such as vermiculite nanosheet, g-C_3N_4 nanosheet [180], boronnitride (BN) nanoplate [181], MXene nanosheet [182], lithium montmorillonite nanoplate [183], and MgAlOH nanosheet [184] are further used as effective nanofillers. Li et al. [182] prepared PEO-LiTFSI composite solid electrolytes with a small amount of $Ti_3C_2T_x$ nanosheets uniformly dispersed in the matrices by a simple aqueous solution mixing method. The addition of the hydrophilic 2D MXene nanoflakes (~ 1 nm in thickness) can weaken the crystallization of PEO and enhance its segment motility. The ionic conductivity of the nanocomposite electrolyte containing 3.6 wt.% MXene was the highest at 28 °C (2.2 × 10^{-5} S·cm^{-1}). Compared with 1D and 2D nanofillers, MXene was more effective in improving the ionic conductivity. It must be noted that MXenes have high electronic conductivity, and the application of high-concentration MXenes in composite electrolyte membrane may cause battery short circuit. Zheng

et al. [185] added single-layered-double-hydroxide nanosheets (SLNs) to PVDF-HFP and obtained robust CPEs, which provided a high room temperature ionic conductivity of 2.2×10^{-4} S·cm^{-1} (25 °C), a superior Li^+ transference number (0.78), and a wide electrochemical window (4.9 V), under a low SLN load (1 wt.%). DFT calculations showed that the SLNs can facilitate the dissociation of LiTFSI and the immobilization of $TFSI^-$, thus enhancing the Li^+ flux in the polymer matrix. Coupled with the enhancement of the mechanical strength of the CPEs, the Li symmetric cells showed a stable cycle (over 900 h at 0.1 mA·cm^{-2}, 25 °C). In addition, all-solid-state Li|$LiFePO_4$ batteries can run stably more than 190 cycles with a high capacity retention rate of 98.6% at 0.1 C and 25 °C. Chen et al. [186] prepared two-dimensional porous graphitic carbon nitride (PGCN) nanosheets by a simple hydrothermal and calcined two-step method, and further obtained a PVDF-HFP/PGCN/LiFSI composite electrolyte film with excellent properties (e.g., high ionic conductivity of 2.3×10^{-4} S·cm^{-1} at 30 °C). The excellent performance of the electrolyte membrane can be attributed to the addition of the PGCN nanosheets containing a large number of nanopores with a specific surface area of up to 53.1 m^2·g, which is conducive to the uniform distribution of PGCN nanosheets in the polymer phase and the formation of rich organic/inorganic interfaces, further enhancing the transmission of lithium ions across the interfaces. The solid Li/$LiFePO_4$ battery showed excellent cycling performance with a 71% capacity retention after 400 cycles at 0.5 C and 26 °C.

3.3.3.4 3D nanofiller

As can be seen from the previous sections, the improvement of ion conductivities of the 0D, 1D, and 2D nanofillers is mostly relied on the rapid interphase conduction between the nanofillers and the polymer matrices. With the increase of the filler ratio, the interphase volume and the conductivity should also increase. However, the nanoparticles tend to aggregate at high concentration, which would destroy the interphase infiltration network and fail to further improve the conductivity. In order to solve this problem, an effective strategy (i.e., solution infusion) is proposed by filling the polymer matrices into 3D nanofiller network structures, which can avoid the nanoparticle agglomeration and meanwhile provide 3D continuous pathways for ion conduction with high nanofiller contents. There are a few ways to construct 3D nanofiller frameworks, such as electrospinning [162, 187], aerogel, hydrogel [188], 3D printing [189], and template methods [190]. Guo et al. [191] prepared a composite polymer electrolyte with 3D porous LLZO networks filled with PEO-Li salt. The 3D garnet framework is fabricated via a polymeric sponge method, using low-cost polyurethane foam as a template. The interconnected 3D garnet frames not only enhance the electrochemical stability, thermal stability, and mechanical stability of the composite electrolyte, but also form a continuous lithium ion transport channel, thereby improving the ionic conductivity. The ionic conductivity of the 3D garnet-based composite electrolyte at 30 °C is 1.2×10^{-4} S·cm^{-1}, about twice that of the garnet particle reinforced composite electrolyte by the traditional solution casting method. Xiong et al. [192] designed a new composite solid electrolyte of PMMA-coated LATP-PVDF-LiTFSI. On one hand, the interconnected LATP@PMMA framework is constructed through the interaction between PVDF and PMMA molecules coated on the LATP particles. On the other hand, the ion transport in the LATP/PVDF interface region is promoted through the coordination of the C–O group and Li^+ in PMMA. Continuous Li^+ transport paths were generated in the LATP framework and the LATP/PVDF interphase, resulting in an excellent ionic conductivity of 1.23×10^{-3} S·cm^{-1} at room temperature. The $LiNi_{0.5}Co_{0.2}Mn_{0.3}O_2$/Li battery has a high capacity retention rate of 91.2% after 150 cycles at 0.5 C.

The commonly-used 3D conductive ceramic frameworks are usually composed of ion-conductive LLZO, LLTO, LAGP, and LATP. High-conductivity composite electrolytes can also be prepared with inert ceramic frameworks with vertical pores such as alumina. Cui et al. [66] have reported composite electrolytes (denoted as APCE) with densely packed, vertically aligned, and continuous nanoscale ceramic/polymer interfaces, using PEO as matrices and surface-modified porous aluminum oxide as the 3D ceramic scaffold (Fig. 25(a)). They believe that the 0D nanoparticle filler-based electrolyte has short and isolated fast-ion conduction pathways, and the nanowire-based electrolyte has longer and more continuous fast-ion transport pathways. To further prolong the ion transport pathways, the authors used anodized aluminum oxides to form directional and vertically-aligned continuous ceramic/polymer interfaces (Fig. 25(b)). The ionic conductivity of the APCE electrolyte is 5.82×10^{-4} S·cm^{-1} (Figs. 25(c) and 25(d)), an order of magnitude higher than that of the original electrolyte (SPE, 1.69×10^{-5} S·cm^{-1}), and about four times higher than those of the 0D nanoparticle-filled electrolyte (CSPE-NPs, 3.13×10^{-5} S·cm^{-1}) and 1D nanowire-filled electrolyte (CSPE-NW, 4.13×10^{-5} S·cm^{-1}). They also calculated that the ceramic/polymer interfacial ion conductivity can reach 10^{-3} S·cm^{-1} at 0 °C.

It should be noted that the thickness of the composite polymer electrolyte films with the ceramic frames is usually large, which seriously affects the energy density of lithium-ion batteries and meanwhile causes the increase of the battery resistance. In addition, the weak and cross-linked ceramic networks may affect the flexibility of the composite electrolytes. In order to achieve high flexibility of composite polymer electrolyte membranes, a few organic materials like PVDF nanofiber [193], polyamide 6 (PA6) microfiber non-woven fabric [194], cellulose nanofiber (CNF) [195], aramid nanofiber (ANF) [73, 196], and polyimide nanofiber [197] are further utilized as 3D nanofiller frameworks. However, the large nanofiller size and the limited contact area and interaction between the non-conductive nanofillers and the polymer matrices may be detrimental to the ionic conductivity. Sun et al. [198] found that the 3D glass fiber frame-supported PEO-LiTFSI electrolyte had a slightly lower ionic conductivity (1.9×10^{-4} S·cm^{-1}) at 60 °C than the pristine PEO-LiTFSI electrolyte, although its mechanical strength, electrochemical window, and lithium dendrite inhibition ability were greatly enhanced.

To improve the ionic conductance of the organic frameworks and their composite electrolytes, Kawakami et al. [197] prepared an ion-conductive PEO-grafted polyimide (PI-g-PEO) nanofiber network by an electrospinning method, and then filled the PEO-LiTFSI electrolyte into the 3D porous PI-g-PEO network to obtain thin and flexible composite polymer electrolytes (Figs. 26(a)–26(c)). The thickness of the PI-g-PEO nanofiber framework-supported PEO-LiTFSI membrane was about 19 μm, similar to the thickness of the pristine nanofiber framework (20 μm). Due to its unique structural integrity of the PI-g-PEO nanofiber framework, the mechanical strength of the solid-state PEO-LiTFSI electrolyte

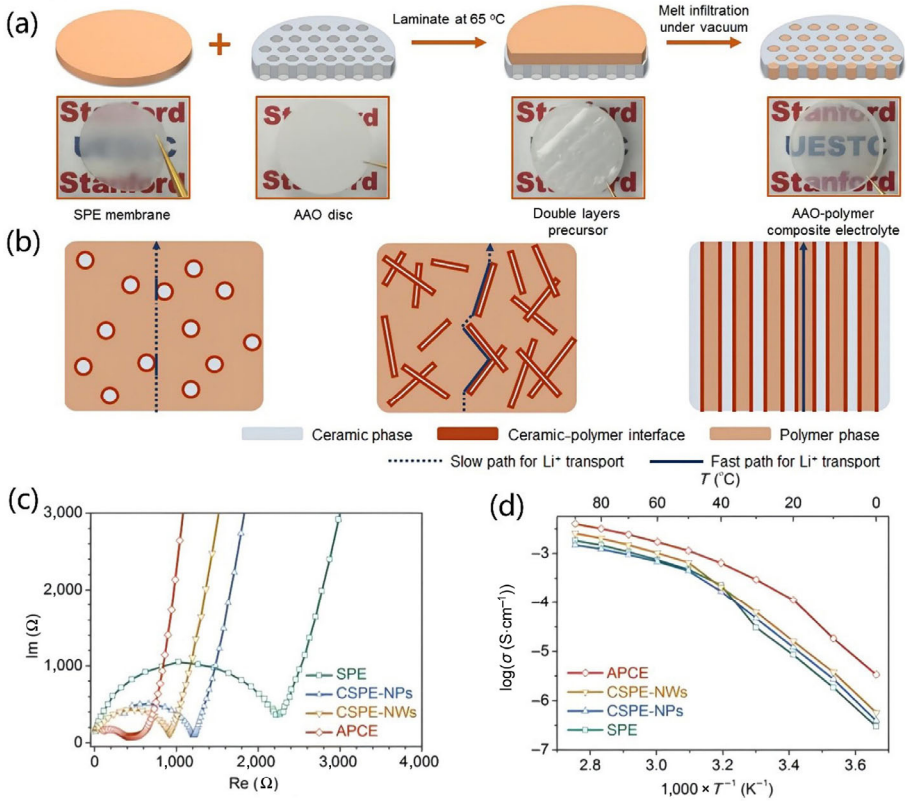

Figure 25 (a) Schematic of fabrication of alumina framework-based composite electrolytes. (b) Schematics of composite electrolyte with three ceramic/polymer interfaces. (c) Impedance spectra measured at room temperature. (d) Temperature dependence of ionic conductivities. Reproduced with permission from Ref. [66], © American Chemical Society 2018.

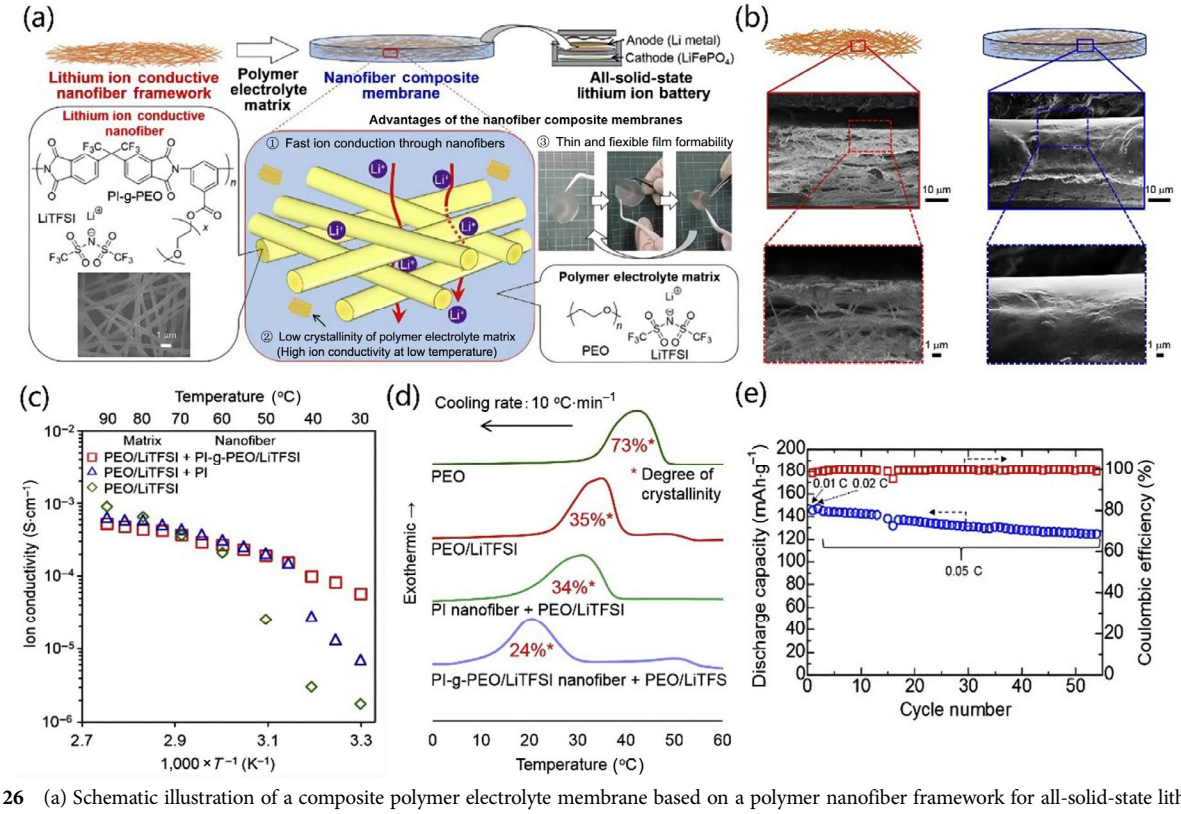

Figure 26 (a) Schematic illustration of a composite polymer electrolyte membrane based on a polymer nanofiber framework for all-solid-state lithium-ion batteries. (b) Cross-sectional SEM images of the PI-g-PEO nanofiber film and the nanofiber-based composite electrolyte. (c) Ion conductivities of PI-g-PEO nanofiber composite (red square), PI nanofiber composite (blue triangle), and PEO/LiTFSI membranes (green diamond). (d) DSC curves of PEO, PEO/LiTFSI, PI nanofiber composite, and PI-g-PEO nanofiber composite membranes. (e) Cycle performance of the coin cell consisted of Li/PI-g-PEO nanofiber composite membrane and $LiFePO_4$ at 0.05 C except the 1st and 2nd cycles at 60 °C. Reproduced with permission from Ref. [197], © Elsevier B.V. 2019.

increased from 0.45 to 3.3 MPa. The PI-g-PEO nanofiber-supported composite electrolyte film also had a low crystallization temperature of 31 °C and a PEO crystallinity of 24% (Fig. 26(d)), resulting in high mobility of the PEO chain segments and the increase of the ionic conductivity of the composite electrolyte film (1.0×10^{-4} S·cm^{-1} at room temperature, Fig. 26(c)). Furthermore, the composite electrolyte-based battery displayed a high discharge capacity of over 120 mAh·g^{-1} after 50 cycles at 0.05 C and 60 °C (Fig. 26(e)). In order to further increase the ionic conductivity of the composite electrolytes, Lee et al. [123] filled a high-ion-conductivity plastic nitrile in a high-strength PET framework film, and the PET nonwoven-supported ETPTA-succinonitrile-LiTFSI composite electrolyte with a thickness of 25 μm showed a high ionic conductivity of 5.7×10^{-4} S·cm^{-1} at 30 °C.

3.3.4 *Synergistic effect*

Above we have introduced three kinds of modification strategies on the polymer electrolytes regarding additives, and each modification method has its own merits and disadvantages. Appropriate addition of these additives can increase the ionic conductivity of the polymer electrolytes, but excessive additives usually result in the decrease in the ionic conductivity or severe degradation of other properties. The utilization of two or more additives may further increase the ionic conductivity or improve other properties based on the synergistic effect. Likewise, the integration of two or three modification methods can also achieve the strengthening effect.

The commonly-used method is the combination of nanoparticle filling and plasticizer addition. Klongkan et al. [115] prepared a PEO-$LiCF_3SO_3$ based composite solid electrolyte by ball milling and hot pressing using nano alumina as filler and DOP and PEG as plasticizers. Al_2O_3 can destroy the ordered arrangement of the polymer side chains, reduce the crystallinity, and further lead to the increase of amorphous phase. At the same time, the plasticizers of DOP and PEG can further increase the amorphous phase content in the polymer electrolyte. The PEO-15 wt.% $LiCF_3SO_3$ electrolyte showed a room-temperature ionic conductivity of the order of 10^{-6} S·cm^{-1}, but the conductivity increased to 10^{-5}–10^{-4} S·cm^{-1} by adding nano Al_2O_3 and plasticizer to the PEO-$LiCF_3SO_3$ SPE. The maximum ionic conductivity of the 20 wt.% DOP-modified PEO-$LiCF_3SO_3$ composite was as high as 7.60×10^{-4} S·cm^{-1}.

Chen et al. [119] synthesized a PEO-based solid electrolyte with a solid oxide lithium ion conductor of LLZO and a SN plasticizer by a solution casting method. The plasticity of SN can effectively solve the interface contact problem between the electrode and the electrolyte, while LLZO can further improve the electrochemical window and mechanical strength of composite electrolyte. Both of them also have positive effects on increasing the concentration of free lithium ion and inhibiting the crystallization of PEO. The ionic conductivity of the PEO-LiTFSI-7.5% LLZO-10% SN electrolyte was the highest at room temperature (1.19×10^{-4} S·cm^{-1}). In addition, the electrolyte had good electrochemical stability (5.5 V vs. Li/Li^+) and good interface compatibility with lithium electrode. The electrolyte-based cells had an initial discharge capacity of 130.2 mAh·g^{-1} and remained 80.0% of the initial capacity after 500 cycles at 1 C. The batteries can also work well at lower temperatures (30 and 45 °C).

In addition to adding plasticizers and nanofillers at the same time, the combination of nanoparticle filling and polymer blending is also proven as an effective modification method. Wang et al. [215] discovered that the Young's modulus (4.73 MPa) of PEO/LLZTO electrolyte was much lower than that of the PVDF-HFP/LLZTO electrolyte (12.3 MPa), but the ionic conductivities of the PEO/LLZTO electrolyte (1.83×10^{-5} and 1.86×10^{-4} S·cm^{-1}) were much higher than those of the PVDF-HFP/LLZTO electrolyte (3.68×10^{-7} and 3.68×10^{-6} S·cm^{-1}) at 21 and 60 °C. Therefore, LLZTO powder was selected as the filler to be added into PEO and PVDF-HFP mixed matrices to prepare composite electrolytes with comprehensively-updated properties. The PVDF-HFP blended electrolyte membrane with 40% LLZTO had a high tensile strength of 3.5 MPa and a modulus of 53.5 MPa (~ 10 times that of PEO/LLZTO membrane) and ionic conductivity of 4.20×10^{-5} S·cm^{-1} at 60 °C. The Li/Li symmetric battery equipped with this new composite electrolyte can cycle steadily over 600 h, while a control battery using the PEO/LLZTO electrolyte short-circuited within 100 h. In addition, the composite electrolyte-based solid-state $LiFePO_4$/Li full battery can maintain 93.4% of initial capacity after 140 cycles. Lim et al. [216] first blended PEO with PMMA and then added silica aerogel particles as inert inorganic fillers to the PEO-PMMA-$LiClO_4$ electrolyte to obtain a solid polymer electrolyte with high ionic conductivity and improved thermal stability. Silica aerogel powder with high specific surface area provided abundant Lewis acid centers, which can induce Lewis acid–base interaction between the polar surface of the ceramic particles and lithium ions, and promote the dissociation of lithium salts. XRD and FTIR analyses showed that the blending of PMMA and PEO can effectively suppress the crystallization of the polymer and lower the glass transition temperature. Due to the synergistic effect of the silica particle and PMMA, the composite electrolyte with PEO:PMMA = 8:1 and 8% silica showed the highest ionic conductivity of 1.35×10^{-4} S·cm^{-1} at 30 °C and excellent mechanical stability.

3.3.5 *Remarks*

Adding organic plasticizers in polymer electrolytes is a commonly-utilized method to increase the ionic conductivity. Due to their high dielectric permittivity, liquid carbonates are usually applied as plasticizers to adjust the polymer interchain interactions and the polymer polar group-Li^+ and anion-Li^+ interactions, thus lowering the activation energy for fast ion motion; however, these solvents can cause electrolyte leakage, flammability, electrochemical instability, and mechanical property degradation. Similarly, adding high-thermostability ionic liquids into the polymer electrolytes can also weaken the polymer segment interaction and promote the polymer segment movement and the lithium salt dissociation, but the mechanical properties also become poor. In contrast, utilizing oligomer polymers can both improve the thermostability and mechanical strength, and meanwhile increase the ionic conductivity by decreasing the polymer matrix crystallinity. As another solid-state plasticizer, succinonitrile imparts a plastic character below its melting point and can greatly increase the ionic conductivity by solvating lithium salts and reducing the polymer crystallinity; however, it has issues such as side reactions with lithium metals and insufficient mechanical properties. Improving the interface stability with lithium anodes by functional additives and confining succinonitrile in high-strength substrates would facilitate their applications in solid-state metallic lithium batteries.

The ionic conductivity and even other properties can be also improved by simply blending two or more polymers, and the increase of the ionic conductivity is usually attributed to the inhibition of the polymer crystallization and the facilitation of the lithium salt dissociation. Of course, the strong interaction between the polymer matrices and the polymer additives would strengthen the mechanical properties, but this may cause the decrease in the ionic conductivity. Thus, the compatibility of the mixed polymers and the interactions between the polymers should be carefully considered when preparing the blend polymer electrolytes.

Similar to the functionality of the abovementioned methods, micro-/nano-particle filling in the polymer electrolytes can also increase the ionic conductivity by inhibiting the polymer matrix crystallinity and facilitating the lithium salt dissociation. Another important advantage of the nanoparticle filling is the formation of many fast-ion pathways at the nanoparticle/polymer matrix interfaces or on the nanofiller surfaces. In comparison with the 0D nanofillers, 1D and 2D nanofillers can make use of their morphological advantages to generate continuous line and surface long-range ion transport channels. The further construction of 3D ion transport pathways (at the interfaces or the 3D substrates) by filling polymer electrolytes in 3D porous frameworks can effectively avoid the agglomeration of the low-dimensional nanofillers, and make high-concentration filling possible, thus significantly improving the ionic conductivity and even the mechanical strength, thermal stability, and electrochemical stability. The adjustion of the interactions between the nanofillers and the polymer matrices/lithium salts would greatly change the polymer crystallinity and the free ion concentration, while the arrangement orientation of the nanoparticles parallel to the electrical field can shorten the ion transport distance for high ionic conductivity.

Each modification strategy has its own advantages and drawbacks as we have mentioned above. The combination of two or more methods would further improve the ionic conductivity or other properties to facilitate the viable application of polymer electrolytes in solid-state batteries based on the synergistic effect.

3.4 Electrolyte micromorphology adjustion

3.4.1 Pore structure

Apart from the chemical composition and structure, the morphology characteristics such as pore and thickness also have an important impact on the electrical and mechanical properties of the solid polymer electrolytes, although there are only a few researches on this issue. The pore size and porosity effect on the GPEs have been deeply studied, and it is found that the porosity, pore size, and pore uniformity determine the ionic conductivity and mechanical strength of the GPEs [217–219]. In general, the GPEs with higher porosity can accommodate more liquid polar electrolytes and thus exhibit higher ionic conductivity, but the mechanical strength would decrease. Moreover, too big pore sizes would reduce the contact area or interface area between the polymer matrices and the liquid electrolyte, which is detrimental to the ionic conductivity. The interconnected pore structure is conducive to the continuous transport of the ions. Thus, it is necessary to exploit polymer matrices with continuous and uniform pores, and proper porosity to get a balance between the high ionic conductivity and the mechanical strength [220].

Extraction and phase inversion methods are usually used to prepare pours polymer matrices for the GPEs with certain mechanical strengths, and the pore structure severely affects the polymer composition, solvent type, and the evaporation time and temperature [221]. The extraction method was found by the researchers in Bellcore Laboratory in 1994 [222, 223]. They prepared porous PVDF-HFP films using low-boiling diethyl ether as an extraction agent with the assistance of the phase separation of the solvents, and found that the high porosity would result in the increase of the ion conductivity and the decrease of the mechanical strength of the gel polymer electrolyte. Later, porous PVDF-HFP/PEG hybrid polymer electrolytes were prepared by the convenient casting method and the following extraction of PEG by water [221]. The PEG molecules were extracted by water from the PVDF-HFP polymer membrane during the casting process to generate pores (Figs. 27(a)–27(c)). The porosity on the ionic conductivity of the electrolyte was also explored, and it was found that with the increase of PEG concentration or the casting time, both the porosity and the ionic conductivity gradually increased. The ion conductivities of all the polymer electrolyte systems were higher than 10^{-3} S·cm^{-1} at room temperature (Figs. 27(d) and 27(f)). The mechanical strength was also improved (Fig. 27(g)). Moreover, the polymer electrolyte composites were stable up to about 5 V (Figs. 27(h) and 27(i)).

Another method for preparing porous polymer matrices such as PVDF-HFP, PAN, PMMA, and PEO is phase inversion, and the generated pores were owing to the different dissolution and evaporation rates of the mixture solvents [224]. Zhou et al. [225] synthesized a poly(B-Vd) which contains cyclic boroxine and cyclic carbonate groups by using polyethylene glycol methyl methacrylate (B-PEGMA) (containing boronic acid monomers) and 4-vinyl-1,3-dioxan-2-one (Vd), and then combined the poly(B-Vd) copolymer with the PVDF polymer matrix to prepare borate-based porous polymer electrolytes (B-PPEs) by the phase inversion method (Fig. 28(a)). With the increase of the poly(B-Vd) content, the pore size in the polymer matrix becomes smaller and the pore distribution is narrower and more uniform (Figs. 28(b), 28(c), and 28(f)). There are well-connected pores inside, which can provide fast conduction channels for lithium ions. The DSC curves showed that the peak intensity of the B-PPE film decreased with the increase of the B-Vd content, indicating that the increase of the B-Vd copolymer and the pores could inhibit the crystallization of PVDF (Fig. 28(h)). This leads to an increase in the ionic conductivity of the B-PPEs, which is 3.12×10^{-4} S·cm^{-1} for the B-PPE0 and 1.32×10^{-3} S·cm^{-1} for the B-PPE40 at 30 °C (Fig. 28(i)). The electrochemical window of the B-PPEs is also expanding (Fig. 28(e)). The introduction of the B-Vd and the pores can also promote the uniform deposition of Li and suppress the growth of the Li dendrite. The Li/B-PPE40/Li battery exhibits a low and stable overpotential, and the polarization voltage held at 11 mV after 1,000 h (Fig. 28(d)). Furthermore, the Li/B-PPE40/$LiFePO_4$ batteries have better cycling performance and higher specific discharge capacity than the B-PPE0-based batteries (Fig. 28(g)).

The commonly-prepared SPEs membranes are dense without porous structures, and the effect of the porosity on the electrical properties is usually ignored. However, recent studies have found that the pore surface is also beneficial to the fast ion transport in the SPEs [219, 226]. Liang et al. [227] prepared a PEO-PMMA-$LiClO_4$-x wt.% phytic acid (PA)

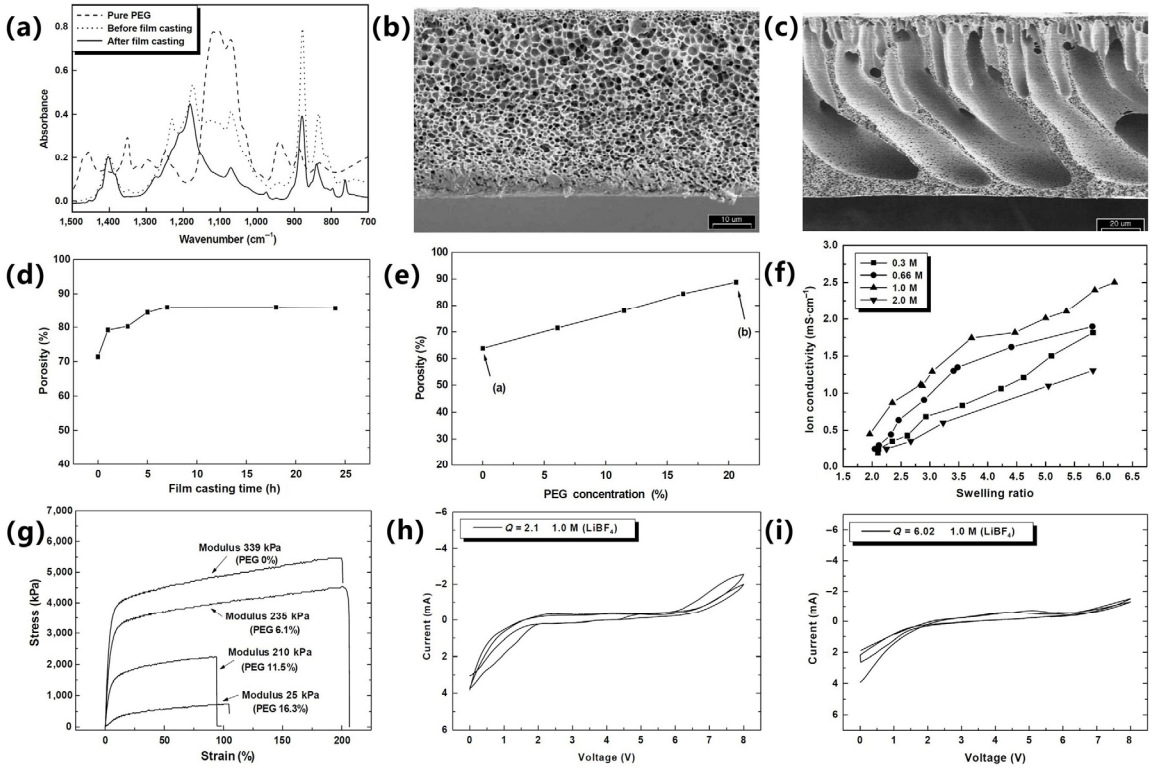

Figure 27 (a) FTIR spectra of the pure PEG and polymer electrolyte films prepared before and after casting process. SEM images of the porous PVDF-HFP/PEG membrane with the incorporated PEG concentrations of (b) 0 wt.% and (c) 20 wt.%. (d) Dependence of the PVDF-HFP/PEG membrane porosity on the film-casting time with the PEG concentration of 15 wt.%. (e) Influence of the PEG concentration on the PVDF-HFP/PEG membrane porosity after immersion in water for 10 h. (f) Effect of the swelling ratio (*Q*) on the ion conductivity of the PVDF-HFP/PEG electrolyte at room temperature with the $LiBF_4$ concentrations of 0.3, 0.66, 1.0, and 2.0 M. (g) Tensile behaviors of the PVDF-HFP/PEG film with 0 wt.%, 6.1 wt.%, 11.5 wt.%, and 16.3 wt.% PEG. Cyclic voltammograms of the PVDF-HFP/PEG electrolyte containing 1 M $LiBF_4$:EC/PC electrolyte with the *Q* of (h) 2.1 and (i) 6.0. Reproduced with permission from Ref. [221], © Elsevier B.V. 2003.

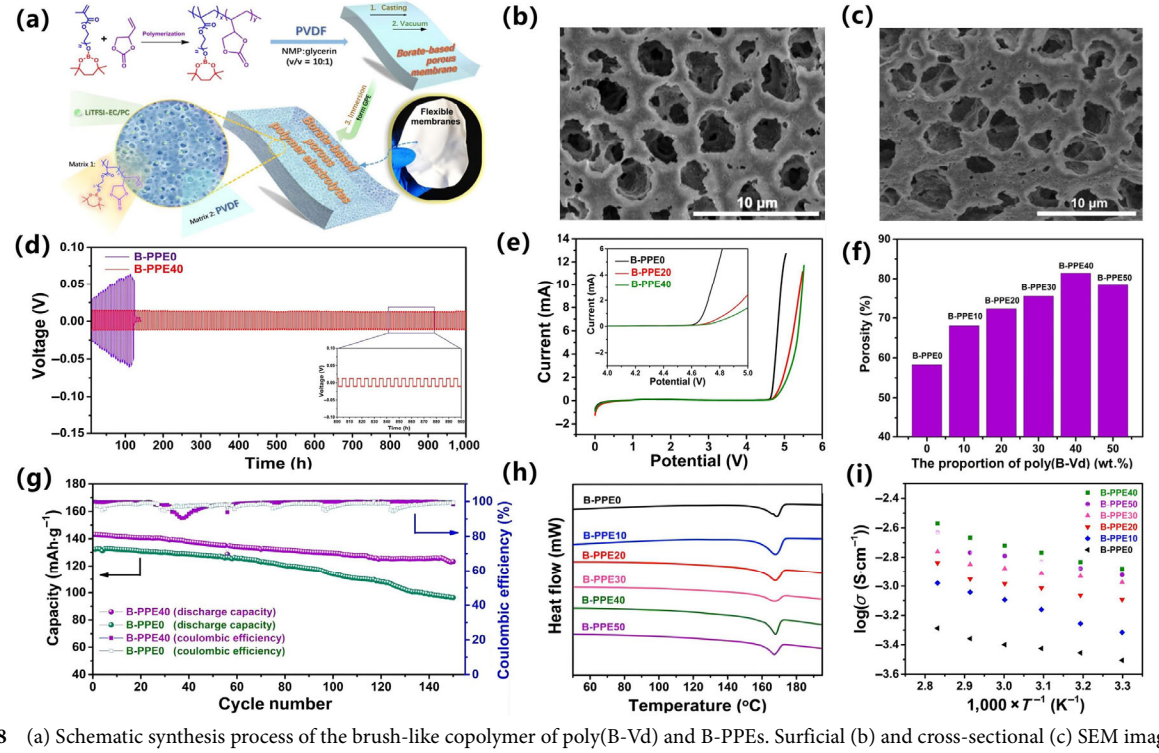

Figure 28 (a) Schematic synthesis process of the brush-like copolymer of poly(B-Vd) and B-PPEs. Surficial (b) and cross-sectional (c) SEM images of the B-PPE40. (d) Charge and discharge curves of the symmetric Li/B-PPE40/Li and Li/B-PPE0/Li cells under 0.2 mA·cm^{-2} at 30 °C. (e) LSV curves of the Li/SS cells with B-PPE0, BPPE20, and B-PPE40. (f) Porosity of B-PPEs with different contents of poly(B-Vd). (g) Cycling performances of the $LiFePO_4$/Li cells using B-PPE0 and B-PPE40 at 0.2 C. (h) DSC curves of B-PPEs. (i) Ionic conductivity dependence with temperature for B-PPEs. Reproduced with permission from Ref. [225], © American Chemical Society 2021.

electrolyte, and then studied the effect of the PA additive content on the morphology, pore structure, and electrochemical performance of the porous electrolyte membrane (Fig. 29(a)). It is confirmed that the addition of PA plays an important role in regulating the electrolyte morphology including the pore size and porosity (Figs. 29(c)–29(f)). The 15 wt.% PA-resulted solid electrolyte with around 20% porosity shows higher ion conductivity of 1.59×10^{-5} S·cm^{-1} than the PA-free electrolyte with around 5% porosity (6.9×10^{-6} S·cm^{-1}) at 20 °C (Fig. 29(b)), and the electrochemical window is above 5 V (Fig. 29(g)).

In addition to the fast ion transport on the pore surface in the porous SPEs, the polymer/polymer and polymer/filler interfaces are also found to be fast-ion transport pathways. Chen et al. [75] applied a simultaneous electrospinning/electrospray method to roll-press PAN and conductive ceramic into thin films, immersed them in $LiClO_4$ solution, and then dried to form electrolyte films (Fig. 30(a)). The FTIR curves show that there is an interaction between Li^+ and the cyanide groups in PAN, and $LiClO_4$ in the composite film is completely dissociated (Fig. 30(b)). In order to verify that Li^+ can be conducted through the polymer/filler interface, the authors changed the diameter of the ZrO_2 particles, but kept the total amount of ZrO_2 unchanged. It was found that the ionic conductivity increased with the decrease of the ZrO_2 particle size (the increasing of specific interfacial area) (Fig. 30(d)). The ionic conductivity was up to 1.16×10^{-3} S·cm^{-1}. In addition, the ionic conductivity also increased with the increase of the ZrO_2 content (Fig. 30(f)). These results show that if there are ceramic fillers in the electrolytes, Li^+ can transport through the polymer/filler interface. Besides, the electrospinning would generate many polymer/polymer interfaces through which Li^+ can transport, and thus the conductivity without the ceramic phase reaches 2.9×10^{-4} S·cm^{-1}, which is much higher than the blade-casted electrolyte (10^{-6}–10^{-7} S·cm^{-1}, Fig. 30(c)). The NMR spectra also confirmed the existence of four Li^+ transport pathways in the electrolyte, i.e., PAN, LLZTO, PAN/PAN interface, and LLZTO/PAN interface (Fig. 30(e)). Moreover, the Li-CNT|PAN/$LiClO_4$:LLZTO|Li-CNT battery can cycle stably for 5,000 h at 1 mA·cm^{-2} with stable overpotentials (Figs. 30(g) and 30(h)).

3.4.2 *Thickness*

The thickness of the solid-state electrolytes has an adverse impact on the overall ionic conductance, internal resistance, gravimetric, and volumetric energies, and even the cost of the solid-state LIBs [228, 229]; however, most of the batteries reported recently are composed of thick SSEs with the thickness of ≥ 100 μm [230]. To achieve high energy densities over 300 Wh·kg^{-1} and 500 Wh·L^{-1}, thin SSEs are quite necessary. The gravimetric energy density of the $LiNi_{0.8}Co_{0.1}Mn_{0.1}O_2$/Li battery can even reach 500 Wh·kg^{-1}, if the polymer electrolyte and the ceramic oxide electrolyte have small thicknesses of 12 and 8 μm, respectively [231, 232]. Although the inorganic electrolytes such as oxides and sulfides have much higher ionic electrolytes than the polymer electrolytes, they also have higher densities than the polymer electrolytes. Thus, it is important to reduce the electrolyte thickness for high-energy-density LIBs. But the brittleness and rigidity of the ceramic electrolytes hinder their preparation of thin films [233]. Of course, the reduction of the thickness of the polymer electrolytes would also cause the loss of the mechanical strength and the safety issues during the fabrication and cycling processes of the solid-state LIBs.

A few physical vapor deposition methods such as pulsed laser deposition, radio frequency magnetron sputtering, chemical vapor deposition, and atomic layer deposition can be used to prepare inorganic thin films [234, 235]. Especially, the magnetron sputtering method has been widely used to fabricate amorphous electrolyte films via the deposition of solid electrolyte particles on substrates by physical sputtering under vacuum condition. The thickness of the electrolyte films prepared by these methods is usually quite thin, even up to several tens of nanometers, which can effectively reduce the impedance of the entire battery. However, these physical deposition methods have a few disadvantages such as high preparation cost, small film area, and low ionic conductivity. The thin electrolyte films also need to be deposited/sputtered

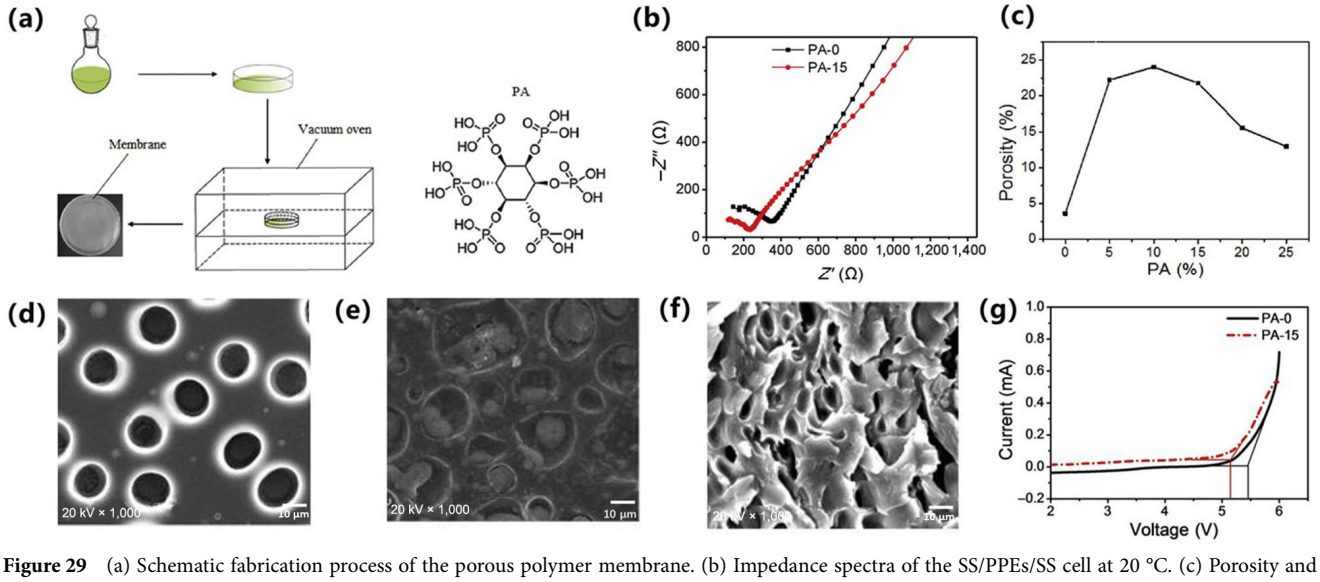

Figure 29 (a) Schematic fabrication process of the porous polymer membrane. (b) Impedance spectra of the SS/PPEs/SS cell at 20 °C. (c) Porosity and liquid electrolyte uptake as a function of the PA weight fraction in the porous membranes. SEM images of the porous PEO-PMMA-$LiClO_4$-15 wt.% PA membranes at the (d) front surface, (e) back surface, and (f) cross section. (g) LSV plots of the PPEs with 0 wt.% and 15 wt.% PA. Reproduced with permission from Ref. [227], © Elsevier B.V. 2015.

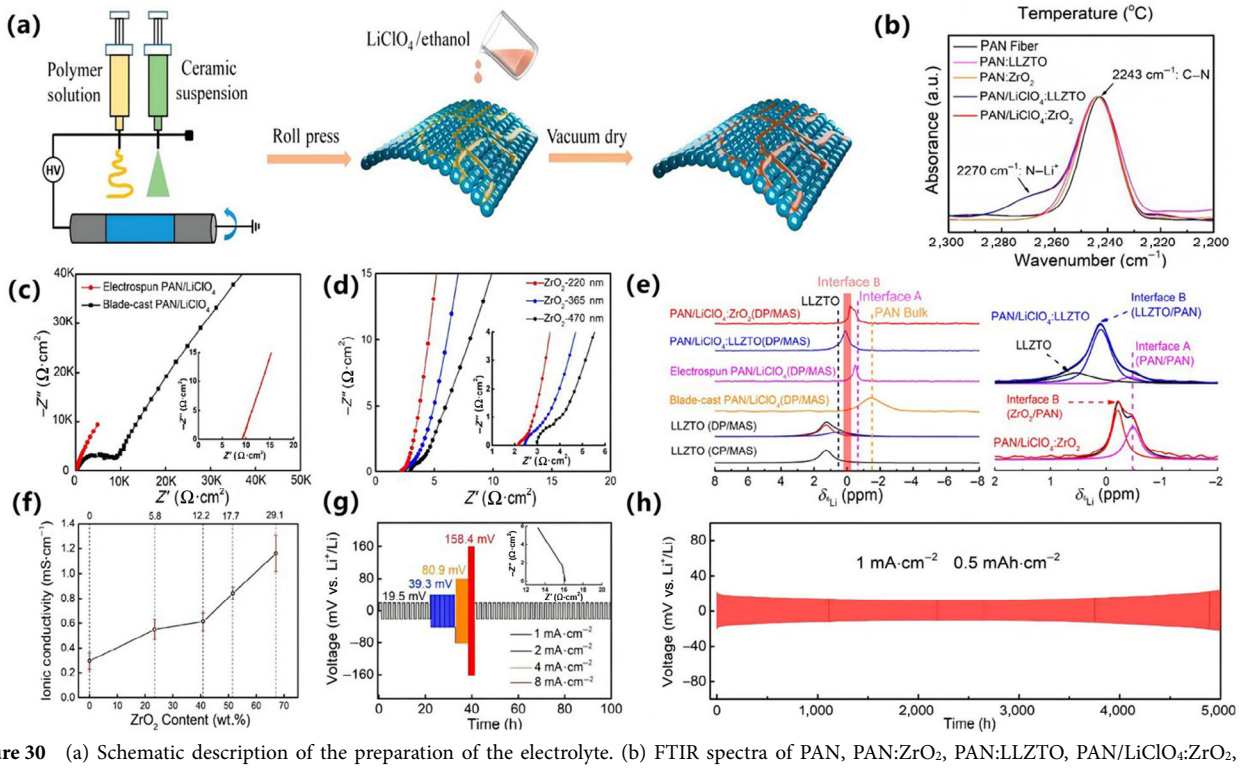

Figure 30 (a) Schematic description of the preparation of the electrolyte. (b) FTIR spectra of PAN, PAN:ZrO_2, PAN:LLZTO, PAN/$LiClO_4$:ZrO_2, and PAN/$LiClO_4$:LLZTO. (c) Nyquist plots of electrospun and blade-casted PAN/$LiClO_4$ samples at 25 °C. (d) Nyquist plots of the PAN/$LiClO_4$:ZrO_2 BISCs with the ZrO_2 particle sizes of 220, 365, and 470 nm. (e) ^{6}Li MAS NMR spectra of the PAN/$LiClO_4$:LLZTO, PAN/$LiClO_4$:ZrO_2, electrospun PAN/$LiClO_4$, and the blade-casted PAN/$LiClO_4$. The right pane exhibits the deconvolution of the BISC spectra. (f) Ionic conductivity of the PAN/$LiClO_4$:ZrO_2 BISCs with different contents of ZrO_2 ranging from 0 wt.% to 67.1 wt.% at 25 °C. (g) Galvanostatic stripping/plating cycles of the symmetric Li-CNT|PAN/$LiClO_4$:LLZTO|Li-CNT cell under different current densities. (h) Extended cycling performance of the Li-CNT|PAN/$LiClO_4$:LLZTO|Li-CNT cell under 1 mA·cm^{-2} and 0.5 mAh·cm^{-2}. Reproduced with permission from Ref. [75], © American Chemical Society 2020.

on a substrate. In addition, high vacuum deposition techniques are extremely expensive and do not present a scalable process for commercial development of the solid-state battery. More importantly, these methods are not applicable in the preparation of solid polymer electrolytes. Ling et al. [236] prepared LATP electrolyte films by the magnetron sputtering technology for thin-film batteries. The LATP films were composed of fine particles, and had smooth surfaces without obvious cracks and pinholes. However, the thin films were difficult to be peeled off from the substrates, and the room-temperature ionic conductivity was only 6.47×10^{-6} S·cm^{-1}. Xu et al. [237] prepared a thin Li-La-Ti-Zr-O electrolyte film with a thickness of 611 nm and an ionic conductivity of 2.83×10^{-6} S·cm^{-1} at room temperature via the radio frequency magnetron co-sputtering using $Li_{0.33}La_{0.56}TiO_3$ and $Li_7La_3Zr_2O_{12}$ powder targets.

Compared to the abovementioned physical deposition methods, solution casting method is a low-cost electrolyte film preparation method by simply pouring the electrolyte solution into an inert mold and then evaporating the solvents, which has been widely used to fabricate flexible polymer electrolytes, but the polymer electrolyte thickness is usually lager than 100 μm for high flexibility and processibility [238]. The thickness can also be changed by adjusting the volume and concentration of the electrolyte solution. To enhance the mechanical strength of the electrolyte films, nanoparticles are usually added into the solution to prepare composite electrolyte films (Table 6). Yang et al. [230] prepared a CPE membrane by the incorporation of $Li_{10}SnP_2S_{12}$ particles into the PEO matrix using a solution-casting method. Because of the uniform distribution of the high-conductivity $Li_{10}SnP_2S_{12}$ particles, the inhibition of the PEO crystallization, and the interactions among the PEO chains, the 1 wt.% $Li_{10}SnP_2S_{12}$ particle-containing CPE film had a maximum ionic conductivity of 1.69×10^{-4} S·cm^{-1} at 50 °C and the highest mechanical strength. Thus, the CPE-based Li-S battery exhibited outstanding electrochemical cycling performance with a high discharge capacity of ~ 1,000 mAh·g^{-1}, high Coulombic efficiency, and excellent cycling stability at 60 °C. Direct casting of the electrolyte solution on the cathode or anode surfaces after the subsequent drying process offers another route to achieving small thickness of the electrolytes, but it should be mentioned that the solvent may destroy the electrode microstructure. Of course, the electrolyte solution can penetrate the pores of the electrodes and greatly improve their physical contact for the continuous ion transport.

Tape casting is also known as doctor blading or knife coating, which is widely utilized to prepare large-area electrodes in LIBs. The tape casting method for preparing ceramic electrolyte films usually contains the following processes: (1) the dispersion of the ceramic electrolyte powders with an organic binder in a solvent; (2) the coating of the homogenous slurry on a flexible substrate using a doctor blade; (3) the evaporation of the solvent for flexible ceramic films with a thickness range of 20–1,000 μm; (4) hot pressing of the dried films to further improve the interconnectivity of the ceramic particles; (5) annealing of the ceramic films to evaporate the organic components and strengthen the connectivity of the ceramic phases for thin and dense ceramic electrolyte films [230]. Chi et al. [239] prepared a thin $Li_{1.4}Al_{0.4}Ge_{1.6}(PO_4)_3$ film with

Table 6 Thin solid-state electrolytes

Preparation method	Electrolyte type	Ionic conductivity ($S \cdot cm^{-1}$, 25 °C)	Thickness (μm)	References
Solution casting	PEO-LiTFSI-$Li_{10}SnP_2S_{12}$	2.3×10^{-4}	30	[230]
Tape casting	$Li_{1.4}Al_{0.4}Ge_{1.6}(PO_4)_3$	3.4×10^{-4}	75	[239]
Tape casting	$Li_{0.34}La_{0.56}TiO_3$	2.0×10^{-5}	25	[234]
Tape casting	Ceramic oxide	1.1×10^{-4} (60 °C)	10	[244]
Hot pressing	Li_2S-P_2S_5	~ 10^{-4}	64	[238]
Cold pressing	Sulfide	2.0×10^{-4}	35	[241]
Solution infusion	PI-g-PEO/PEO-LiTFSI	~ 10^{-4}	19	[197]
Solution infusion	PE/PMMA-PS/PEG-LiTFSI	1.9×10^{-5}	10	[242]
Solution infusion	PE/PEO-LiTFSI	10^{-5} (30 °C)	8	[243]
Solution infusion	PI/PEO-LiTFSI	2.3×10^{-4} (30 °C)	9	[233]
Solution infusion	Vermiculite/PEO-PAN-LiTFSI	2.1×10^{-4}	4	[232]

a thickness of 75 μm and a high ionic conductivity of 3.4×10^{-4} $S \cdot cm^{-1}$ at 25 °C by the tape casting method. The high ionic conductivity of the sample was ascribed to the increase of the relative density by the proper heat-treating process, which can effectively reduce the resistance of the grain boundary. Wang et al. [234] prepared a freestanding ceramic electrolyte film of perovskite-type LLTO with a thickness of 25 μm by the tape casting method (Figs. 31(a)–31(f)). Compared to the cold pressing-resulted thick electrolyte with a thickness of > 200 μm, the tape casting-resulted thin film showed a high ionic conductivity of 2.0×10^{-5} $S \cdot cm^{-1}$ at room temperature and a high flexural strength of 264 MPa. The solid-state LIBs with 41 μm thick LLTO films exhibited an initial capacity of 145 $mAh \cdot g^{-1}$ and a high capacity retention ratio of 86% after 50 cycles. Though the obvious advantages such as the scalability for large-area electrolyte film production and the reduction of the preparation cost, the electrolyte preparation is complicated and energy consuming, because of the processes such as the planetary ball milling and hot pressing. The utilization of the toxic solvent is also harmful to the environment.

Ceramic electrolyte pellets with high thickness are usually prepared by cold pressing of the electrolyte powders in a mold and then calcinating them at high temperatures. To reduce the electrolyte thickness and preparation cost while maintaining the flexibility of the electrolytes, cold pressing has been developed by facilely putting the electrolyte powders (or the electrolyte powders with non-polar solvents) into the pores of the porous scaffolds under high pressure. Jung et al. [240] prepared thin and bendable sulfide electrolyte films with a thickness of ~ 70 μm by pressing soft sulfide particles into

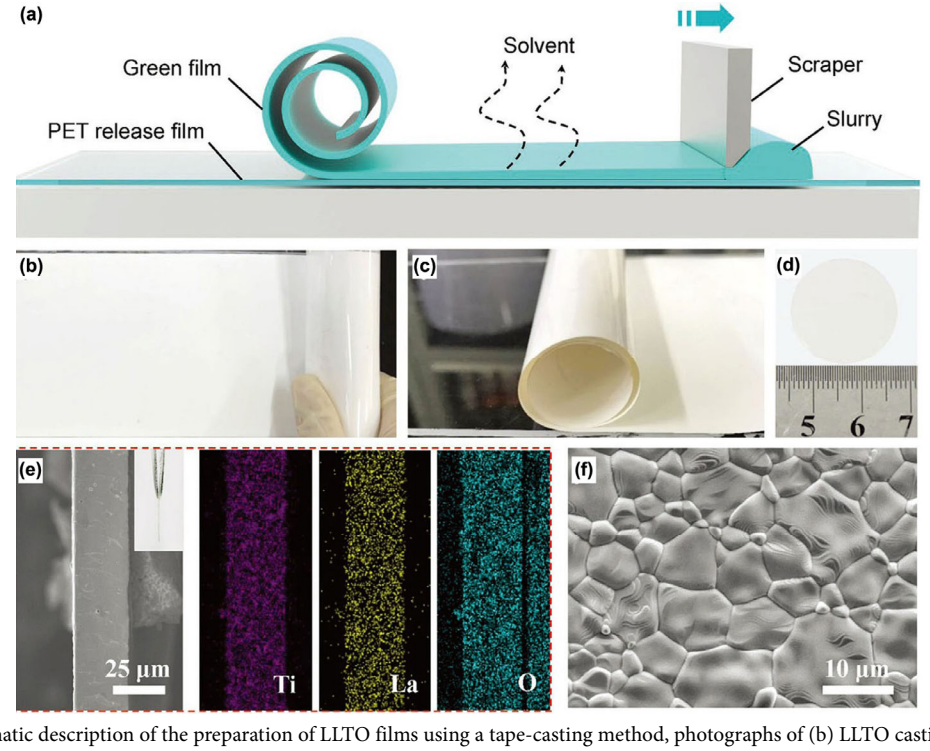

Figure 31 (a) Schematic description of the preparation of LLTO films using a tape-casting method, photographs of (b) LLTO casting film on PET release film after drying, (c) LLTO scroll film after being stripped off from the PET film, and (d) LLTO casting film disk with a diameter of 22 mm, and (e) cross-sectional SEM images (inset is a photograph) with EDS mapping and (f) surface SEM image of the LLTO ceramic film after sintering at 1,260 °C. Reproduced with permission from Ref. [234], © WILEY-VCH Verlag GmbH & Co. KGaA, Weinheim 2019.

polyparaphenylene terephthalamide (PPTA) NW scaffolds. Due to the effective mechanical supporting by the high-strength PPTA, the sulfide electrolyte films had high flexibility and the ionic conductivity reached 2.0 × 10^{-4} S·cm^{-1} at room temperature. Moreover, the energy density of the LCO/LTO cells with the thin electrolyte films increased by approximately a factor of 3 (to 44 Wh·kg^{-1}), compared to the conventional all-solid-state cells without the NW scaffold. Yao et al. [241] prepared an ultra-thin free-standing sulfide electrolyte film with a thickness of ~ 35 μm by cold pressing of polydopamine-coated Li_6PS_5Cl particles. Because of the high ionic conductivity (0.2 mS·cm^{-1} at room temperature) and the small thickness of the electrolyte films, the energy density of the full cells with 6.37 mg·cm^{-2} cathode loading reached 284.4 Wh·kg^{-1}.

Apart from the cold pressing method, hot pressing is also exploited to prepare ceramic electrolyte films and even polymer electrolyte films. The applied heat can easily melt the polymers or the organic binders and evaporate the solvents. The utilization of the binders can enhance the flexibility of the electrolyte films, but the low-conductivity binders have a negative impact on the conductivity of the electrolyte films after the hot-pressing process. Thus, the content of the binders should be minimized to balance the flexibility and the ionic conductivity. Zhang et al. [238] prepared an electrolyte film with a thickness of 64 μm by the hot pressing method. The electrolyte film also had high flexibility and room-temperature ionic conductivity of ~ 10^{-4} S·cm^{-1}, because of the penetration of the *in situ* derived polymer matrix in the void space between the solid ceramic particles.

Compared to the aforesaid methods, solution infusion method is considered as one of the most important routes to preparing thin CPE membranes by infusing the electrolyte solution/slurry into porous substrates and then evaporating the solvents. The ionic conductivity of the CPE films is determined by the porous substrates (e.g., the intrinsic ionic conductivity) and the interaction between the porous substrates and the polymer electrolytes, while the thickness is mainly relied on the porous substrates (e.g., the thickness and the mechanical strength). As we have mentioned in Section 3.3.3, the porous ceramic electrolytes (e.g., LLZO, LLTO, LAGP, and LATP) with high ionic conductivity have been used as substrates to prepare CPE membranes for high ionic conductivity and mechanical strength; however, the membranes are too brittle and inflexible, and the thickness is usually higher than 100 μm [187–189, 191, 232]. To reduce the thickness and meanwhile increase the flexibility of the electrolyte membranes, organic substrates composed of PVDF nanofiber [193], PA6 microfiber non-woven fabric [194], CNF [195], ANF [73, 196], polyimide nanofiber [233, 197], and polyethylene separator [242, 243] are further utilized to prepared CPEs. Nevertheless, the organic substrate-supported CPE films have much lower ionic conductivity than the ceramic electrolyte substrate-supported CPEs, because of the low intrinsic conductivity and high content of the organic substrates. Adjusting the interaction between the substrates and the polymer matrices/lithium salts to decrease the polymer matrix crystallinity and facilitate the lithium salt dissociation offers an important way to increase the ionic conductivity of the CPE films.

3.4.3 Remarks

A few methods such as extraction and phase inversion have been used to prepare porous polymer matrices for obtaining gel polymer electrolytes, and the pore size and porosity have an important impact on the ionic conductivity and mechanical strength of the gel polymer electrolytes. In comparison, solid polymer electrolytes are usually prepared by solution casting or doctor blading methods, and the polymer matrices are dense without porous structure. However, recent studies discover that the pore surface is conducive to fast ion transport in solid polymer electrolytes, and appropriate porosity results in high ionic conductivity. A few characterizations such as NMR and TEM further verify the fast-ion transport pathways at the polymer/polymer interface. Thus, the control on the porous structure (e.g., interconnected pores and porosity) of the solid polymer electrolytes offers another viable way to obtaining high-conductivity electrolytes. It should also be mentioned that too high porosity (or too big pore) could cause deteriorative mechanical strength and poor physical contact with the electrodes. Moreover, the development of novel porous electrolyte preparation processes will become a new research hotspot.

In comparison of the pore structure (determining the electrolyte conductivity), the thickness of the electrolytes has an important impact on both the overall conductance of the electrolytes and the internal resistance and energy density (even cost) of the batteries. Of course, reducing the electrolyte thickness may cause the deterioration of the electrolyte strength and the short circuit of the batteries. Physical vapor deposition technologies are usually utilized to prepare ultrathin ceramic electrolytes with the thickness of ≤ 1 μm for low-area-density batteries; however, the physical deposition methods have the disadvantages such as low electrolyte conductivity and high cost. In comparison, tape casting and hot-/cold-pressing technologies are low-cost methods to prepare thin membranes of inorganic electrolytes. Solution casting is a commonly-used method to prepare polymer electrolytes due to its facile process and low cost, but the electrolyte thickness is usually higher than 100 μm. To obtain polymer electrolytes with lower thickness, nanoparticles are added in the electrolytes to enhance the mechanical strength or the polymer electrolytes are directly deposited on the electrode surface. Filling polymer electrolytes in flexible porous organic substrates offers a quite important route to obtaining ultrathin composite electrolytes, but the intrinsic non-conductivity nature of the organic substrates affects the overall conductivity of the electrolytes. An effective way to increase the conductivity of the electrolyte films is adjusting the interaction between the substrates and the polymer matrices/lithium salts to decrease the polymer matrix crystallinity and facilitate the lithium salt dissociation.

4 Conclusions

Polymer electrolytes are regarded as one of the most important solid-state electrolytes, because of their comprehensive merits such as high flexibility, excellent physical contact with the electrodes, film formation ability, and low cost. The utilization of polymer electrolytes is believed to greatly improve the safety and energy density of lithium-ion batteries; however, one of the main obstacles is the insufficient ionic conductivity of the electrolytes especially below their melting points. By scrutinizing the microstructure characteristics and the ion migration behaviors, we disclose the ion conduction mechanisms of the polymer electrolytes. The ion transport involves the ion hopping in adjacent sites and the polymer segmental motion. The ionic conductivity is mainly relied on the free ion concentration, the ionic hopping velocity along the polymer

chains, and the interfacial fast-ion pathways. Based on these analyses, this paper further summarizes the up-to-date progress made in the polymer electrolytes with the focus on the polymer structure design, lithium salt type, additive engineering, and electrolyte morphology control.

As for the polymer molecular structure design, ethylene oxide groups are usually combined with other polymer units to construct copolymer structures with low polymer crystallinity or glass-transition temperature. Compared to the block, star, and graft copolymers with possible mechanical strength degradation, the design of cross-linking interpenetrating networks has dual advantages of the reduction of the crystalline domain and the enhancement of the mechanical properties, and thus has attracted more and more attention. It should be highlighted that the increase of the ionic conductivity should not sacrifice other properties especially the mechanical strength and the electrochemical compatibility with the electrode materials, which is always ignored. Ideal cross-linking initiators and novel copolymer structure design are therefore become more important for comprehensively-updated polymer electrolytes. Same to the polymer matrices, lithium salts are also indispensable in polymer electrolytes, and their properties have important effects on the polymer electrolytes and the battery. Although there are many lithium salts, none of them possesses the comprehensive advantages of high dissociation ability, wide electrochemical window, good compatibility with other battery components, high safety, low cost, etc. It is necessary to exploit novel lithium salts with large anion radius and weak interaction between the positive and negative ions for high-conductivity electrolytes. The overall performance of the polymer electrolytes can also be strengthened by combining two or more lithium salts with different molecular structures and properties with assistance of the synergic effect on the electrical, thermal, and electrochemical properties.

In addition to the modification on the polymer electrolytes themselves, a lot of organic micro-molecules, polymer molecules, and micro-/nano-particles are introduced into polymer electrolytes as additives to increase the ionic conductivity by facilitating the polymer segment mobility, increasing the carrier concentration, or forming fast-ion pathways. High-dielectric-permittivity carbonates, ionic liquids, and plastic materials are commonly used as plasticizers to adjust the polymer interchain interactions, and the polymer polar group-Li^+ and anion-Li^+ interactions, and lower the activation energy for fast ion motion, thus greatly increasing the ionic conductivity; however, these plasticizers are related to the issues such as poor thermostability, low mechanical strength, and electrochemical instability with the electrodes. In comparison with the organic plasticizers, the introduction of other polymers by simple blending can increase both the mechanical strength and ionic conductivity of polymer electrolytes by inhibiting the polymer crystallization and facilitating the lithium salt dissociation, but the compatibility and interactions between the polymers should be carefully considered. Different from the organic plasticizers and polymer additives, the utilization of nanoparticle fillers can improve the overall performance of the polymer electrolytes, and the increase in the ionic conductivity is not only attributed to the inhibition of polymer matrix crystallinity (or the decrease of the T_g) and the facilitation of lithium salt dissociation, but also to the formation of fast-ion pathways at the nanofiller/polymer interfaces (and the ion transport pathways in the electrolyte filler phase). The particle size, chemical composition, surficial functional groups/charges, and shape have important impacts on the ionic conductivity, and it is generally recognized that the formation of continuous fast-ion pathways in 1D, 2D, and 3D nanofiller-based electrolytes is conducive to the ionic conductivity; however, the nanoparticle filling induces a few problems such as severe aggregation and disordered distribution of the nanoparticles. Thus, it is important to control the particle arrangement and the interaction between the nanofillers and the polymer matrices/lithium salts. Of course, each modification strategy has its own advantages and drawbacks, and the effective combination of two or more methods would further improve the ionic conductivity or other properties based on the synergistic effect.

Apart from the composition and structure, the micromorphology characteristics such as pore and thickness also play an important role in the ion conduction of polymer electrolytes. Especially, recent researches have confirmed the fast ion transport behaviors at the pore surface and even the polymer/polymer interface. Novel methods are needed to effectively adjust the porous structure for high-conductivity polymer electrolytes without sacrificing the mechanical properties, and meanwhile the electrode preparation methods may be changed to enhance the physical interface contact between the polymer electrolytes and the active electrode materials. Another route to improve the overall ionic conductance of the electrolytes is decreasing the electrolyte thickness, which is also helpful for increasing the energy density of the batteries. Nevertheless, the commonly-used solution casting and tape casting methods are not suitable for preparing thin polymer electrolytes of ≤ 100 μm in thickness. To obtain thin polymer electrolyte membranes, nanofillers are usually introduced into the electrolytes for high mechanical strength and film processibility. Direct deposition of thin polymer electrolyte layers on the electrodes offers an important way to improve the electrolyte/electrode contact, but the electrode integrity should not be destroyed during the deposition process. In stark contrast, solution infusion technology is a quite effective method to produce ultrathin (≤ 30 μm) composite polymer electrolytes by filling polymer electrolytes in flexible porous substrates, and the pore structure and the interaction between the substrates and the polymer matrices/lithium salts need to be well adjusted to further increase the ionic conductivity.

Though the numerous studies on the ion transport behaviors in the polymer electrolytes, there are still a few questions that must be answered: (1) What is the highest ionic conductivity of the polymer electrolytes, and how the polymer chain distribution affects the ion migration? Based on the analyses of the ion conduction mechanisms and the modification strategies on the polymer molecular structure design, lithium salt exploitation, additive engineering, and the electrolyte micromorphology adjustion, we can easily conclude that especially the polymer segment migration and interfacial ion transport mechanisms play important roles in increasing the ionic conductivity, and the nanofiller/polymer interfaces are proven to exhibit high conductivities same to the liquid electrolytes through the numerical simulation methods. High ionic conductivities up to 10^{-5}–10^{-3} S·cm^{-1} have been achieved at room temperature by the above-mentioned modification strategies, and solid polymer electrolytes with abundant, continuous, and well-aligned interfaces are expected to further increase the ionic conductivity up to the level of liquid electrolytes (10^{-3}–10^{-2} S·cm^{-1} at room temperature). (2) How the interfacial ion conduction phenomenon comes out, and what is the nature of the fast-ion pathways at the nanofiller/polymer

interfaces? A few advanced technologies such as ssNMR and HAADF-TEM/EELS have proven the existence of fast-ion pathways at the nanofiller/polymer and polymer/polymer interfaces, and the finite element analysis further discloses the high ionic conductivities of the interfacial areas. Other advanced technologies such as neutron diffraction highly sensitive to light elements (e.g., H, Li, or O) may be suitable for revealing the Li^+ transport pathways. The Lewis acid–base theory and space-charge layer theory have been applied to explain the fast-ion transport pathways at the interfacial regions, but the numerical simulation methods such as density functional theory calculations and molecular dynamics simulations should be further utilized to explore the nature of the fast-ion pathways. (3) Which method can afford green and scalable preparation of flexible, thin, and high-conductivity electrolyte membranes without compromising other properties? The conventional methods such as solution casting are simple and scalable to prepare electrolyte membranes with large thickness, which is detrimental to the ion conduction and the energy density of batteries. Because of the high ionic conductivity of the interfacial regions, novel methods such as electrospinning may be capable of fabricating flexible, thin, and high-conductivity polymer electrolytes with continuous interfaces. The exploitation of novel modification methods would further facilitate the large-scale application of polymer electrolytes in high-safety and high-energy-density batteries.

Acknowledgements

This work was supported partially by project of the State Key Laboratory of Alternate Electrical Power System with Renewable Energy Sources(Nos. LAPS21004 and LAPS202114), the Hebei Natural Science Foundation (No. E2022502022), the National Natural Science Foundation of China (Nos. 52272200, 51972110, 52102245, and 52072121), the Beijing Science and Technology Project (No. Z211100004621010), the Beijing Natural Science Foundation (Nos. 2222076 and 2222077), the Huaneng Group Headquarters Science and Technology Project (No. HNKJ20-H88), the 2022 Strategic Research Key Project of Science and Technology Commission of the Ministry of Education, the China Postdoctoral Science Foundation (No. 2022M721129), the Fundamental Research Funds for the Central Universities (Nos. 2022MS030, 2021MS028, 2020MS023, and 2020MS028), and the NCEPU "Double First-Class" Program.

Declaration of conflicting interests

The authors declare no conflicting interests regarding the content of this article.

References

[1] Yue, J. P.; Yan, M.; Yin, Y. X.; Guo, Y. G. Progress of the interface design in all-solid-state Li-S batteries. *Adv. Funct. Mater.* **2018**, *28*, 1707533.

[2] Schnell, J.; Gunther, T.; Knoche, T.; Vieider, C.; Köhler, L.; Just, A.; Keller, M.; Passerini, S.; Reinhart, G. All-solid-state lithium-ion and lithium metal batteries-paving the way to large-scale production. *J. Power Sources* **2018**, *382*, 160–175.

[3] Nitta, N.; Wu, F. X.; Lee, J. T.; Yushin, G. Li-ion battery materials: Present and future. *Mater. Today* **2015**, *18*, 252–264.

[4] Lv, F.; Wang, Z. Y.; Shi, L. Y.; Zhu, J. F.; Edström, K.; Mindemark, J.; Yuan, S. Challenges and development of composite solid-state electrolytes for high-performance lithium ion batteries. *J. Power Sources* **2019**, *441*, 227175.

[5] Liu, Y.; Xu, B. Q.; Zhang, W. Y.; Li, L. L.; Lin, Y. H.; Nan, C. W. Composition modulation and structure design of inorganic-in-polymer composite solid electrolytes for advanced lithium batteries. *Small* **2020**, *16*, 1902813.

[6] Sastre, J.; Futscher, M. H.; Pompizi, L.; Aribia, A.; Priebe, A.; Overbeck, J.; Stiefel, M.; Tiwari, A. N.; Romanyuk, Y. E. Blocking lithium dendrite growth in solid-state batteries with an ultrathin amorphous Li-La-Zr-O solid electrolyte. *Commun. Mater.* **2021**, *2*, 76.

[7] Wang, Y.; Zanelotti, C. J.; Wang, X. E.; Kerr, R.; Jin, L. Y.; Kan, W. H.; Dingemans, T. J.; Forsyth, M.; Madsen, L. A. Solid-state rigid-rod polymer composite electrolytes with nanocrystalline lithium ion pathways. *Nat. Mater.* **2021**, *20*, 1255–1263.

[8] Raj, V.; Venturi, V.; Kankanallu, V. R.; Kuiri, B.; Viswanathan, V.; Aetukuri, N. P. B. Direct correlation between void formation and lithium dendrite growth in solid-state electrolytes with interlayers. *Nat. Mater.* **2022**, *21*, 1050–1056.

[9] Janek, J.; Zeier, W. G. A solid future for battery development. *Nat. Energy* **2016**, *1*, 16141.

[10] Ko, J.; Yoon, Y. S. Recent progress in LiF materials for safe lithium metal anode of rechargeable batteries: Is LiF the key to commercializing Li metal batteries? *Ceram. Int.* **2019**, *45*, 30–49.

[11] Lee, M. J.; Han, J.; Lee, K.; Lee, Y. J.; Kim, B. G.; Jung, K. N.; Kim, B. J.; Lee, S. W. Elastomeric electrolytes for high-energy solid-state lithium batteries. *Nature* **2022**, *601*, 217–222.

[12] Ye, L. H.; Li, X. A dynamic stability design strategy for lithium metal solid state batteries. *Nature* **2021**, *593*, 218–222.

[13] Shimonishi, Y.; Zhang, T.; Imanishi, N.; Im, D.; Lee, D. J.; Hirano, A.; Takeda, Y.; Yamamoto, O.; Sammes, N. A study on lithium/air secondary batteries—Stability of the NASICON-type lithium ion conducting solid electrolyte in alkaline aqueous solutions. *J. Power Sources* **2011**, *196*, 5128–5132.

[14] Murugan, R.; Thangadurai, V.; Weppner, W. Fast lithium ion conduction in garnet-type $Li_7La_3Zr_2O_{12}$. *Angew. Chem., Int. Ed.* **2007**, *46*, 7778–7781.

[15] Stramare, S.; Thangadurai, V.; Weppner, W. Lithium lanthanum titanates: A review. *Chem. Mater.* **2003**, *15*, 3974–3990.

[16] Kamaya, N.; Homma, K.; Yamakawa, Y.; Hirayama, M.; Kanno, R.; Yonemura, M.; Kamiyama, T.; Kato, Y.; Hama, S.; Kawamoto, K. et al. A lithium superionic conductor. *Nat. Mater.* **2011**, *10*, 682–686.

[17] Mizuno, F.; Hayashi, A.; Tadanaga, K.; Tatsumisago, M. New, highly ion-conductive crystals precipitated from Li_2S-P_2S_5 glasses. *Adv. Mater.* **2005**, *17*, 918–921.

[18] Efthimiadis, J.; Annat, G. J.; Efthimiadis, J.; Forsyth, M.; MacFarlane, D. R. Solid state ion transport and phase behaviour in composites of N,N-methyl propylpyrrolidinium tetrafluoroborate and amorphous polyethylene oxide. *Phys. Chem. Chem. Phys.* **2003**, *5*, 5558–5564.

[19] Alarco, P. J.; Abu-Lebdeh, Y.; Abouimrane, A.; Armand, M. The plastic-crystalline phase of succinonitrile as a universal matrix for solid-state ionic conductors. *Nat. Mater.* **2004**, *3*, 476–481.

[20] Zhao, B. Q.; Yang, M. X.; Li, J. Y.; Li, S. M.; Zhang, G.; Liu, S. Q.; Cui, Y. H.; Liu, H. Cellulose-based plastic crystal electrolyte membranes with enhanced interface for solid-state lithium batteries. *Energy Technol.* **2021**, *9*, 2100114.

[21] Wang, Z. Q.; Tan, R.; Wang, H. B.; Yang, L. Y.; Hu, J. T.; Chen, H. B.; Pan, F. A metal-organic-framework-based electrolyte with nanowetted interfaces for high-energy-density solid-state lithium battery. *Adv. Mater.* **2018**, *30*, 1704436.

[22] Shen, L.; Wu, H. B.; Liu, F.; Brosmer, J. L.; Shen, G. R.; Wang, X. F.; Zink, J. I.; Xiao, Q. F.; Cai, M.; Wang, G. et al. Creating lithium-ion electrolytes with biomimetic ionic channels in metal-organic frameworks. *Adv. Mater.* **2018**, *30*, 1707476.

[23] Jeong, K.; Park, S.; Jung, G. Y.; Kim, S. H.; Lee, Y. H.; Kwak, S. K.; Lee, S. Y. Solvent-free, single lithium-ion conducting covalent organic frameworks. *J. Am. Chem. Soc.* **2019**, *141*, 5880–5885.

[24] Fenton, D. E.; Parker, J. M.; Wright, P. V. Complexes of alkali metal ions with poly(ethylene oxide). *Polymer* **1973**, *14*, 589.

[25] Armand, M. Polymer solid electrolytes-an overview. *Solid State Ionics* **1983**, *9–10*, 745–754.

[26] Feuillade, G.; Perche, P. Ion-conductive macromolecular gels and membranes for solid lithium cells. *J. Appl. Electrochem.* **1975**, *5*, 63–69.
[27] Xue, Z. G.; He, D.; Xie, X. L. Poly(ethylene oxide)-based electrolytes for lithium-ion batteries. *J. Mater. Chem. A* **2015**, *3*, 19218–19253.
[28] Long, L. Z.; Wang, S. J.; Xiao, M.; Meng, Y. Z. Polymer electrolytes for lithium polymer batteries. *J. Mater. Chem. A* **2016**, *4*, 10038–10069.
[29] Young, W. S.; Kuan, W. F.; Epps III, T. H. Block copolymer electrolytes for rechargeable lithium batteries. *J. Polym. Sci. Part B Pol. Phys.* **2014**, *52*, 1–16.
[30] Zhou, Q.; Ma, J.; Dong, S. M.; Li, X. F.; Cui, G. L. Intermolecular chemistry in solid polymer electrolytes for high-energy-density lithium batteries. *Adv. Mater.* **2019**, *31*, 1902029.
[31] Bannister, D. J.; Davies, G. R.; Ward, I. M.; McIntyre, J. E. Ionic conductivities for poly(ethylene oxide) complexes with lithium salts of monobasic and dibasic acids and blends of poly(ethylene oxide) with lithium salts of anionic polymers. *Polymer* **1984**, *25*, 1291–1296.
[32] Reinoso, D. M.; Frechero, M. A. Strategies for rational design of polymer-based solid electrolytes for advanced lithium energy storage applications. *Energy Storage Mater.* **2022**, *52*, 430–464.
[33] Borodin, O.; Smith, G. D. Mechanism of ion transport in amorphous poly(ethylene oxide)/litfsi from molecular dynamics simulations. *Macromolecules* **2006**, *39*, 1620–1629.
[34] Mao, G. M.; Perea, R. F.; Howells, W. S.; Price, D. L.; Saboungi, M. L. Relaxation in polymer electrolytes on the nanosecond timescale. *Nature* **2000**, *405*, 163–165.
[35] Mindemark, J.; Lacey, M. J.; Bowden, T.; Brandell, D. Beyond PEO-alternative host materials for Li^+-conducting solid polymer electrolytes. *Prog. Polym. Sci.* **2018**, *81*, 114–143.
[36] Sun, C. W.; Liu, J.; Gong, Y. D.; Wilkinson, D. P.; Zhang, J. J. Recent advances in all-solid-state rechargeable lithium batteries. *Nano Energy* **2017**, *33*, 363–386.
[37] Dirican, M.; Yan, C. Y.; Zhu, P.; Zhang, X. W. Composite solid electrolytes for all-solid-state lithium batteries. *Mater. Sci. Eng. R Rep.* **2019**, *136*, 27–46.
[38] Stoeva, Z.; Martin-Litas, I.; Staunton, E.; Andreev, Y. G.; Bruce, P. G. Ionic conductivity in the crystalline polymer electrolytes PEO_6:$LiXF_6$, X = P, As, Sb. *J. Am. Chem. Soc.* **2003**, *125*, 4619–4626.
[39] Gadjourova, Z.; Andreev, Y. G.; Tunstall, D. P.; Bruce, P. G. Ionic conductivity in crystalline polymer electrolytes. *Nature* **2001**, *412*, 520–523.
[40] Aziz, S. B.; Woo, T. J.; Kadir, M. F. Z.; Ahmed, H. M. A conceptual review on polymer electrolytes and ion transport models. *J. Sci. Adv. Mater. Dev.* **2018**, *3*, 1–17.
[41] Ratner, M. A.; Johansson, P.; Shriver, D. F. Polymer electrolytes: Ionic transport mechanisms and relaxation coupling. *MRS Bull.* **2011**, *25*, 31–37.
[42] Yang, H.; Wu, N. Q. Ionic conductivity and ion transport mechanisms of solid-state lithium-ion battery electrolytes: A review. *Energy Sci. Eng.* **2022**, *10*, 1643–1671.
[43] Baskaran, R.; Selvasekarapandian, S.; Kuwata, N.; Kawamura, J.; Hattori, T. Structure, thermal, and transport properties of PVAc-$LiClO_4$ solid polymer electrolytes. *J. Phys. Chem. Solids* **2007**, *68*, 407–412.
[44] Zhang, C. H.; Gamble, S.; Ainsworth, D.; Slawin, A. M. Z.; Andreev, Y. G.; Bruce, P. G. Alkali metal crystalline polymer electrolytes. *Nat. Mater.* **2009**, *8*, 580–584.
[45] Liu, M.; Zhang, S. N.; van Eck, E. R. H.; Wang, C.; Ganapathy, S.; Wagemaker, M. Improving Li-ion interfacial transport in hybrid solid electrolytes. *Nat. Nanotechnol.* **2022**, *17*, 959–967.
[46] Xia, Y. Y.; Xu, N.; Du, L. L.; Cheng, Y.; Lei, S. L.; Li, S. J.; Liao, X. B.; Shi, W. C.; Xu, L.; Mai, L. Q. Rational design of ion transport paths at the interface of metal-organic framework modified solid electrolyte. *ACS Appl. Mater. Interfaces* **2020**, *12*, 22930–22938.
[47] Zhang, X. X.; Oh, T. S.; Fergus, J. W. Densification of ta-doped garnet-type $Li_{6.75}La_3Zr_{1.75}Ta_{0.25}O_{12}$ solid electrolyte materials by sintering in a lithium-rich air atmosphere. *J. Electrochem. Soc.* **2019**, *166*, A3753–A3759.
[48] Yang, L.; Dai, Q. S.; Liu, L.; Shao, D. S.; Luo, K. L.; Jamil, S.; Liu, H.; Luo, Z. G.; Chang, B. B.; Wang, X. Y. Rapid sintering method for highly conductive $Li_7La_3Zr_2O_{12}$ ceramic electrolyte. *Ceram Int.* **2020**, *46*, 10917–10924.
[49] Mackanic, D. G.; Michaels, W.; Lee, M.; Feng, D. W.; Lopez, J.; Qin, J.; Cui, Y.; Bao, Z. N. Crosslinked poly(tetrahydrofuran) as a loosely coordinating polymer electrolyte. *Adv. Energy Mater.* **2018**, *8*, 1800703.
[50] Fu, J. F.; Lu, Q.; Shang, D. P.; Chen, L. Y.; Jiang, Y.; Xu, Y. F.; Yin, J. T.; Dong, X.; Deng, W.; Yuan, S. A novel room temperature POSS ionic liquid-based solid polymer electrolyte. *J. Mater. Sci.* **2018**, *53*, 8420–8435.
[51] Li, Y. H.; Zhang, L. B.; Sun, Z. J.; Gao, G. X.; Lu, S. Y.; Zhu, M.; Zhang, Y. F.; Jia, Z. Y.; Xiao, C. H.; Bu, H. T. et al. Hexagonal boron nitride induces anion trapping in a polyethylene oxide based solid polymer electrolyte for lithium dendrite inhibition. *J. Mater. Chem. A* **2020**, *8*, 9579–9589.
[52] Mindemark, J.; Sun, B.; Törmä, E.; Brandell, D. High-performance solid polymer electrolytes for lithium batteries operational at ambient temperature. *J. Power Sources* **2015**, *298*, 166–170.
[53] Tang, W. J.; Tang, S.; Zhang, C. J.; Ma, Q. T.; Xiang, Q.; Yang, Y. W.; Luo, J. Y. Simultaneously enhancing the thermal stability, mechanical modulus, and electrochemical performance of solid polymer electrolytes by incorporating 2D sheets. *Adv. Energy Mater.* **2018**, *8*. 1800866.
[54] Utpalla, P.; Sharma, S. K.; Sudarshan, K.; Deshpande, S. K.; Sahu, M.; Pujari, P. K. Investigating the correlation of segmental dynamics, free volume characteristics, and ionic conductivity in poly(ethylene oxide)-based electrolyte: A broadband dielectric and positron annihilation spectroscopy study. *J. Phys. Chem. C* **2020**, *124*, 4489–4501.
[55] Devaux, D.; Bouchet, R.; Glé, D.; Denoyel, R. Mechanism of ion transport in PEO/LiTFSI complexes: Effect of temperature, molecular weight, and end groups. *Solid State Ionics* **2012**, *227*, 119–127.
[56] Yahsi, U.; Deligöz, H.; Tav, C.; Ulutaş, K.; Değer, D.; Yılmaztürk, S.; Erdemci, G.; Coşkun, B.; Yılmazoğlu, M.; Yakut, Ş. Ionic conductivity of PVDF-co-HFP/$LiClO_4$ in terms of free volume defects probed by positron annihilation lifetime spectroscopy. *Radiat. Eff. Defect Solids* **2019**, *174*, 214–228.
[57] Williams, M. L.; Landel, R. F.; Ferry, J. D. The temperature dependence of relaxation mechanisms in amorphous polymers and other glass-forming liquids. *J. Am. Chem. Soc.* **2002**, *77*, 3701–3707.
[58] Arya, A.; Sharma, A. L. Polymer electrolytes for lithium ion batteries: A critical study. *Ionics* **2017**, *23*, 497–540.
[59] Carvalho, L. M.; Guégan, P.; Cheradame, H.; Gomes, A. S. Variation of the mesh size of PEO-based networks filled with TFSILi: From an Arrhenius to WLF type conductivity behavior. *Eur. Polym. J.* **2000**, *36*, 401–409.
[60] Carvalho, L. M.; Guegan, P.; Cheradame, H.; Gomes, A. S. Synthesis and electrochemical characterization of crosslinked poly(ethylene oxide) containing $LiN(CF_3SO_2)_2$. *Eur. Polym. J.* **1997**, *33*, 1741–1745.
[61] Liang, C. C. Conduction characteristics of the lithium iodide-aluminum oxide solid electrolytes. *J. Electrochem. Soc.* **1973**, *120*, 1289.
[62] Phipps, J. B.; Whitmore, D. H. Interfacial conduction in lithium iodide containing inert oxides. *J. Power Sources* **1983**, *9*, 373–378.
[63] Nakamura, O.; Goodenough, J. B. Conductivity enhancement of lithium bromide monohydrate by Al_2O_3 particles. *Solid State Ionics* **1982**, *7*, 119–123.
[64] Bunde, A.; Dieterich, W.; Roman, E. Dispersed ionic conductors and percolation theory. *Phys. Rev. Lett.* **1985**, *55*, 5–8.
[65] Liu, W.; Lee, S. W.; Lin, D. C.; Shi, F. F.; Wang, S.; Sendek, A. D.; Cui, Y. Enhancing ionic conductivity in composite polymer electrolytes with well-aligned ceramic nanowires. *Nat. Energy* **2017**, *2*, 17035.
[66] Zhang, X. K.; Xie, J.; Shi, F. F.; Lin, D. C.; Liu, Y. Y.; Liu, W.; Pei, A.; Gong, Y. J.; Wang, H. X.; Liu, K. et al. Vertically aligned and continuous nanoscale ceramic–polymer interfaces in composite solid

polymer electrolytes for enhanced ionic conductivity. *Nano Lett*. **2018**, *18*, 3829–3838.
[67] Kalnaus, S.; Sabau, A. S.; Tenhaeff, W. E.; Dudney, N. J.; Daniel, C. Design of composite polymer electrolytes for Li ion batteries based on mechanical stability criteria. *J. Power Sources* **2012**, *201*, 280–287.
[68] Liu, M.; Cheng, Z.; Ganapathy, S.; Wang, C.; Haverkate, L. A.; Tułodziecki, M.; Unnikrishnan, S.; Wagemaker, M. Tandem interface and bulk Li-ion transport in a hybrid solid electrolyte with microsized active filler. *ACS Energy Lett*. **2019**, *4*, 2336–2342.
[69] Wang, W. M.; Yi, E.; Fici, A. J.; Laine, R. M.; Kieffer, J. Lithium ion conducting poly(ethylene oxide)-based solid electrolytes containing active or passive ceramic nanoparticles. *J. Phys. Chem. C* **2017**, *121*, 2563–2573.
[70] Yang, T.; Zheng, J.; Cheng, Q.; Hu, Y. Y.; Chan, C. K. Composite polymer electrolytes with $Li_7La_3Zr_2O_{12}$ garnet-type nanowires as ceramic fillers: Mechanism of conductivity enhancement and role of doping and morphology. *ACS Appl. Mater. Interfaces* **2017**, *9*, 21773–21780.
[71] Xu, H. H.; Chien, P. H.; Shi, J. J.; Li, Y. T.; Wu, N.; Liu, Y. Y.; Hu, Y. Y.; Goodenough, J. B. High-performance all-solid-state batteries enabled by salt bonding to perovskite in poly(ethylene oxide). *Proc. Natl. Acad. Sci. USA* **2019**, *116*, 18815–18821.
[72] Zheng, J.; Wang, P. B.; Liu, H. Y.; Hu, Y. Y. Interface-enabled ion conduction in $Li_{10}GeP_2S_{12}$-poly(ethylene oxide) hybrid electrolytes. *ACS Appl. Energy Mater*. **2019**, *2*, 1452–1459.
[73] Liu, L. H.; Lyu, J.; Mo, J. S.; Yan, H. J.; Xu, L. L.; Peng, P.; Li, J. R.; Jiang, B.; Chu, L. H.; Li, M. C. Comprehensively-upgraded polymer electrolytes by multifunctional aramid nanofibers for stable all-solid-state Li-ion batteries. *Nano Energy* **2020**, *69*, 104398.
[74] Borodin, O.; Smith, G. D.; Bandyopadhyaya, R.; Redfern, P.; Curtiss, L. A. Molecular dynamics study of nanocomposite polymer electrolyte based on poly(ethylene oxide)/$LiBF_4$. *Modell. Simul. Mater. Sci. Eng*. **2004**, *12*, S73–S89.
[75] Hu, C. J.; Shen, Y. B.; Shen, M.; Liu, X.; Chen, H. W.; Liu, C. H.; Kang, T.; Jin, F.; Li, L.; Li, J. et al. Superionic conductors via bulk interfacial conduction. *J. Am. Chem. Soc*. **2020**, *142*, 18035–18041.
[76] Fang, R. Y.; Xu, B. Y.; Grundish, N. S.; Xia, Y.; Li, Y. T.; Lu, C. W.; Liu, Y. J.; Wu, N.; Goodenough, J. B. Li_2S_6-integrated PEO-based polymer electrolytes for all-solid-state lithium-metal batteries. *Angew. Chem., Int. Ed*. **2021**, *60*, 17701–17706.
[77] Zheng, Y.; Yao, Y. Z.; Ou, J. H.; Li, M.; Luo, D.; Dou, H. Z.; Li, Z. Q.; Amine, K.; Yu, A. P.; Chen, Z. W. A review of composite solid-state electrolytes for lithium batteries: Fundamentals, key materials, and advanced structures. *Chem. Soc. Rev*. **2020**, *49*, 8790–8839.
[78] Yang, L. X.; Luo, D.; Zheng, Y.; Yang, T. Z.; Ma, Q. Y.; Nie, Y. H.; Dou, H. Z.; Zhang, Y. G.; Huang, R.; Yu, A. P. et al. Heterogeneous nanodomain electrolytes for ultra-long-life all-solid-state lithium-metal batteries. *Adv. Funct. Mater*. **2022**, *32*, 2204778.
[79] Li, R. Y.; Hua, H. M.; Zeng, Y. J.; Yang, J.; Chen, Z. Q.; Zhang, P.; Zhao, J. B. Promote the conductivity of solid polymer electrolyte at room temperature by constructing a dual range ionic conduction path. *J. Energy Chem*. **2022**, *64*, 395–403.
[80] Meabe, L.; Huynh, T. V.; Lago, N.; Sardon, H.; Li, C. M.; O'Dell, L. A.; Armand, M.; Forsyth, M.; Mecerreyes, D. Poly(ethylene oxide carbonates) solid polymer electrolytes for lithium batteries. *Electrochim. Acta* **2018**, *264*, 367–375.
[81] Vancaeyzeele, C.; Nguyen, G. T. M.; Michan, A. L.; Viallon, M.; Michal, C. A.; Vidal, F. Lithium-based oligomer ionic liquid for solvent-free conducting materials. *Polymer* **2018**, *142*, 337–347.
[82] Zeng, Z. Q.; Chen, X.; Sun, M. J.; Jiang, Z. P.; Hu, W.; Yu, C.; Cheng, S. J.; Xie, J. Nanophase-separated, elastic epoxy composite thin film as an electrolyte for stable lithium metal batteries. *Nano Lett*. **2021**, *21*, 3611–3618.
[83] Aldalur, I.; Martinez-Ibañez, M.; Piszcz, M.; Rodriguez-Martinez, L. M.; Zhang, H.; Armand, M. Lowering the operational temperature of all-solid-state lithium polymer cell with highly conductive and interfacially robust solid polymer electrolytes. *J. Power Sources* **2018**, *383*, 144–149.
[84] Guan, T. Y.; Qian, S. J.; Guo, Y. K.; Cheng, F. Y.; Zhang, W. Q.; Chen, J. Star brush block copolymer electrolytes with high ambient-temperature ionic conductivity for quasi-solid-state lithium batteries. *ACS Mater. Lett*. **2019**, *1*, 606–612.
[85] Wang, S.; Wang, A. L.; Yang, C. K.; Gao, R.; Liu, X.; Chen, J.; Wang, Z. N.; Zeng, Q. H.; Liu, X. F.; Zhou, H. H. et al. Six-arm star polymer based on discotic liquid crystal as high performance all-solid-state polymer electrolyte for lithium-ion batteries. *J. Power Sources* **2018**, *395*, 137–147.
[86] Khurana, R.; Schaefer, J. L.; Archer, L. A.; Coates, G. W. Suppression of lithium dendrite growth using cross-linked polyethylene/poly(ethylene oxide) electrolytes: A new approach for practical lithium-metal polymer batteries. *J. Am. Chem. Soc*. **2014**, *136*, 7395–7402.
[87] Tong, Y. F.; Lyu, H.; Xu, Y. Z.; Prasad Thapaliya, B.; Li, P. P.; Sun, X. G.; Dai, S. All-solid-state interpenetrating network polymer electrolytes for long cycle life of lithium metal batteries. *J. Mater. Chem. A* **2018**, *6*, 14847–14855.
[88] Park, C. K.; Zhang, Z. W.; Xu, Z. Q.; Kakirde, A.; Kang, K.; Chai, C.; Au, G.; Cristo, L. Variables study for the fast charging lithium ion batteries. *J. Power Sources* **2007**, *165*, 892–896.
[89] Aravindan, V.; Gnanaraj, J.; Madhavi, S.; Liu, H. K. Lithium-ion conducting electrolyte salts for lithium batteries. *Chem. —Eur. J*. **2011**, *17*, 14326–14346.
[90] Banitaba, S. N.; Semnani, D.; Fakhrali, A.; Ebadi, S. V.; Heydari-Soureshjani, E.; Rezaei, B.; Ensafi, A. A. Electrospun PEO nanofibrous membrane enable by LiCl, $LiClO_4$, and LiTFSI salts: A versatile solvent-free electrolyte for lithium-ion battery application. *Ionics* **2020**, *26*, 3249–3260.
[91] Arya, A.; Sharma, A. L. A glimpse on all-solid-state Li-ion battery (ASSLIB) performance based on novel solid polymer electrolytes: A topical review. *J. Mater. Sci*. **2020**, *55*, 6242–6304.
[92] Yang, H.; Zhuang, G. V.; Ross, P. N. Jr. Thermal stability of $LiPF_6$ salt and Li-ion battery electrolytes containing $LiPF_6$. *J. Power Sources* **2006**, *161*, 573–579.
[93] Ibrahim, S.; Yassin, M. M.; Ahmad, R.; Johan, M. R. Effects of various $LiPF_6$ salt concentrations on PEO-based solid polymer electrolytes. *Ionics* **2011**, *17*, 399–405.
[94] Varishetty, M. M.; Qiu, W. L.; Gao, Y.; Chen, W. Structure, electrical, and optical properties of (PVA/$LiAsF_6$) polymer composite electrolyte films. *Polym. Eng. Sci*. **2010**, *50*, 878–884.
[95] Zhang, S. S.; Xu, K.; Jow, T. R. Study of $LiBF_4$ as an electrolyte salt for a Li-ion battery. *J. Electrochem. Soc*. **2002**, *149*, A586–A590.
[96] Wang, X. Y.; Li, S. Y.; Zhang, W. D.; Wang, D.; Shen, Z. Y.; Zheng, J. P.; Zhuang, H. L.; He, Y.; Lu, Y. Y. Dual-salt-additive electrolyte enables high-voltage lithium metal full batteries capable of fast-charging ability. *Nano Energy* **2021**, *89*, 106353.
[97] Liu, Y.; Xie, K.; Pan, Y.; Li, Y. J.; Lu, W.; Liu, S. K.; Zheng, C. M. Impacts of lithium tetrafluoroborate and lithium difluoro(oxalate)borate as additives on the storage life of Li-ion battery at elevated temperature. *Ionics* **2018**, *24*, 1617–1628.
[98] Whba, R. A. G.; TianKhoon, L.; Su'ait, M. S.; Rahman, M. Y. A.; Ahmad, A. Influence of binary lithium salts on 49% poly(methyl methacrylate) grafted natural rubber based solid polymer electrolytes. *Arab. J. Chem*. **2020**, *13*, 3351–3361.
[99] Fahmi, E. M.; Ahmad, A.; Nazeri, N. N. M.; Hamzah, H.; Razali, H.; Rahman, M. Y. A. Effect of $LiBF_4$ salt concentration on the properties of poly (ethylene oxide)-based composite polymer electrolyte. *Int. J. Electrochem. Sci*. **2012**, *7*, 5798–5804.
[100] Noor, S. A. M.; Ahmad, A.; Talib, I. A.; Rahman, M. Y. A. Morphology, chemical interaction, and conductivity of a PEO-ENR50 based on solid polymer electrolyte. *Ionics* **2010**, *16*, 161–170.
[101] Zygadło-Monikowska, E.; Florjańczyk, Z.; Rogalska-Jońska, E.; Werbanowska, A.; Tomaszewska, A.; Langwald, N.; Golodnitsky, D.; Peled, E.; Kovarsky, R.; Chung, S. H. et al. Lithium ion transport of solid electrolytes based on PEO/CF_3SO_3Li and aluminum carboxylate. *J. Power Sources* **2007**, *173*, 734–742.
[102] Radzir, N. N. M.; Hanifah, S. A.; Ahmad, A.; Hassan, N. H.; Bella, F. Effect of lithium bis(trifluoromethylsulfonyl)imide salt-doped UV-cured glycidyl methacrylate. *J. Solid State Electr*. **2015**, *19*, 3079–3085.

[103] Han, H. B.; Zhou, S. S.; Zhang, D. J.; Feng, S. W.; Li, L. F.; Liu, K.; Feng, W. F.; Nie, J.; Li, H.; Huang, X. J. et al. Lithium bis(fluorosulfonyl)imide (LiFSI) as conducting salt for nonaqueous liquid electrolytes for lithium-ion batteries: Physicochemical and electrochemical properties. *J. Power Sources* **2011**, *196*, 3623–3632.
[104] Itoh, T.; Nakamura, K.; Uno, T.; Kubo, M. Thermal and electrochemical properties of poly(2,2-dimethoxypropylene carbonate)-based solid polymer electrolyte for polymer battery. *Solid State Ionics* **2018**, *317*, 69–75.
[105] Appetecchi, G. B.; Zane, D.; Scrosati, B. PEO-based electrolyte membranes based on $LiBC_4O_8$ salt. *J. Electrochem. Soc.* **2004**, *151*, A1369–A1374.
[106] Barbosa, P. C.; Rodrigues, L. C.; Silva, M. M.; Smith, M. J. Characterization of pTMCnLiPF$_6$ solid polymer electrolytes. *Solid State Ionics* **2011**, *193*, 39–42.
[107] Perumal, P.; Christopher Selvin, P.; Selvasekarapandian, S.; Sivaraj, P. Structural and electrical properties of bio-polymer pectin with $LiClO_4$ solid electrolytes for lithium ion polymer batteries. *Mater. Today Proc.* **2019**, *8*, 196–202.
[108] Chong, W. G.; Osman, Z. The effect of carbonate-phthalate plasticizers on structural, morphological, and electrical properties of polyacrylonitrile-based solid polymer electrolytes. *J. Polym. Res.* **2014**, *21*, 381.
[109] Zhang, Z. Y.; Antonio, R. G.; Choy, K. L. Boron nitride enhanced polymer/salt hybrid electrolytes for all-solid-state lithium ion batteries. *J. Power Sources* **2019**, *435*, 226736.
[110] Tao, S. D.; Li, J.; Hu, R.; Wang, L. H.; Chi, Z. X.; Li, T. F. $3Li_2S$-$2MoS_2$ filled composite polymer PVDF-HFP/LiODFB electrolyte with excellent interface performance for lithium metal batteries. *Appl. Surf. Sci.* **2021**, *536*, 147794.
[111] Baskoro, F.; Wong, H. Q.; Yen, H. J. Strategic structural design of a gel polymer electrolyte toward a high efficiency lithium-ion battery. *ACS Appl. Energy Mater.* **2019**, *2*, 3937–3971.
[112] Banitaba, S. N.; Semnani, D.; Heydari-Soureshjani, E.; Rezaei, B.; Ensafi, A. A. The effect of concentration and ratio of ethylene carbonate and propylene carbonate plasticizers on characteristics of the electrospun PEO-based electrolytes applicable in lithium-ion batteries. *Solid State Ionics* **2020**, *347*, 115252.
[113] Fan, L.; Wei, S. Y.; Li, S. Y.; Li, Q.; Lu, Y. Y. Recent progress of the solid-state electrolytes for high-energy metal-based batteries. *Adv. Energy Mater.* **2018**, *8*, 1702657.
[114] Pan, J.; Zhang, Y. C.; Wang, J.; Bai, Z. C.; Cao, R. G.; Wang, N. N.; Dou, S. X.; Huang, F. Q. A quasi-double-layer solid electrolyte with adjustable interphases enabling high-voltage solid-state batteries. *Adv. Mater.* **2022**, *34*, 2107183.
[115] Klongkan, S.; Pumchusak, J. Effects of nano alumina and plasticizers on morphology, ionic conductivity, thermal, and mechanical properties of PEO-$LiCF_3SO_3$ solid polymer electrolyte. *Electrochim. Acta* **2015**, *161*, 171–176.
[116] Guo, Q. P.; Han, Y.; Wang, H.; Xiong, S. Z.; Sun, W. W.; Zheng, C. M.; Xie, K. Flame retardant and stable $Li_{1.5}Al_{0.5}Ge_{1.5}(PO_4)_3$-supported ionic liquid gel polymer electrolytes for high safety rechargeable solid-state lithium metal batteries. *J. Phys. Chem. C* **2018**, *122*, 10334–10342.
[117] Rathika, R.; Suthanthiraraj, S. A. Influence of 1-ethyl-3-methylimidazolium bis (trifluoromethyl sulfonyl) imide plasticization on zinc-ion conducting PEO/PVDF blend gel polymer electrolyte. *J. Mater. Sci. Mater. Electron.* **2018**, *29*, 19632–19643.
[118] MacFarlane, D. R.; Forsyth, M. Plastic crystal electrolyte materials: New perspectives on solid state ionics. *Adv. Mater.* **2001**, *13*, 957–966.
[119] Chen, F.; Zha, W. P.; Yang, D. J.; Cao, S. Y.; Shen, Q.; Zhang, L. M.; Sadoway, D. R. All-solid-state lithium battery fitted with polymer electrolyte enhanced by solid plasticizer and conductive ceramic filler. *J. Electrochem. Soc.* **2018**, *165*, A3558–A3565.
[120] Fan, L. Z.; Wang, X. L.; Long, F.; Wang, X. Enhanced ionic conductivities in composite polymer electrolytes by using succinonitrile as a plasticizer. *Solid State Ionics* **2008**, *179*, 1772–1775.
[121] Zha, W. P.; Li, J. Y.; Li, W. W.; Sun, C. Z.; Wen, Z. Y. Anchoring succinonitrile by solvent-Li^+ associations for high-performance solid-state lithium battery. *Chem. Eng. J.* **2021**, *406*, 126754.
[122] Liu, Y. L.; Zhao, Y.; Lu, W.; Sun, L. Q.; Lin, L.; Zheng, M.; Sun, X. L.; Xie, H. M. PEO based polymer in plastic crystal electrolytes for room temperature high-voltage lithium metal batteries. *Nano Energy* **2021**, *88*, 106205.
[123] Choi, K. H.; Cho, S. J.; Kim, S. H.; Kwon, Y. H.; Kim, J. Y.; Lee, S. Y. Thin, deformable, and safety-reinforced plastic crystal polymer electrolytes for high-performance flexible lithium-ion batteries. *Adv. Funct. Mater.* **2014**, *24*, 44–52.
[124] Wang, F. R.; Li, L. B.; Yang, X. Y.; You, J.; Xu, Y. P.; Wang, H.; Ma, Y.; Gao, G. X. Influence of additives in a PVDF-based solid polymer electrolyte on conductivity and Li-ion battery performance. *Sustainable Energy Fuels* **2018**, *2*, 492–498.
[125] Das, S.; Ghosh, A. Charge carrier relaxation in different plasticized PEO/PVDF-HFP blend solid polymer electrolytes. *J. Phys. Chem. B* **2017**, *121*, 5422–5432.
[126] Jinisha, B.; Anilkumar, K. M.; Manoj, M.; Pradeep, V. S.; Jayalekshmi, S. Development of a novel type of solid polymer electrolyte for solid state lithium battery applications based on lithium enriched poly (ethylene oxide) (PEO)/poly (vinyl pyrrolidone) (PVP) blend polymer. *Electrochim. Acta* **2017**, *235*, 210–222.
[127] Choudhary, S. Effects of amorphous silica nanoparticles and polymer blend compositions on the structural, thermal, and dielectric properties of PEO-PMMA blend based polymer nanocomposites. *J. Polym. Res.* **2018**, *25*, 116.
[128] Dhatarwal, P.; Sengwa, R. J. Influence of solid polymer electrolyte preparation methods on the performance of (PEO-PMMA)-$LiBF_4$ films for lithium-ion battery applications. *Polym Bull.* **2018**, *75*, 5645–5666.
[129] Li, J. L.; Zhu, L.; Xu, J. N.; Jing, M. X.; Yao, S. S.; Shen, X. Q.; Li, S. J.; Tu, F. Y. Boosting the performance of poly(ethylene oxide)-based solid polymer electrolytes by blending with poly(vinylidene fluoride-co-hexafluoropropylene) for solid-state lithium-ion batteries. *Int. J. Energy Res.* **2020**, *44*, 7831–7840.
[130] Liu, L. H.; Mo, J. S.; Li, J. R.; Liu, J. X.; Yan, H. J.; Lyu, J.; Jiang, B.; Chu, L. H.; Li, M. C. Comprehensively-modified polymer electrolyte membranes with multifunctional PMIA for highly-stable all-solid-state lithium-ion batteries. *J. Energy Chem.* **2020**, *48*, 334–343.
[131] Wang, H.; Lin, C.; Yan, X. H.; Wu, A. M.; Shen, S. Y.; Wei, G. H.; Zhang, J. L. Mechanical property-reinforced PEO/PVDF/$LiClO_4$/SN blend all solid polymer electrolyte for lithium ion batteries. *J. Electroanal. Chem.* **2020**, *869*, 114156.
[132] Shenbagavalli, S.; Muthuvinayagam, M.; Revathy, M. S. Preparation and characterization of proton (H^+) conducting solid blend polymer electrolytes based on PEO/P(VdF-HFP) incorporated with NH_4SCN. *J. Non-Cryst. Solids* **2022**, *579*, 121368.
[133] Lv, Z. L.; Tang, Y.; Dong, S. M.; Zhou, Q.; Cui, G. L. Polyurethane-based polymer electrolytes for lithium Batteries: Advances and perspectives. *Chem. Eng. J* **2022**, *430*, 132659.
[134] Yu, X. Y.; Xiao, M.; Wang, S. J.; Zhao, Q. Q.; Meng, Y. Z. Fabrication and characterization of PEO/PPC polymer electrolyte for lithium-ion battery. *J. Appl. Polym. Sci.* **2010**, *115*, 2718–2722.
[135] Zhang, J. J.; Zhao, J. H.; Yue, L. P.; Wang, Q. F.; Chai, J. C.; Liu, Z. H.; Zhou, X. H.; Li, H.; Guo, Y. G.; Cui, G. L. et al. Safety-reinforced poly(propylene carbonate)-based all-solid-state polymer electrolyte for ambient-temperature solid polymer lithium batteries. *Adv. Energy Mater.* **2015**, *5*, 1501082.
[136] Nourisabet, T.; Aval, H. J.; Shidpour, R.; Naji, L. Fabrication of a PEO-PVDF blend based polymer composite electrolyte with extremely high ionic conductivity via the addition of LLTO nanowires. *Solid State Ionics* **2022**, *377*, 115885.
[137] Mallaiah, Y.; Jeedi, V. R.; Swarnalatha, R.; Raju, A.; Reddy, S. N.; Chary, A. S. Impact of polymer blending on ionic conduction mechanism and dielectric properties of sodium based PEO-PVDF solid polymer electrolyte systems. *J. Phys. Chem. Solids* **2021**, *155*, 110096.

[138] Rocco, A. M.; Pereira, R. P. Solid electrolytes based on poly(ethylene oxide)/poly(4-vinyl phenol-co-2-hydroxyethyl methacrylate) blends and $LiClO_4$. *Solid State Ionics* **2015**, *279*, 78–89.
[139] Li, Y. J.; Fan, C. Y.; Zhang, J. P.; Wu, X. L. A promising PMHS/PEO blend polymer electrolyte for all-solid-state lithium ion batteries. *Dalton Trans*. **2018**, *47*, 14932–14937.
[140] Patla, S. K.; Ray, R.; Asokan, K.; Karmakar, S. Investigation of ionic conduction in PEO-PVDF based blend polymer electrolytes. *J. Appl. Phys*. **2018**, *123*, 125102.
[141] Glynos, E.; Petropoulou, P.; Mygiakis, E.; Nega, A. D.; Pan, W. Y.; Papoutsakis, L.; Giannelis, E. P.; Sakellariou, G.; Anastasiadis, S. H. Leveraging molecular architecture to design new, all-polymer solid electrolytes with simultaneous enhancement in modulus and ionic conductivity. *Macromolecules* **2018**, *51*, 2542–2550.
[142] B. Puthirath, A.; Patra, S.; Pal, S.; M, M.; Puthirath Balan, A.; S, J.; Tharangattu N, N. Transparent flexible lithium ion conducting solid polymer electrolyte. *J. Mater. Chem. A* **2017**, *5*, 11152–11162.
[143] Bao, J. J.; Qu, X. B.; Qi, G. Q.; Huang, Q. K.; Wu, S. F.; Tao, C.; Gao, M. H.; Chen, C. H. Solid electrolyte based on waterborne polyurethane and poly(ethylene oxide) blend polymer for all-solid-state lithium ion batteries. *Solid State Ionics* **2018**, *320*, 55–63.
[144] Liang, H. P.; Zarrabeitia, M.; Chen, Z.; Jovanovic, S.; Merz, S.; Granwehr, J.; Passerini, S.; Bresser, D. Polysiloxane-based single-ion conducting polymer blend electrolyte comprising small-molecule organic carbonates for high-energy and high-power lithium-metal batteries. *Adv. Energy Mater*. **2022**, *12*, 2200013.
[145] Zhao, Y. B.; Bai, Y.; Bai, Y. P.; An, M. Z.; Chen, G. R.; Li, W. D.; Li, C.; Zhou, Y. F. A rational design of solid polymer electrolyte with high salt concentration for lithium battery. *J. Power Sources* **2018**, *407*, 23–30.
[146] Li, Z. G.; Mogensen, R.; Mindemark, J.; Bowden, T.; Brandell, D.; Tominaga, Y. Ion-conductive and thermal properties of a synergistic poly(ethylene carbonate)/poly(trimethylene carbonate) blend electrolyte. *Macromol. Rapid Commun*. **2018**, *39*, 1800146.
[147] Vignarooban, K.; Dissanayake, M. A. K. L.; Albinsson, I.; Mellander, B. E. Effect of TiO_2 nano-filler and EC plasticizer on electrical and thermal properties of poly(ethylene oxide) (PEO) based solid polymer electrolytes. *Solid State Ionics* **2014**, *266*, 25–28.
[148] Masoud, E. M.; El-Bellihi, A. A.; Bayoumy, W. A.; Mousa, M. A. Organic–inorganic composite polymer electrolyte based on PEO-$LiClO_4$ and nano-Al_2O_3 filler for lithium polymer batteries: Dielectric and transport properties. *J. Alloys Compd*. **2013**, *575*, 223–228.
[149] Li, W. W.; Zhang, S. P.; Wang, B. R.; Gu, S.; Xu, D.; Wang, J. N.; Chen, C. H.; Wen, Z. Y. Nanoporous adsorption effect on alteration of the Li^+ diffusion pathway by a highly ordered porous electrolyte additive for high-rate all-solid-state lithium metal batteries. *ACS Appl. Mater. Interfaces* **2018**, *10*, 23874–23882.
[150] Wu, N.; Chien, P. H.; Qian, Y. M.; Li, Y. T.; Xu, H. H.; Grundish, N. S.; Xu, B. Y.; Jin, H. B.; Hu, Y. Y.; Yu, G. H. et al. Enhanced surface interactions enable fast Li^+ conduction in oxide/polymer composite electrolyte. *Angew. Chem., Int. Ed*. **2020**, *59*, 4131–4137.
[151] Liang, Y.; Liu, Y.; Chen, D.; Dong, L.; Guang, Z.; Liu, J.; Yuan, B.; Yang, M.; Dong, Y.; Li, Q. et al. Hydroxyapatite functionalization of solid polymer electrolytes for high-conductivity solid-state lithium-ion batteries. *Mater. Today Energy* **2021**, *20*, 100694.
[152] Ma, C.; Dai, K.; Hou, H. S.; Ji, X. B.; Chen, L. B.; Ivey, D. G.; Wei, W. F. High ion-conducting solid-state composite electrolytes with carbon quantum dot nanofillers. *Adv. Sci*. **2018**, *5*, 1700996.
[153] Liu, R. P.; He, P.; Wu, Z. R.; Guo, F.; Huang, B.; Wang, Q.; Huang, Z. Y.; Wang, C.-A.; Li, Y. T., PEO/hollow mesoporous polymer spheres composites as electrolyte for all solid state lithium ion battery. *J. Electroanal. Chem.* **2018**, *822*, 105–111.
[154] Wang, S.; Liu, X.; Wang, A. L.; Wang, Z. N.; Chen, J.; Zeng, Q. H.; Jiang, X. R.; Zhou, H. H.; Zhang, L. Y., High-performance all-solid-state polymer electrolyte with controllable conductivity pathway formed by self-assembly of reactive discogen and immobilized via a facile photopolymerization for a lithium-ion battery. *ACS Appl. Mater. Interfaces* **2018**, *10*, 25273–25284.
[155] Fu, X. W.; Li, C. H.; Wang, Y.; Kovatch, L. P.; Scudiero, L.; Liu, J.; Zhong, W. H. Building ion-conduction highways in polymeric electrolytes by manipulating protein configuration. *ACS Appl. Mater. Interfaces* **2018**, *10*, 4726–4736.
[156] Zhu, K.; Liu, Y. X.; Liu, J. A fast charging/discharging all-solid-state lithium ion battery based on PEO-MIL-53(Al)-LiTFSI thin film electrolyte. *RSC Adv*. **2014**, *4*, 42278–42284.
[157] Wu, J. F.; Guo, X. MOF-derived nanoporous multifunctional fillers enhancing the performances of polymer electrolytes for solid-state lithium batteries. *J. Mater. Chem. A* **2019**, *7*, 2653–2659.
[158] Gutiérrez-Pardo, A.; Pitillas Martinez, A. I.; Otaegui, L.; Schneider, M.; Roters, A.; Llordés, A.; Aguesse, F.; Buannic, L. Will the competitive future of solid state Li metal batteries rely on a ceramic or a composite electrolyte? *Sustainable Energy Fuels* **2018**, *2*, 2325–2334.
[159] Zhao, Y. R.; Huang, Z.; Chen, S. J.; Chen, B.; Yang, J.; Zhang, Q.; Ding, F.; Chen, Y. H.; Xu, X. X. A promising PEO/LAGP hybrid electrolyte prepared by a simple method for all-solid-state lithium batteries. *Solid State Ionics* **2016**, *295*, 65–71.
[160] Chen, S. J.; Wang, J. Y.; Zhang, Z. H.; Wu, L. B.; Yao, L. L.; Wei, Z. Y.; Deng, Y. H.; Xie, D. J.; Yao, X. Y.; Xu, X. X. *In situ* preparation of poly(ethylene oxide)/Li_3PS_4 hybrid polymer electrolyte with good nanofiller distribution for rechargeable solid-state lithium batteries. *J. Power Sources* **2018**, *387*, 72–80.
[161] Cao, J.; Wang, L.; He, X. M.; Fang, M.; Gao, J.; Li, J. J.; Deng, L. F.; Chen, H.; Tian, G. Y.; Wang, J. L. et al. *In situ* prepared nano-crystalline TiO_2-poly(methyl methacrylate) hybrid enhanced composite polymer electrolyte for Li-ion batteries. *J. Mater. Chem. A* **2013**, *1*, 5955–5961.
[162] Fu, K.; Gong, Y. H.; Dai, J. Q.; Gong, A.; Han, X. G.; Yao, Y. G.; Wang, C. W.; Wang, Y. B.; Chen, Y. N.; Yan, C. Y. et al. Flexible, solid-state, ion-conducting membrane with 3D garnet nanofiber networks for lithium batteries. *Proc. Natl. Acad. Sci. USA* **2016**, *113*, 7094–7099.
[163] Zheng, J.; Tang, M. X.; Hu, Y. Y. Lithium ion pathway within $Li_7La_3Zr_2O_{12}$-polyethylene oxide composite electrolytes. *Angew. Chem., Int. Ed*. **2016**, *55*, 12538–12542.
[164] Zheng, J.; Hu, Y. Y. New insights into the compositional dependence of Li-ion transport in polymer-ceramic composite electrolytes. *ACS Appl. Mater. Interfaces* **2018**, *10*, 4113–4120.
[165] Zhang, J. J.; Zang, X.; Wen, H. J.; Dong, T. T.; Chai, J. C.; Li, Y.; Chen, B. B.; Zhao, J. W.; Dong, S. M.; Ma, J. et al. High-voltage and free-standing poly(propylene carbonate)/$Li_{6.75}La_3Zr_{1.75}Ta_{0.25}O_{12}$ composite solid electrolyte for wide temperature range and flexible solid lithium ion battery. *J. Mater. Chem. A* **2017**, *5*, 4940–4948.
[166] Zhai, H. W.; Xu, P. Y.; Ning, M. Q.; Cheng, Q.; Mandal, J.; Yang, Y. A flexible solid composite electrolyte with vertically aligned and connected ion-conducting nanoparticles for lithium batteries. *Nano Lett*. **2017**, *17*, 3182–3187.
[167] Liu, X. Q.; Peng, S.; Gao, S. Y.; Cao, Y. C.; You, Q. L.; Zhou, L. Y.; Jin, Y. C.; Liu, Z. H.; Liu, J. Y. Electric-field-directed parallel alignment architecting 3D lithium-ion pathways within solid composite electrolyte. *ACS Appl. Mater. Interfaces* **2018**, *10*, 15691–15696.
[168] Lin, D. C.; Liu, W.; Liu, Y. Y.; Lee, H. R.; Hsu, P. C.; Liu, K.; Cui, Y. High ionic conductivity of composite solid polymer electrolyte via *in situ* synthesis of monodispersed SiO_2 nanospheres in poly(ethylene oxide). *Nano Lett*. **2016**, *16*, 459–465.
[169] Huang, Z. Y.; Pang, W. Y.; Liang, P.; Jin, Z. H.; Grundish, N.; Li, Y. T.; Wang, C. A. A dopamine modified $Li_{6.4}La_3Zr_{1.4}Ta_{0.6}O_{12}$/PEO solid-state electrolyte: Enhanced thermal and electrochemical properties. *J. Mater. Chem. A* **2019**, *7*, 16425–16436.
[170] Zhang, P.; Yang, L. C.; Li, L. L.; Ding, M. L.; Wu, Y. P.; Holze, R. Enhanced electrochemical and mechanical properties of P(VDF-HFP)-based composite polymer electrolytes with SiO_2 nanowires. *J. Membrane Sci*. **2011**, *379*, 80–85.
[171] Liu, W.; Liu, N.; Sun, J.; Hsu, P. C.; Li, Y. Z.; Lee, H. W.; Cui, Y. Ionic conductivity enhancement of polymer electrolytes with ceramic nanowire fillers. *Nano Lett*. **2015**, *15*, 2740–2745.

[172] Sheng, O. W.; Jin, C. B.; Luo, J. M.; Yuan, H. D.; Huang, H.; Gan, Y. P.; Zhang, J.; Xia, Y.; Liang, C.; Zhang, W. K. et al. $Mg_2B_2O_5$ nanowire enabled multifunctional solid-state electrolytes with high ionic conductivity, excellent mechanical properties, and flame-retardant performance. *Nano Lett*. **2018**, *18*, 3104–3112.
[173] Liu, W.; Lin, D. C.; Sun, J.; Zhou, G. M.; Cui, Y. Improved lithium ionic conductivity in composite polymer electrolytes with oxide-ion conducting nanowires. *ACS Nano* **2016**, *10*, 11407–11413.
[174] Pignanelli, F.; Romero, M.; Faccio, R.; Fernández-Werner, L.; Mombrú, A. W. Enhancement of lithium-ion transport in poly(acrylonitrile) with hydrogen titanate nanotube fillers as solid polymer electrolytes for lithium-ion battery applications. *J. Phys. Chem. C* **2018**, *122*, 1492–1499.
[175] Guo, X. Q.; Peng, W. J.; Wu, Y. Q.; Guo, H. J.; Wang, Z. X.; Li, X. H.; Ke, Y.; Wu, L. J.; Fu, H. K.; Wang, J. X. $Al_4B_2O_9$ nanorods-modified solid polymer electrolytes with decent integrated performance. *Sci. China Mater*. **2021**, *64*, 296–306.
[176] Gomari, S.; Esfandeh, M.; Ghasemi, I. All-solid-state flexible nanocomposite polymer electrolytes based on poly(ethylene oxide): Lithium perchlorate using functionalized graphene. *Solid State Ionics* **2017**, *303*, 37–46.
[177] Yuan, M. Y.; Erdman, J.; Tang, C. Y.; Ardebili, H. High performance solid polymer electrolyte with graphene oxide nanosheets. *RSC Adv*. **2014**, *4*, 59637–59642.
[178] Shim, J.; Kim, D. G.; Kim, H. J.; Lee, J. H.; Baik, J. H.; Lee, J. C. Novel composite polymer electrolytes containing poly(ethylene glycol)-grafted graphene oxide for all-solid-state lithium-ion battery applications. *J. Mater. Chem. A* **2014**, *2*, 13873–13883.
[179] Ye, Y. S.; Wang, H.; Bi, S. G.; Xue, Y.; Xue, Z. G.; Zhou, X. P.; Xie, X. L.; Mai, Y. W. High performance composite polymer electrolytes using polymeric ionic liquid-functionalized graphene molecular brushes. *J. Mater. Chem. A* **2015**, *3*, 18064–18073.
[180] Sun, Z. J.; Li, Y. H.; Zhang, S. Y.; Shi, L.; Wu, H.; Bu, H. T.; Ding, S. J. g-C_3N_4 nanosheets enhanced solid polymer electrolytes with excellent electrochemical performance, mechanical properties, and thermal stability. *J. Mater. Chem. A* **2019**, *7*, 11069–11076.
[181] An, H. W.; Liu, Q. S.; An, J. L.; Liang, S. T.; Wang, X. F.; Xu, Z. W.; Tong, Y. J.; Huo, H.; Sun, N.; Wang, Y. L. et al. Coupling two-dimensional fillers with polymer chains in solid polymer electrolyte for room-temperature dendrite-free lithium-metal batteries. *Energy Storage Mater*. **2021**, *43*, 358–364.
[182] Pan, Q. W.; Zheng, Y. W.; Kota, S.; Huang, W. C.; Wang, S. J.; Qi, H.; Kim, S.; Tu, Y. F.; Barsoum, M. W.; Li, C. Y. 2D MXene-containing polymer electrolytes for all-solid-state lithium metal batteries. *Nanoscale Adv*. **2019**, *1*, 395–402.
[183] Chen, L.; Li, W. X.; Fan, L. Z.; Nan, C. W.; Zhang, Q. Intercalated electrolyte with high transference number for dendrite-free solid-state lithium batteries. *Adv. Funct. Mater*. **2019**, *29*, 1901047.
[184] Wang, Q.; Wu, J. F.; Yu, Z. Y.; Guo, X. Composite polymer electrolytes reinforced by two-dimensional layer-double-hydroxide nanosheets for dendrite-free lithium batteries. *Solid State Ionics* **2020**, *347*, 115275.
[185] Xia, S. X.; Yang, B. B.; Zhang, H. B.; Yang, J. H.; Liu, W.; Zheng, S. Y. Ultrathin layered double hydroxide nanosheets enabling composite polymer electrolyte for all-solid-state lithium batteries at room temperature. *Adv. Funct. Mater*. **2021**, *31*, 2101168.
[186] Sun, Y. Y.; Jin, F.; Li, J.; Liu, B. T.; Chen, X.; Dong, H. C.; Mao, Y. Y.; Gu, W.; Xu, J. J.; Shen, Y. B. et al. Composite solid electrolyte for solid-state lithium batteries workable at room temperature. *ACS Appl. Energy Mater.* **2020**, *3*, 12127–12133.
[187] Li, D.; Chen, L.; Wang, T. S.; Fan, L. Z. 3D fiber-network-reinforced bicontinuous composite solid electrolyte for dendrite-free lithium metal batteries. *ACS Appl. Mater. Interfaces* **2018**, *10*, 7069–7078.
[188] Bae, J.; Li, Y. T.; Zhang, J.; Zhou, X. Y.; Zhao, F.; Shi, Y.; Goodenough, J. B.; Yu, G. H. A 3D nanostructured hydrogel-framework-derived high-performance composite polymer lithium-ion electrolyte. *Angew. Chem., Int. Ed*. **2018**, *57*, 2096–2100.
[189] Zekoll, S.; Marriner-Edwards, C.; Hekselman, A. K. O.; Kasemchainan, J.; Kuss, C.; Armstrong, D. E. J.; Cai, D. Y.; Wallace, R. J.; Richter, F. H.; Thijssen, J. H. J. et al. Hybrid electrolytes with 3D bicontinuous ordered ceramic and polymer microchannels for all-solid-state batteries. *Energy Environ. Sci*. **2018**, *11*, 185–201.
[190] Gong, Y. H.; Fu, K.; Xu, S. M.; Dai, J. Q.; Hamann, T. R.; Zhang, L.; Hitz, G. T.; Fu, Z. Z.; Ma, Z. H.; McOwen, D. W. et al. D. Lithium-ion conductive ceramic textile: A new architecture for flexible solid-state lithium metal batteries. *Mater. Today* **2018**, *21*, 594–601.
[191] Li, Z.; Sha, W. X.; Guo, X. Three-dimensional garnet framework-reinforced solid composite electrolytes with high lithium-ion conductivity and excellent stability. *ACS Appl. Mater. Interfaces* **2019**, *11*, 26920–26927.
[192] Jin, Y. M.; Zong, X.; Zhang, X. B.; Liu, C. J.; Li, D.; Jia, Z. G.; Li, G.; Zhou, X. G.; Wei, J. H.; Xiong, Y. P. Interface regulation enabling three-dimensional $Li_{1.3}Al_{0.3}Ti_{1.7}(PO_4)_3$-reinforced composite solid electrolyte for high-performance lithium batteries. *J. Power Sources* **2021**, *501*, 230027.
[193] Gao, L.; Li, J. X.; Ju, J. G.; Wang, L. Y.; Yan, J.; Cheng, B. W.; Kang, W. M.; Deng, N. P.; Li, Y. T. Designing of root-soil-like polyethylene oxide-based composite electrolyte for dendrite-free and long-cycling all-solid-state lithium metal batteries. *Chem. Eng. J*. **2020**, *389*, 124478.
[194] Gao, L.; Sarmad, B.; Li, J. X.; Cheng, B. W.; Kang, W. M.; Deng, N. P. Application of polyamide 6 microfiber non-woven fabrics in the large-scale production of all-solid-state lithium metal batteries. *J. Power Sources* **2020**, *475*, 228663.
[195] Qin, H. F.; Fu, K.; Zhang, Y.; Ye, Y. H.; Song, M. Y.; Kuang, Y. D.; Jang, S. H.; Jiang, F.; Cui, L. F. Flexible nanocellulose enhanced Li^+ conducting membrane for solid polymer electrolyte. *Energy Storage Mater*. **2020**, *28*, 293–299.
[196] Liu, L. H.; Lyu, J.; Mo, J. S.; Peng, P.; Li, J. R.; Jiang, B.; Chu, L. H.; Li, M. C. Flexible, high-voltage, ion-conducting composite membranes with 3D aramid nanofiber frameworks for stable all-solid-state lithium metal batteries. *Sci. China Mater*. **2020**, *63*, 703–718.
[197] Watanabe, T.; Inafune, Y.; Tanaka, M.; Mochizuki, Y.; Matsumoto, F.; Kawakami, H. Development of all-solid-state battery based on lithium ion conductive polymer nanofiber framework. *J. Power Sources* **2019**, *423*, 255–262.
[198] Yang, X. F.; Sun, Q.; Zhao, C. T.; Gao, X. J.; Adair, K. R.; Liu, Y. L.; Luo, J.; Lin, X. T.; Liang, J. N.; Huang, H. et al. High-areal-capacity all-solid-state lithium batteries enabled by rational design of fast ion transport channels in vertically-aligned composite polymer electrodes. *Nano Energy* **2019**, *61*, 567–575.
[199] Pal, P.; Ghosh, A. Influence of TiO_2 nano-particles on charge carrier transport and cell performance of PMMA-$LiClO_4$ based nano-composite electrolytes. *Electrochim. Acta* **2018**, *260*, 157–167.
[200] Wang, Q. J.; Song, W. L.; Fan, L. Z.; Song, Y. Flexible, high-voltage, and free-standing composite polymer electrolyte membrane based on triethylene glycol diacetate-2-propenoic acid butyl ester copolymer for lithium-ion batteries. *J. Membrane Sci*. **2015**, *492*, 490–496.
[201] Li, Z.; Huang, H. M.; Zhu, J. K.; Wu, J. F.; Yang, H.; Wei, L.; Guo, X. Ionic conduction in composite polymer electrolytes: Case of PEO:Ga-LLZO composites. *ACS Appl. Mater. Interfaces* **2019**, *11*, 784–791.
[202] Karthik, K.; Murugan, R. Lithium garnet based free-standing solid polymer composite membrane for rechargeable lithium battery. *J. Solid State Electr*. **2018**, *22*, 2989–2998.
[203] Zhang, X.; Liu, T.; Zhang, S. F.; Huang, X.; Xu, B. Q.; Lin, Y. H.; Xu, B.; Li, L. L.; Nan, C. W.; Shen, Y. Synergistic coupling between $Li_{6.75}La_3Zr_{1.75}Ta_{0.25}O_{12}$ and poly(vinylidene fluoride) induces high ionic conductivity, mechanical strength, and thermal stability of solid composite electrolytes. *J. Am. Chem. Soc*. **2017**, *139*, 13779–13785.
[204] Cheng, S. H. S.; He, K. Q.; Liu, Y.; Zha, J. W.; Kamruzzaman, M.; Ma, R. L. W.; Dang, Z. M.; Li, R. K. Y.; Chung, C. Y. Electrochemical performance of all-solid-state lithium batteries using inorganic lithium garnets particulate reinforced PEO/$LiClO_4$ electrolyte. *Electrochim. Acta* **2017**, *253*, 430–438.

[205] Zhao, Y. R.; Wu, C.; Peng, G.; Chen, X. T.; Yao, X. Y.; Bai, Y.; Wu, F.; Chen, S. J.; Xu, X. X. A new solid polymer electrolyte incorporating $Li_{10}GeP_2S_{12}$ into a polyethylene oxide matrix for all-solid-state lithium batteries. *J. Power Sources* **2016**, *301*, 47–53.

[206] Xu, X. Y.; Hou, G. M.; Nie, X. K.; Ai, Q.; Liu, Y.; Feng, J. K.; Zhang, L.; Si, P. C.; Guo, S. R.; Ci, L. J. $Li_7P_3S_{11}$/poly(ethylene oxide) hybrid solid electrolytes with excellent interfacial compatibility for all-solid-state batteries. *J. Power Sources* **2018**, *400*, 212–217.

[207] Bao, W. D.; Zhao, L. Q.; Zhao, H. J.; Su, L. X.; Cai, X. C.; Yi, B. L.; Zhang, Y.; Xie, J. Vapor phase infiltration of ZnO quantum dots for all-solid-state PEO-based lithium batteries. *Energy Storage Mater*. **2021**, *43*, 258–265.

[208] Sasikumar, M.; Raja, M.; Krishna, R. H.; Jagadeesan, A.; Sivakumar, P.; Rajendran, S. Influence of hydrothermally synthesized cubic-structured $BaTiO_3$ ceramic fillers on ionic conductivity, mechanical integrity, and thermal behavior of P(VDF-HFP)/PVAc-based composite solid polymer electrolytes for lithium-ion batteries. *J. Phys. Chem. C* **2018**, *122*, 25741–25752.

[209] Zhu, P.; Yan, C. Y.; Dirican, M.; Zhu, J. D.; Zang, J.; Selvan, R. K.; Chung, C. C.; Jia, H.; Li, Y.; Kiyak, Y. et al. $Li_{0.33}La_{0.557}TiO_3$ ceramic nanofiber-enhanced polyethylene oxide-based composite polymer electrolytes for all-solid-state lithium batteries. *J. Mater. Chem. A* **2018**, *6*, 4279–4285.

[210] Fan, R.; Liu, C.; He, K. Q.; Cheng, S. H. S.; Chen, D. Z.; Liao, C. Z.; Li, R. K. Y.; Tang, J. N.; Lu, Z. G. Versatile strategy for realizing flexible room-temperature all-solid-state battery through a synergistic combination of salt affluent PEO and $Li_{6.75}La_3Zr_{1.75}Ta_{0.25}O_{12}$ nanofibers. *ACS Appl. Mater. Interfaces* **2020**, *12*, 7222–7231.

[211] Gao, L.; Luo, S. B.; Li, J. X.; Cheng, B. W.; Kang, W. M.; Deng, N. P. Core–shell structure nanofibers-ceramic nanowires based composite electrolytes with high Li transference number for high-performance all-solid-state lithium metal batteries. *Energy Storage Mater*. **2021**, *43*, 266–274.

[212] Zhang, Z.; Huang, Y.; Gao, H.; Li, C.; Huang, J. X.; Liu, P. B. 3D glass fiber cloth reinforced polymer electrolyte for solid-state lithium metal batteries. *J. Membrane Sci*. **2021**, *621*, 118940.

[213] Chen, L.; Li, Y. T.; Li, S. P.; Fan, L. Z.; Nan, C. W.; Goodenough, J. B. PEO/garnet composite electrolytes for solid-state lithium batteries: From "ceramic-in-polymer" to "polymer-in-ceramic". *Nano Energy* **2018**, *46*, 176–184.

[214] Wang, Y. T.; Ju, J. W.; Dong, S. M.; Yan, Y. Y.; Jiang, F.; Cui, L. F.; Wang, Q. L.; Han, X. Q.; Cui, G. L. Facile design of sulfide-based all solid-state lithium metal battery: *In situ* polymerization within self-supported porous argyrodite skeleton. *Adv. Funct. Mater*. **2021**, *31*, 2101523.

[215] Wang, T. R.; Zhang, R. Q.; Wu, Y. M.; Zhu, G. N.; Hu, C. C.; Wen, J. Y.; Luo, W. Engineering a flexible and mechanically strong composite electrolyte for solid-state lithium batteries. *J. Energy Chem*. **2020**, *46*, 187–190.

[216] Lim, Y. S.; Jung, H. A.; Hwang, H. Fabrication of PEO-PMMA-$LiClO_4$-based solid polymer electrolytes containing silica aerogel particles for all-solid-state lithium batteries. *Energies* **2018**, *11*, 2559.

[217] Xu, Y. J.; Gao, L. N.; Wu, X. Z.; Zhang, S. Z.; Wang, X. L.; Gu, C. D.; Xia, X. H.; Kong, X. Q.; Tu, J. P. Porous composite gel polymer electrolyte with interfacial transport pathways for flexible quasi solid lithium-ion batteries. *ACS Appl. Mater. Interfaces* **2021**, *13*, 23743–23750.

[218] Tsai, C. Y.; Peng, K. J.; Wang, C. F.; Liu, Y. L. Creation of lithium-ion-conducting channels in gel polymer electrolytes through non-solvent-induced phase separation for high-rate lithium-ion batteries. *ACS Sustainable Chem. Eng*. **2020**, *8*, 2138–2146.

[219] Tsai, C. Y.; Liu, Y. L. Building up ion-conduction pathways in solid polymer electrolytes through surface and pore functionalization of PVDF porous membranes with ionic conductors. *J. Membrane Sci*. **2022**, *651*, 120456.

[220] Zhang, S. S.; Xu, K.; Jow, T. R. EIS study on the formation of solid electrolyte interface in Li-ion battery. *Electrochim. Acta* **2006**, *51*, 1636–1640.

[221] Chung, N. K.; Kwon, Y. D.; Kim, D. Thermal, mechanical, swelling, and electrochemical properties of poly(vinylidene fluoride)-co-hexafluoropropylene/poly(ethylene glycol) hybrid-type polymer electrolytes. *J. Power Sources* **2003**, *124*, 148–154.

[222] Du Pasquier, A.; Zheng, T.; Amatucci, G. G.; Gozdz, A. S. Microstructure effects in plasticized electrodes based on PVDF-HFP for plastic Li-ion batteries. *J. Power Sources* **2001**, *97–98*, 758–761.

[223] Du Pasquier, A.; Warren, P. C.; Culver, D.; Gozdz, A. S.; Tarascon, J. M. Plastic PVDF-HFP electrolyte laminates prepared by a phase-inversion process. *Solid State Ionics* **2000**, *135*, 249–257.

[224] Ren, Z.; Liu, Y. Y.; Sun, K. N.; Zhou, X. L.; Zhang, N. Q. A microporous gel electrolyte based on poly(vinylidene fluoride-co-hexafluoropropylene)/fully cyanoethylated cellulose derivative blend for lithium-ion battery. *Electrochim. Acta* **2009**, *54*, 1888–1892.

[225] Zhou, B. H.; Zhou, Y.; Lai, L. J.; Chen, Z. L.; Li, J. J.; Jiang, Y. L.; Liu, J.; Wang, Z. P.; Xue, Z. G. Fabrication of borate-based porous polymer electrolytes containing cyclic carbonate for high-performance lithium metal batteries. *ACS Appl. Energy Mater*. **2021**, *4*, 9582–9593.

[226] Feng, J. W.; Ao, X. H.; Lei, Z. W.; Wang, J.; Deng, Y. H.; Wang, C. Y. Hollow nanotubular clay composited comb-like methoxy poly(ethylene glycol) acrylate polymer as solid polymer electrolyte for lithium metal batteries. *Electrochim. Acta* **2020**, *340*, 135995.

[227] Liang, B.; Jiang, Q. B.; Tang, S. Q.; Li, S. L.; Chen, X. Porous polymer electrolytes with high ionic conductivity and good mechanical property for rechargeable batteries. *J. Power Sources* **2016**, *307*, 320–328.

[228] Wu, J. Y.; Yuan, L. X.; Zhang, W. X.; Li, Z.; Xie, X. L.; Huang, Y. H. Reducing the thickness of solid-state electrolyte membranes for high-energy lithium batteries. *Energy Environ. Sci*. **2021**, *14*, 12–36.

[229] Zhou, M. H.; Liu, R. L.; Jia, D. Y.; Cui, Y.; Liu, Q. T.; Liu, S. H.; Wu, D. C. Ultrathin yet robust single lithium-ion conducting quasi-solid-state polymer-brush electrolytes enable ultralong-life and dendrite-free lithium-metal batteries. *Adv. Mater*. **2021**, *33*, 2100943.

[230] Yang, X. F.; Adair, K. R.; Gao, X. J.; Sun, X. L. Recent advances and perspectives on thin electrolytes for high-energy-density solid-state lithium batteries. *Energy Environ. Sci*. **2021**, *14*, 643–671.

[231] Gao, J.; Shao, Q. J.; Chen, J. Lithiated Nafion-garnet ceramic composite electrolyte membrane for solid-state lithium metal battery. *J. Energy Chem*. **2020**, *46*, 237–247.

[232] He, F.; Tang, W. J.; Zhang, X. Y.; Deng, L. J.; Luo, J. Y. High energy density solid state lithium metal batteries enabled by sub-5 μm solid polymer electrolytes. *Adv. Mater*. **2021**, *33*, 2105329.

[233] Wan, J. Y.; Xie, J.; Kong, X.; Liu, Z.; Liu, K.; Shi, F. F.; Pei, A.; Chen, H.; Chen, W.; Chen, J. et al. Ultrathin, flexible, solid polymer composite electrolyte enabled with aligned nanoporous host for lithium batteries. *Nat. Nanotechnol*. **2019**, *14*, 705–711.

[234] Jiang, Z. Y.; Wang, S. Q.; Chen, X. Z.; Yang, W. L.; Yao, X.; Hu, X. C.; Han, Q. Y.; Wang, H. H. Tape-casting $Li_{0.34}La_{0.56}TiO_3$ ceramic electrolyte films permit high energy density of lithium-metal batteries. *Adv. Mater*. **2020**, *32*, 1906221.

[235] Balaish, M.; Gonzalez-Rosillo, J. C.; Kim, K. J.; Zhu, Y. T.; Hood, Z. D.; Rupp, J. L. M. Processing thin but robust electrolytes for solid-state batteries. *Nat. Energy* **2021**, *6*, 227–239.

[236] Ling, Q.; Yu, Z. Z.; Xu, H. R.; Zhu, G. S.; Zhang, X. Y.; Zhao, Y. Y.; Yu, A. B. Preparation and electrical properties of amorphous Li-Al-Ti-P-O thin film electrolyte. *Mater. Lett*. **2016**, *169*, 42–45.

[237] Nong, J.; Xu, H. R.; Yu, Z. Z.; Zhu, G. S.; Yu, A. B. Properties and preparation of Li-La-Ti-Zr-O thin film electrolyte. *Mater. Lett*. **2015**, *154*, 167–169.

[238] Whiteley, J. M.; Taynton, P.; Zhang, W.; Lee, S. H. Ultra-thin solid-state Li-ion electrolyte membrane facilitated by a self-healing polymer matrix. *Adv. Mater*. **2015**, *27*, 6922–6927.

[239] Zhang, M.; Huang, Z.; Cheng, J. F.; Yamamoto, O.; Imanishi, N.;

Chi, B.; Pu, J.; Li, J. Solid state lithium ionic conducting thin film $Li_{1.4}Al_{0.4}Ge_{1.6}(PO_4)_3$ prepared by tape casting. *J. Alloys Compd*. **2014**, *590*, 147–152.
[240] Nam, Y. J.; Cho, S. J.; Oh, D. Y.; Lim, J. M.; Kim, S. Y.; Song, J. H.; Lee, Y. G.; Lee, S. Y.; Jung, Y. S. Bendable and thin sulfide solid electrolyte film: A new electrolyte opportunity for free-standing and stackable high-energy all-solid-state lithium-ion batteries. *Nano Lett*. **2015**, *15*, 3317–3323.
[241] Liu, G. Z.; Shi, J. M.; Zhu, M. T.; Weng, W.; Shen, L.; Yang, J.; Yao, X. Y. Ultra-thin free-standing sulfide solid electrolyte film for cell-level high energy density all-solid-state lithium batteries. *Energy Storage Mater*. **2021**, *38*, 249–254.
[242] Wang, Z. Y.; Shen, L.; Deng, S. G.; Cui, P.; Yao, X. Y. 10 μm-thick high-strength solid polymer electrolytes with excellent interface compatibility for flexible all-solid-state lithium-metal batteries. *Adv. Mater*. **2021**, *33*, 2100353.
[243] Wu, J. Y.; Rao, Z. X.; Cheng, Z. X.; Yuan, L. X.; Li, Z.; Huang, Y. H. Ultrathin, flexible polymer electrolyte for cost-effective fabrication of all-solid-state lithium metal batteries. *Adv. Energy Mater*. **2019**, *9*, 1902767.
[244] Chen, W. P.; Duan, H.; Shi, J. L.; Qian, Y. M.; Wan, J.; Zhang, X. D.; Sheng, H.; Guan, B.; Wen, R.; Yin, Y. X. et al. Bridging interparticle Li^+ conduction in a soft ceramic oxide electrolyte. *J. Am. Chem. Soc*. **2021**, *143*, 5717–5726.

Dongmei Zhang is currently a PhD candidate in Prof. Meicheng Li's New Energy Materials and Devices group at the North China Electric Power University. Her research interest is focused on the nano-/micro-materials for solid-state battery application.

Xianglong Meng is currently a master candidate majoring in Power Engineering at the New Energy School of North China Electric Power University. He received his bachelor's degree in New Energy Science and Engineering from North China Electric Power University in 2016. His current research focus on the design and synthesis of composite solid electrolytes suitable for lithium metal batteries.

Wenyan Hou is a postgraduate of Department of Electrical Engineering at Xi'an Jiaotong University and State Key Laboratory of Electrical Insulation and Power Equipment. Her main research interests focus on all-solid-state electrolytes for lithium-ion batteries.

Lehao Liu is a researcher in North China Electric Power University. He finished his PhD defense in 2016 in Northwestern Polytechnical University under the supervision of Prof. Tiehu Li. He was a joint-training PhD student at University of Michigan for 26 months with the guidance of Prof. Nicholas A. Kotov. After graduation, he began to work as a chief engineer in CITIC Guoan MGL Power Source Technology Company. His research interest focuses on nano-/micro-materials for energy storage.

Meicheng Li is a professor in North China Electric Power University. He is the Dean of School of New Energy. He obtained his PhD degree at Harbin Institute of Technology in 2001. He worked in University of Cambridge as research fellow from 2004 to 2006. His research topic is New Energy Materials and Devices, such as solar cells and lithium/sodium ion battery, and other solar devices, sensors, etc. He has contributed more than 300 peer-reviewed articles in journals such as *Nature Energy*, *Joule*, *Advanced Materials*, *Energy & Environmental Science*, etc.